Organic Reactions of Gallium Phosphide and Silicon Surfaces for Stability and Dye Sensitization

by

Elizabeth S. Brown

A dissertation submitted in partial fulfillment
of the requirements for the degree of
Doctor of Philosophy
(Chemistry)
in the University of Michigan
2016

Doctoral Committee:

Associate Professor Stephen Maldonado, Chair
Professor Adam J. Matzger
Professor Michael D. Morris
Professor Bradford Orr

DEDICATION

For my parents

ACKNOWLEDGMENTS

They say it takes a village to raise a child. I would argue it also takes a village to successfully graduate a PhD program. I am grateful for everyone I have interacted with from my formative years through today. You have all shaped me with your support and love.

Without the support and encouragement of my research mentor, Prof. Stephen Maldonado, my PhD would not have been possible. I appreciate all your help in pursuing my research project and developing my career. I feel very fortunate to have found not just a home, but a family, in your lab. For starting my career towards a PhD in chemistry, I would like to thank Prof. Robert McGaff for teaching me how to apply the scientific method to a research setting. I would like to acknowledge our funding agencies for supporting my research, primarily the U.S. Department of Energy, the University of Michigan Chemistry Department, and the Susan Lipschutz Award through Rackham Graduate School.

I also would not have made it through my PhD degree without the support and advice of my peers. From all the iterations of the Maldonado lab, I would like to thank all past and present lab members. I've been so glad to be your labmate. In particular, I would like to thank Dr. Sabrina Peczoncyzk for teaching me all about surface chemistry and sharing in the caretaking of Xaiver the XPS. I'd like to thank Dr. Zhijie Wang for his welcoming personality, Dr. Junsi Gu for his willingness to help everyone at the drop of a hat, Dr. Wen Wen for making me feel included. Thanks to Eli Fahrenkrug for going through all the stages of the PhD with me and for all our chats. Thank you to Susu Lee, Luyao Ma, Tim Zhang, Josh DeMuth, Titi Shidayo for keeping our lab fun, friendly, and running smoothly. This lab was a second home and great people like you all are the main reason for that. Sofiya Hlynchuk, I am so glad to leave Xaiver and the surface projects in your capable hands—we couldn't have found a smarter or more hardworking person if we tried. Thanks to my collaborators, Prof. Ksenija Glusac, Stefan Ilic, Prof. Nicolai

Lehnert, Dr. Shawn Eady, for helping me to learn about different types of chemistry and sharing fresh ideas and approaches through our discussions and Skype meetings. Lastly, I would like to thank my committee members, Prof. Adam Matzger, Prof. Michael Morris, and Prof. Brad Orr, for their suggestions and guidance throughout the milestones of my PhD.

I would like to thank the support staff in the chemistry department. For the secretaries and administration, thank you for running such a great program. For Margarita Bekiares, thank you for listening when I needed it. For Cornelius Wright and Liz Oxford, thank you for answering my many (many) questions about the business side of being a graduate student. For Tracy Stevenson, thank you for making Chemistry a safe place to work and for all your help with FEMMES events. I would like to thank Steve Donajkowski and the machine shop for helping us to repair the XPS during times of distress.

The broader community at the University of Michigan has been amazing. Contributions from faculty, staff, other students, and 'townies' make this a great place to be a graduate student. I learned a lot through the many workshops hosted by Rackham and the Department of Chemistry. Student run groups also impacted my time at Michigan significantly, especially FEMMES. To all the past and future executive board members and many people who I have convinced to volunteer with FEMMES, thank you for encouraging, inspiring, and supporting me and facilitating the sharing of our love of science with the youth in the area. I'm really proud of us and what we are working towards.

Thank you to my friends and support system from Ann Arbor (Julia Bourg, Jenny Wong, Joanna Thielen, Pooja Pandit, Dr. Jess Donehue Flynn, Dr. Kayla Pyper) and beyond (Sasha Mala Chihak, Katie Challis, Susan VandenLangenberg, Julia Dlugopolski, Jasmine Johnson, Kevin Mauthe). I am so lucky to have you all in my life to keep me grounded and sane.

To Tim, my love, thank you for your support and understanding as we went through this journey together. I remember your support during all the late nights in lab,

your encouragement while listening to my frustrations, cheering me up while eating our lunches together in the conference rooms, the advice you gave me about organic chemistry, all the chemicals you lent to me, proofreading each other's documents and listening to practice talks, dropping by for morning hugs or quick advice …This was the beginning of our story and I am excited to see where our next adventure takes us.

Thank you to my siblings, Jennifer and Bill, and to their families (Ryan, Cassandra, Brenna, Dylan, Morgan, Noelle, Serena) as well as my Grandma Rita and Aunt Carla and Candy for your unconditional love and for visiting me in faraway Michigan. I have been so blessed in knowing you and in being known by you.

Finally, thank you to my parents, Steve Brown and Karin Weiss Brown, for without whom I would be lost. Your love, support, and advice have been the most precious blessing. I am so fortunate to be your daughter. Mom-- you've finally got a doctor in the family. Brownsketeers forever.

TABLE OF CONTENTS

DEDICATION ii
ACKNOWLEDGMENTS iii
LIST OF FIGURES ix
LIST OF TABLES xiv
LIST OF EQUATIONS xv
LIST OF APPENDICES xvi

CHAPTER

1. Introduction 1
   1.1 Background 1
   1.2 Gallium Phosphide 2
   1.3 Thesis Summary 6
   1.4 References 9
2. Wet Chemical Functionalization of GaP(111)B Through a Williamson Ether-type Reaction 13
   2.1 Introduction 13
   2.2 Experimental 14
      2.2.1 Materials and Chemicals 14
      2.2.2 Etching 15
      2.2.3 X-ray Photoelectron Spectroscopy 15
      2.2.5 Infrared Spectroscopy 22
      2.2.5 Static Sessile Drop Contact Angle Measurements 22
      2.2.6 Electrode Fabrication and Photoelectrochemical Cell Design 22
      2.2.7 Photoelectrochemical Measurements 22
   2.3 Results 23
      2.3.1 Characterization of Etched GaP(111)B 23
      2.3.2 Reaction of Etched GaP(111)B with Alkyl and Benzyl Halides 26
      2.3.3 Base Promoters 36

2.3.4 Sub-Band Gap Photoelectrochemical Measurements 42
2.3.5 Sensitization of GaP(111)B with Chemisorbed Coomassie Blue Dye 42
2.4 Discussion 46
2.5 Summary 52
2.6 References 53
3. Photoelectrochemical Properties of CH_3-Terminated P-type GaP(111)A 57
3.2 Experimental 58
3.2.1 Materials and Chemicals 58
3.2.2 Electrode Fabrication 59
3.2.3 Chlorination and Grignard Reaction Sequence of Electrodes 59
3.2.4 Experimental Surface Characterization 59
3.2.5 Electrochemical Impedance Spectroscopy 60
3.2.6 Photoelectrochemical Measurements 63
3.3 Results 64
3.3.1 Impedance Characteristics of p-GaP(111)A Electrodes in Aqueous Solution 64
3.3.2 Band Edge Energetics of Native and CH_3-terminated p-GaP(111)A Electrodes in Aqueous Solution 64
3.3.3 Cathodic Stability of p-GaP Photoelectrodes 66
3.3.4 Non-sensitized Sub-bandgap Photoresponse of Etched and CH_3-terminated p-GaP(111)A 70
3.3.5 Sensitized Sub-bandgap Photoresponse of Etched and CH_3-terminated p-GaP(111)A 72
3.4 Dicussion 75
3.4.1 Surface Energetics of CH_3-terminated GaP 75
3.4.2 Stability of Surface Bonds at CH_3-terminated GaP 76
3.4.3 Surface Defect Density of CH_3-terminated GaP 77
3.5 Summary 78
3.6 References 79
4. Chemically Modified Si(111) Surfaces Simultaneously Demonstrating Hydrophilicity, Resistance Against Oxidation, and Low Trap State Densities 83
4.1 Introduction 83
4.2 Experimental 84
4.2.1 Materials and Chemicals 84
4.2.2 Sample Preparation 85
4.2.3 Preparation of *1* and *1a* 87

4.2.4 Preparation of *2*, *2a*, *2b* and *2c* 87
4.2.5 Preparation of *3*, *3a*, *3b* and *3c* 87
4.2.6 Nucleophilic Reaction with 4-(trifluoromethyl)benzyl bromide. 87
4.2.7 X-ray Photoelectron Spectroscopy 88
4.2.8 Infrared Spectroscopy 95
4.2.9 Static Sessile Drop Contact Angle Measurements 95
4.2.10 Surface Recombination Velocity Measurement 95
4.3 Results 96
4.3.1. Passivated Surfaces Featuring Chemisorbed Primary Alcohols (1a) 96
4.3.2 Passivated Surfaces Featuring Chemisorbed Diols 106
4.3.3 Passivated Surfaces Featuring Chemisorbed Phenylamine 109
4.4 Dicussion 110
4.5 Summary 114
4.6 References 116
Appendices 121

LIST OF FIGURES

Figure 1.1. Solar absorptivity (α^{-1}) and the separation of the majority carrier (electrons) and minority carriers (holes) for (a) conventional planar GaP junction and (b) electrochemically-etched, macroporous GaP. Figure originally published in Price, et al.[13] 3
Figure 1.2 Zincblende crystal structure of gallium phosphide. Figure originally published in Peczoncyzk, et al.[44] 5
Figure 2.1 Illustration of Partial Layers t_1 and t_2 on GaP(111)B Reacted with *p*-(trifluoromethyl)benzyl bromide. 19
Figure 2.2 Difference spectra between high resolution P 2p XP spectra of (red) GaP(111)A etched with concentrated H_2SO_4 and (black) GaP(111)B etched with concentrated H_2SO_4. The difference between the two spectra is shown in blue. 24
Figure 2.3 Representative spectra of reaction of GaP(111)B with BH_3•THF at 0°C for 3 h with (a) B 1s peak at 189 eV in XP spectra difficult to distinguish from the P 2s peak and corresponding P-oxide at 186.1 eV and 190.8 eV, respectively, and (b) no signal at 2400 cm^{-1} indicating B-H stretching in the GATR-FTIR spectrum. Vertical scale bar = 1.0 x 10^{-4} absorbance units..... 27
Figure 2.4 Representative GATR-FTIR spectra of the (a) -CH_3/-CH_2 stretching region and (b) P-O-C stretching region for etched GaP(111)B (black) and GaP(111)B reacted with $C_{18}H_{37}Br$ and KHMDS for 1 h at 60°C (red). Vertical scale bar = 5 x 10^{-4} absorbance units. Spectra are offset for clarity. 31
Figure 2.5 GATR-FTIR spectra showing the symmetric and asymmetric –CH_2- and –CH_3 stretching modes of GaP(111)B after reaction with (a) $C_{14}H_{29}Br$ after 1 h and (b) $C_{10}H_{21}Br$ with KHMDS after 3 h. Vertical scale bar = 2.5 x 10^{-4} absorbance units. Spectra have been baseline corrected. 32
Figure 2.6 GATR-FTIR of GaP(111)B reacted with *p*-$CF_3C_6H_4CH_2Br$ showing (a) -CH_3/ -CH_2- stretches, (b) P-O-C stretches, and (c) several peaks for –CF_3 groups off of a benzene ring. Vertical scale bars = 1.0 x 10^{-3} absorbance units. 33
Figure 2.7 Increased signal intensity in the high resolution C 1s XP spectrum after reaction of GaP(111)B with $C_{18}H_{37}Br$ for 1 h. 34
Figure 2.8 High-resolution XP spectra of (a) C 1s and (b) F 1s for GaP(111)B before and after reaction with *p*-$CF_3C_6H_4CH_2Br$ and KHMDS. 35
Figure 2.9 Water contact angle of etched (red triangles) and $C_{18}H_{37}$-terminated GaP(111)B (black squares) after time aging in water. Error bars indicate one standard deviation..... 38
Figure 2.10 Measured oxide thickness (black triangles, left *y*-axis) and monolayer coverage (red squares, right *y*-axis) observed for GaP(111)B after reaction with *p*-$CF_3C_6H_4CH_2Br$ for 1 hour at T = 60°C followed by a 3 hour immersion in water with varying pH. 39
Figure 2.11 The calculated oxide thickness of etched (red triangles) and $C_{18}H_{37}$-terminated (black squares) GaP(111)B over time in ambient conditions. 40

Figure 2.12 Monolayer coverages of p-$CF_3C_6H_4CH_2$- on GaP(111)B after reaction with p-$CF_3C_6H_4CH_2Br$ for 1 h at T = 60°C using several different base promoters (TEA = triethylamine; KBuO = potassium butoxide; DBU = 1,8-diazabicycloundec-7-ene; KHMDS= potassium bis(trimethylsilyl)amide). Arrows indicate the range of monolayer coverage values obtained under the same conditions in the absence of any base promoter. 41
Figure 2.13 Contact angle data for GaP(111)B reaction with $C_{18}H_{37}Br$ (closed squares) or $C_{10}H_{21}Br$ (open circles) in the presence of a series of bases..... 43
Figure 2.14 Monolayer coverage of *p*-$CF_3C_6H_4CH_2$- on GaP(111)B without (open circles) or with KHMDS (closed squares) at *T* = 60°C for different reaction times. 44
Figure 2.15 Wavelength-dependent external quantum yields for photocurrent for p-type GaP(111)B after reaction with concentrated H_2SO_4 and alkyl bromides ($C_nH_{2n+1}Br$, where *n* = 10, 14, 18). 45
Figure 2.16 High resolution XP spectra of GaP(111)B after etching (black) and after reaction with CB-I in methanol in the dark. (a) Both P 2p spectra show negligible oxide formation at 133 eV. CB-I reacted GaP(111)B exhibited increased intensity at (b) 168.0 eV in the S 2p spectrum and at (c) ~400 eV in the N 1s spectrum. The difference spectrum (blue trace) is included for clarity. (d) Some Cl 2p signal remains after reaction. 47
Figure 2.17 Wavelength-dependent external quantum yield for photocurrent at p-type GaP(111)B before and after attachment of Coommassie Blue dye. 48
Figure 2.18 External QY response of p-type GaP(111)B reacted with CB-I (solid line) and the same electrode again after several measurements and one week under vacuum (dashed line). 49
Figure 3.1 XP (a) survey spectrum and (b) high-resolution P 2p or (c) C 1s spectra of p-GaP(111)A electrode after subsequent reaction with PCl_5 in chlorobenzene and CH_3MgCl in THF. In (a), no signature of excess reagents was observed. In (b), no oxidation of the electrode was observed at 133 eV. In (c), the shoulder at 282.7 eV was present after reaction of the electrode with CH_3MgCl. 61
Figure 3.2 Bode plots for (a-d) a representative acid etched and (e-h) a representative CH_3-terminated GaP(111)A electrodes immersed in N_2-purged aqueous solution containing 1 M KCl, 0.002 M $EuCl_2$, 0.002 M $EuCl_3$, and acetate buffer (pH = 4). 65
Figure 3.3 a) Representative plots of the squared reciprocal capacitance values at *f* = 103 Hz as a function of electrochemical potential for etched and CH_3-terminated p-type GaP(111)A electrodes in N_2-saturated solution containing 1 M KCl, 0.002 M $EuCl_2$, 0.002 M $EuCl_3$, and acetate buffer (pH = 4). Measurements were performed in the dark and plots are normalized to electrode area. b) Flat-band potentials of etched and CH_3-terminated p-GaP(111)A as a function of pH. Error bars indicate the standard error mean over five etched and six CH_3-terminated electrodes. 67
Figure 3.4 Idealized schematic depiction of the stabilities of native and CH_3-terminated p-GaP(111)A photoelectrode interfaces after sustained passage of cathodic current. 68
Figure 3.5 The current-voltage characteristics for p-type GaP(111)A photoelectrodes in N_2-purged aqueous solution containing 0.1 M H_3PO_4 while illuminated with 100 mW cm^{-2}. (a) Photoresponses for an etched p-GaP(111)A photoelectrode (solid line) at the start and (dashed line) after 15 h of continuous illumination at *E* = -2.5 V vs Ag/AgCl. (b) Photoresponses for a CH_3-terminated p-GaP(111)A photoelectrode (solid line) at the start

and (dashed line) after 15 h of continuous illumination at E = -2.5 V vs Ag/AgCl. (c) High resolution Ga 3d XP spectra of etched (bottom) and CH_3-terminated (top) p-GaP(111)A photoelectrodes before and after continuous illumination at E = -2.5 V vs Ag/AgCl for 15 h. The Ga 3d peak shift is highlighted by a dashed line (18.65 eV) for aged etched electrodes, a dot-dashed line for both before electrodes (19.0 eV), and a solid line for aged CH_3-terminated electrode (18.9 eV). 69
Figure 3.6 a) Schematic depiction of a p-type GaP photoelectrode under depletion conditions in contact with an electrolyte. Photoexcitation is shown for band-to-band transition from the absorption of supra-bandgap light and for band-to-state transition for sub-bandgap light. The dotted lines show excitation from supra-bandgap or sub-bandgap light. b) Wavelength-dependent external quantum yields measured at E = -0.6 V vs. Ag/AgCl bias in deaerated 0.1 M KCl solution for etched and CH_3-terminated p-GaP(111) photoelectrodes. 71
Figure 3.7 a) The measured external quantum yield at 645 nm for etched and CH_3-terminated GaP(111)A photoelectrodes at E = -0.6 V vs. Ag/AgCl in 0.1 M KCl as a function of dye (Brilliant Green) concentration. b) Wavelength-dependent external quantum yields measured for etched and CH_3-terminated GaP(111)A photoelectrodes. Measurement conditions were as in (a) with [Brilliant Green] = 16 μM. 74
Figure 4.1 Chemical modification routes for Si surfaces outlined in this work. 86
Figure 4.2 Surface Labeled with t_1 and t_2. 90
Figure 4.3 Modified Si(111) surfaces after reaction with 4-(trifluoromethyl)benzyl bromide. 93
Figure 4.4 Comparison of (*a*) Si 2p XP and (*b*) infrared spectra for freshly prepared type *1* and *1a* surfaces. (*c*) Comparison of F 1s XP spectra before and after reaction of a type *1a* surface with 4-(trifluoromethyl)benzyl bromide. All spectra offset vertically for clarity. Representative microwave photoconductivity transients presented as (*d*) normalized and (*e*) natural log signal vs time. 98
Figure 4.5 GATR-FTIR of *1* and *1a* surfaces in the COH bend region. Scale bar indicates 2 x 10^{-4} A.U. Spectra were baseline corrected and offset for clarity. 99
Figure 4.6 GATR-FTIR of *1* and *1a* surfaces. Scale bar indicates 2 x 10^{-4} A.U. Spectra were baseline corrected and offset for clarity. 100
Figure 4.7 Representative etherification reaction, showing reaction *1a* with TFB with base promotor (KHMDS). 102
Figure 4.8 High resolution F 1s XP spectra of pristine *1a* (bottom) and after reaction with OFP (top). Spectra offset for clarity. 103
Figure 4.9 (*a*) Comparison of Si 2p XP spectra for freshly prepared type *2* and *2a* surfaces. (*b*) Infrared spectra showing the CO stretches, -OH bend, and CH bend for type *2a* surfaces. (*c*) Comparison of F 1s XP spectra before and after reaction of a type *2a* surface with 4-(trifluoromethyl)benzyl bromide. (*d*) Comparison of Si 2p XP spectra for freshly prepared type *2b* and *2c* surfaces. All spectra offset vertically for clarity. Representative microwave photoconductivity transients presented as (*e*) normalized and (*f*) natural log signal vs time. 107
Figure 4.10 High resolution F 1s XP spectra after etherification reaction of TFB with (a) *2c* and (b) *3c*. 108
Figure 4.11 GATR-FTIR of surface *3*. Scale bar is 1 x 10^{-4} A.U. 111

Figure 4.12 (*a*) Comparison of Si 2p XP spectra for freshly prepared type *3* and *3a* surfaces. (*b*) High resolution N1s XP spectrum of a freshly prepared type *3a* surface. (*c*) Comparison of infrared spectra for freshly prepared type *3* and *3a* surfaces. (*d*) Comparison of F 1s XP spectra before and after reaction of a type *3a* surface with 4-(trifluoromethyl)benzyl bromide. (*e*) Comparison of Si 2p XP spectra for freshly prepared type *3b* and *3c* surfaces. All spectra offset vertically for clarity. Representative microwave photoconductivity transients presented as (*f*) normalized and (*g*) natural log signal vs time. 112
Figure A.1 Schemes determined for a) phosphorus atop atoms of planar GaP(111)B and b) gallium atop atoms of planar GaP(111)A. 123
Figure A.2 High resolution XP spectra of a) F 1s region of GaP NW after etching (bottom) and after reaction with TFB. Spectra offset for clarity. XP spectra of b) C 1s region of GaP NW after reaction with TFB. 125
Figure A.3 SEM of GaP NW after a) 15 min and b) 30 min in NCS solution. Micrographs courtesy of Dr. W.Wen. 126
Figure A.4 High resolution XP a) Cl 2p and b) Au 4f spectra of samples after chlorination with NCS for 15 min (black) or 30 min (red) and after reaction with CH_3MgCl (blue and pink, respectively). Spectra are offset for clarity. 128
Figure A.5 High resolution XP a) P 2p, b) N 1s, c) S 2p, and d) Cl 2p spectra for GaP NW reacted with modified Coomassie Blue dye. 130
Figure A.6 High resolution F 1s XP spectra of modified GaP NW. Increased signal at 688 eV was observed from etched NW (black) to spectra taken immediately after reaction with TFB (red). Peak signal changes after aging reacted NW samples in water for 4 h (blue), 8 h (pink), and 12 h (green). Spectra are normalized and offset for clarity. 131
Figure A.7 High resolution XP P 2p spectra for modified GaP NW immediately after reaction (bottom traces) and after several hours oxidation in water (4 h, 8 h, 12 h). Each spectra is offset a small amount for clarity. Each modified surface is grouped together, where etched is black, TFB-reacted is green, NCS (15 min) and CH_3MgCl is blue, and NCS (30 min) and CH_3MgCl is red. 132
Figure B.1 Band diagram for GaP etched (orange), after modification with PCl_5 and subsequently CH_3MgCl (red), and the HOMO and LUMO levels for the hole-injecting dye. 136
Figure B.2 External quantum yield measured in the sub-band gap region of GaP (>550 nm) for 10 μM a) pinacyanol chloride, b) Stains All, or c) Coomassie Blue in 1 M KCl electrolyte. Etched GaP(111)A responses are shown in black and CH_3-terminated GaP(111)A responses are shown in red. 138
Figure B.3 External quantum yield measured in the sub-band gap region of GaP (>550 nm) for 10 μM a) ethyl violet and b) indocyanine green in 1 M KCl electrolyte. Etched GaP(111)A responses are shown in black and CH_3-terminated GaP(111)A responses are shown in red. 139
Figure C.1 High resolution Si 2p XP spectra for Si(111) reacted with PCl_5 and then a) $TMSCF_3$ for 1 h, b) $TMSCF_3$ for 1 h followed by sonication in methanol, and c) $TMSCF_3$ for 3 h. 147
Figure C.2 High resolution Si 2p XP spectra for Si(111) reacted with PCl_5 and then with Mg^0 and a) $PhSCF_3$ for 4 h and b) $PhSCF_3$ for 24 h at 0^0C, followed by sonication in methanol. 148

Figure C.3 High resolution a) Si 2p and b) F 1s XP spectra for Si(111) reacted with PCl_5 and subsequently with $PhSO_2CF_3$ and Mg^0 for 5 h at room temperature (black), for 2 h at 0°C (red), and for 5 h at 0°C (blue). Spectra are offset for clarity. 149
Figure C.4 High resolution Si 2p XP spectra for Si(111) reacted with PCl_5 and then with $PhSO_2CF_3$ and Mg^0 a) for 2 h at 0°C and b) for 2 h at -30°C. Procedure for these reactions required the reagents to be mixed prior to adding to the Cl-Si(111). 152
Figure C.5 High resolution XP spectra of Cl-Si(111) after reaction with $PhSO_2CF_3$ and Mg^0 in DMF at -30°C for different reaction times. Blue traces indicate reactions where all reagents are mixed together before adding Si substrate while green traces indicate reactions where all reagents were injected simultaneously into a vessel containing the Si substrate. 153
Figure C.6 High resolution a) F 1s and b) Cl 2p XP spectra for Cl-Si(111) reacted at -30°C with Mg^0 and $PhSCF_3$ for 24 h (green) or $PhSO_2CF_3$ for 2 h (red), 5 h (blue), or 24 h (green). 154
Figure C.7 Representative high resolution F 1s XP spectra for Cl-Si(111) reacted at -30°C with Mg^0 and $PhSO_2CF_3$ for 2 h in the presence of $HgCl_2$ (blue) or potassium butoxide (red) additives. 155
Figure C.8 High resolution a) Si 2p, b) F 1s, and c) Cu 2p XP spectra of several reaction conditions of Cl-Si(111) reacted with $TMSCF_3$ with CuCl, 1,10-phenathroline, and potassium butoxide in DMF. 157
Figure C.9 High resolution a) Si 2p, b) F 1s, and c) Cu 2p XP spectra of two sections of the same wafer after reaction of Cl-Si(111) with $TMSCF_3$ with CuCl, 1,10-phenathroline, and potassium butoxide in DMF at 55°C for 18 h. One section, termed 'clean', looked optically shiny after rinsing while another section contained a plaque that was not removable by sonication in different solvents, termed 'residue. 158
Figure C.10 High resolution a) Si 2p and b) F 1s XP spectra for Cl-Si(111) with $TMSCF_3$ with CuCl, 1,10-phenathroline, and potassium butoxide in DMF at 55°C for 18 h (black) and after 1 day in ambient conditions (gray). 159

LIST OF TABLES

Table 2.1 Monolayer Coverage Calculation Parameters for Various Reactants. 18
Table 2.2 Monolayer Coverage Calculation Parameters for Various Reactants. 21
Table 2.3 Reaction Parameters of GaP(111)B Surfaces. 25
Table 2.4 XPS Peak Positions and Intensities of Functionalized GaP(111)B. 28
Table 2.5 Reaction Parameters of GaP(111)B Surfaces. 29
Table 2.6 Contact Angle Data for Treated GaP(111)B. 30
Table 2.7 XPS Peak Positions and Intensities of Functionalized GaP(111)B. 37
Table 3.1 Average External Quantum Yield of GaP(111)A at 650 nm. 73
Table 4.1 Monolayer Coverage Calculation Parameters for Various Reactants. 91
Table 4.2 Monolayer Coverage and Fractional Coverage (θ) of Modified Si(111) Surfaces. 94
Table 4.3 Contact Angle Data for Modified Si(111) Surfaces. 101
Table 4.4 Calculated SRV Values in cm s^{-1} Over Time in Ambient Conditions for N=3. 104
Table 4.5 Average Oxide Thickness of Modified Si(111) Surfaces in nm. 105
Table A.1 Contact Angle Values for Modified NW Samples. 129
Table C.1 Contact Angle Values for $TMSCF_3$ Reactions 146
Table C.2 Contact Angle Values for $PhSCF_3$ and $PhSO_2CF_3$. 150
Table C.3 Lifetime and Surface Recombination Velocity of Modified Si(111). 160

LIST OF EQUATIONS

Equation 2.1 Simplified Overlayer Model Equation for Oxide Thickness. 16
Equation 2.2 Equation for Electron Escape Depth. 16
Equation 2.3 Equation for Mean Diameter. 16
Equation 2.4 Equation for Full Substrate Overlayer Model. 17
Equation 2.5 Equation for Monolayer Coverage. 17
Equation 2.6 Monolayer Coverage Calculation Derived From Three-Layer Model. 17
Equation 2.7 Equation for Relationship Between Thickness of the Three Layers of the Overlayer 20
Equation 2.8 Relationship Between Thickness of Three Layers and Total Overlayer Thickness. 20
Equation 2.9 Monolayer Coverage Calculation. 20
Equation 3.1 Equation for Impedance of Photoelectrochemical Cell with Small Solution Resistance. 60
Equation 3.2 Relationship Between Total Impedance and Space-Charge Capacitance. 62
Equation 3.3 Mott-Schottky Relation. 62
Equation 3.4 Relationship Between Flat-Band Potential and Valence Band Potential. 63
Equation 4.1 Simplified Substrate Overlayer Equation. 88
Equation 4.2 Electron Escape Depth Calculation. 88
Equation 4.3 Mean Diameter Calculation. 89
Equation 4.4 Three-Layer Model for Monolayer Calculation. 89
Equation 4.5 Relationship Between Two Sub-Layers in Three-Layer Model 92
Equation 4.6 Relationship Between Total Overlayer Thickness and Two Sub-Layers 92
Equation 4.7 Monolayer Coverage Relationship. 92
Equation 4.8 Relationship Between Lifetime and Surface Recombination Velocity. 96
Equation 4.9 Relationship Between Lifetime and Surface Recombination Velocity when Wafer Thickness Is Small. 96
Equation C.1 Relation between lifetime and surface state recombination velocity. 144
Equation C.2 Approximation for surface state recombination velocity. 145

LIST OF APPENDICES

Appendix A…….....121
Appendix B……..135
Appendix C……..142

CHAPTER 1
Introduction

1.1 BACKGROUND

With a growing world population, energy demand is projected to double current usage by 2050.[1] The impact of burning fossil fuels is a known contributor to global climate change, following a 40% rise in anthropogenic carbon dioxide (CO_2) emissions since the Industrial Revolution.[2,3] Governments from countries around the world have recognized that if this trend continues, the potential threat to ecosystems looms over the livelihoods of their constituents. Correspondingly, many countries have pledged to increasing renewable energy sources within infrastructure through programs like the United States Department of Energy SunShot initiative, aiming for $0.06 per kWh by 2020,[4] and the Paris Agreement (2015), where the United Nations Framework Convention for Climate Change pledged to reduce carbon dioxide emissions by 2020.[5] The mission of SunShot states their goal to "re-establish American technological and market leadership, improve the nation's energy independence, and strengthen U.S. economic competitiveness while fighting climate change."[4] Environmentally friendly, renewable energy sources, including hydrothermal, hydroelectric, wind harvesting, and solar energy conversion, are not only desired for their environment impacts but for geopolitical and economic purposes. Solar energy is the most abundant renewable energy source available, hitting the earth with more energy in one hour than is globally consumed in one year.[6]

A myriad of materials, device structures, and mechanisms for solar energy storage have been studied and optimized, with benefits and challenges for each system. High efficiency solar energy conversion cells include triple-junction cells composed of crystalline III-V semiconductors, which operate at 41% efficiency under concentrated illumination,[7] and silicon (Si) cells at 1 sun with 25% efficiency.[8] Once the solar energy is harvested and converted to electrical energy, it can be stored as electrical energy in a

battery system. However, state-of-the-art lithium ion battery performance degrades upon cycling.[9,10] An alternative is to store energy in the form of chemical bonds, much like processes found in nature such as photosynthesis.[11]

1.2 GALLIUM PHOSPHIDE

Crystalline inorganic semiconductors electrode materials in photoelectrochemical systems can form chemical fuels from external bias or even from sunlight. Small and wide band gap semiconductors, Si (1.1 eV) and titanium dioxide (TiO_2) (3.2 eV), respectively, have been widely studied in this purpose. One method for solar energy capture, which utilizes low grade TiO_2 nanoparticles, employs adsorbed dye in order to increase the fraction of the solar spectrum that was captured.[12] III-V semiconductors are also potential photoelectrode materials due to their superior optoelectronic properties. In particular, gallium phosphide (GaP) has a mid-sized band gap (2.26 eV) which allows an appreciable amount of photocurrent (10 mA cm^{-2}) *and* photovoltage (~1.7 V) to drive bond-forming electrochemical reactions.[13] With GaP, the reduction of CO_2 to CH_3OH has been shown with nearly 100% Faradaic efficiencies. [14-16] GaP has also been explored as a photocathode for the reduction of H^+ *(aq)* to H_2*(g)*.[17,18]

The bandgap position and inherent stability of GaP are uniquely suited for dye sensitized photoelectrochemical cells. For sensitization, n-type photoanodes such as TiO_2 have been exhaustively studied, where a photoexcited electron from the dye is injected into the semiconductor valence band.[19] The charge transfer kinetics and bonding modes are well-known for these systems (e.g. ruthenium-polypyridine dyes on TiO_2).[12,20] However, little is known about the transfer of an electron from the valence band of a p-type semiconductor to a photoexcited dye, i.e., sensitized hole-injection. Other p-type materials studied in this way, such as NiO and CuSCN, have small bulk carrier mobilities ($\mu_p << 1$ cm^2 V^{-1} s^{-1}) which complicates measurements of hole injection processes.[21,22] Conversion efficiencies on dye-sensitized p-NiO have only reached 2.5%,[23,24] compared with n-type DSSC systems reaching 13%.[25] Conversely, p-type GaP has better charge carrier mobility ($\mu_p \sim 300$ cm^2 V^{-1} s^{-1}). Further development and understanding of p-GaP systems will complement knowledge of n-type SC systems allowing for construction of tandem photovoltaics or photoelectrochemical cells.

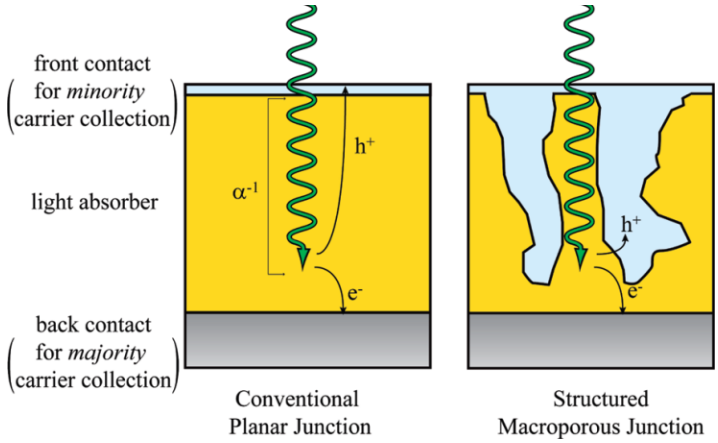

Figure 1.1. Solar absorptivity (α^{-1}) and the separation of the majority carrier (electrons) and minority carriers (holes) for (a) conventional planar GaP junction and (b) electrochemically-etched, macroporous GaP. Figure originally published in Price, et al.[13]

Two key features that inhibit further development of GaP as a photoelectrode material are (1) the inefficient absorption of 'long' wavelength light due to an indirect band gap and (2) the chemical instability of native GaP surfaces towards oxidation and chemical attack. The first challenge was addressed through development of nanostructured, high aspect ratio morphologies.[13,18,26,27] Nanostructured GaP maximizes the depth of light absorption in one direction and minimizes the required distance for charge carrier collection (Figure 1.1). The second challenge of instability is exacerbated in high surface area nanostructured materials that feature non-uniform surface chemistries. Native oxides form rapidly on GaP surfaces in ambient conditions which lead to a high density of surface traps (1 defect/100 surface atoms).[28,29] Native oxides on GaP are neither stable nor electrically passivating, unlike thermal oxides on Si surfaces. Chemical functionalization of single crystalline Si surfaces lowers the content of surface defects, on the order of 1 defect/1,000,000 surface atoms.[30-33] Chemical control over both atop Ga and atop P atoms on surfaces may similarly impart long-lasting stability for GaP photoelectrodes.

To date, several different surface chemistry approaches have been used to modify the interfacial properties of GaP. Attachment of sulfides and thiols has been demonstrated, adapted from surface reactions developed for gold or gallium arsenide.[34-38] Such surfaces had poor stability in air and water over time.[37] Furthermore, evidence both supporting and refuting proposed P-S bonding, as well as the presence of Ga-S bonding, has been presented, indicating surfaces with undefined bonding.[34-36,38,39]

An alternative reaction strategy for GaP through the grafting of alkene or azide containing molecules using UV light after an etching step in hydrogen plasma is known.[37,40-42] Without the hydrogen plasma pretreatment, high oxide and lower surface coverage was observed after grafting.[37] Ga-H terminated GaP surfaces cannot be prepared by any known wet chemical treatments tested.[39]

A more recent approach for surface functionalization of GaP is the grafting of a conjugated polymer on GaP(100). After treatment with oxygen plasma and etching with buffered hydrofluoric acid/ammonium fluoride solution, GaP was grafted with 4-vinylpyridine under UV light, which continues to polymerize with itself under these conditions.[43] Cobaloxime molecules were subsequently reacted with the pyridines

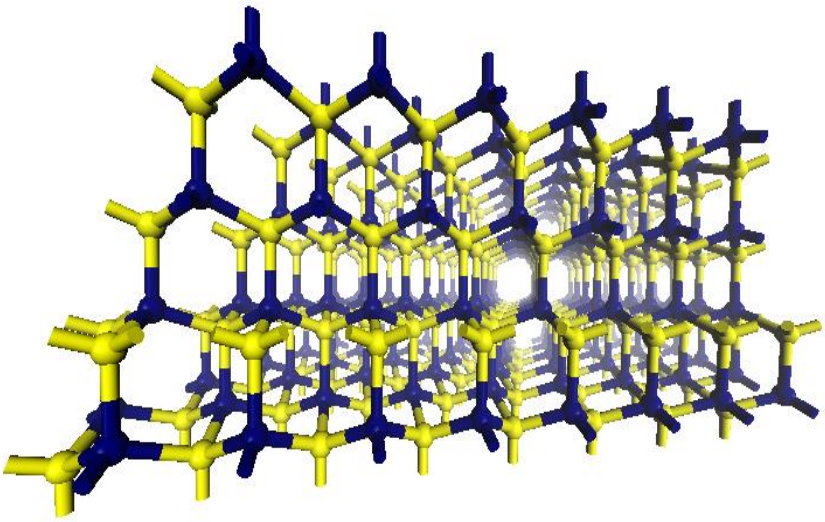

Figure 1.2 Zincblende crystal structure of gallium phosphide. Figure originally published in Peczoncyzk, et al.[44]

tethered to the GaP surface in the presence of triethylamine base, exhibiting some activity under illumination.[43,45] However, thick layers of polymer block inherent light absorption of GaP complicating this method.

The approach of our lab is to understand and manipulate the chemistry *at the molecular level* of semiconductor surface atoms with organic groups through wet-chemical reactions without hindering the inherent photoelectrochemical properties of the substrate. To better understand the bonding of atop atoms, different planes of the zincblende structure of crystalline GaP were considered (Figure 1.2). The (111) crystal planes isolate one atom type and have ideally one site available for bonding. Chlorination/Grignard reaction sequences have been developed to decorate GaP(111)A with organic groups such as $–CH_3$ and $–C_{18}H_{37}$ groups.[46] These surfaces were stable against oxidation on the order of months and showed stability during electrochemical testing.[46] When olefin molecules with reactive terminal groups were covalently bonded to GaP(111)A, secondary reactivity was demonstrated through three separate pathways.[47] The evidence for further reactivity through these reaction strategies opened ideas for covalent attachment of molecules of interest, such as dyes, catalysts, or sensors. Of particular interest is the possibility of dye attachment. P-type GaP has previously been shown to facilitate hole injection from a physisorbed dye to increase the total number of photons utilized from sunlight.[48,49] Presently, only physical adsorption through attractive van der Waals forces was used to attach a dye to the GaP surface. The weak interactions cause the resulting properties of adsorbed layers to be difficult to predict.[50] Covalent attachment could provide better stability and possibly better charge transfer through the interfacial layer. Additionally, covalently bound dye systems could be used to study other components of the system, such as redox mediator.

1.3 THESIS SUMMARY

In this thesis, the development of reaction strategies of atop P atoms of GaP(111)B surfaces were demonstrated, producing surfaces that were somewhat resistant against oxidation in aqueous solutions, facilitated covalent attachment of a dye, and resulted in favorable interfacial energetics for heterogeneous charge transfer through reduced number of surface states. The photoelectrochemical properties of p-type

GaP(111)A electrodes before and after a two-step chlorination/Grignard reaction sequence have been assessed for cathodic stability, valence band edge shift, and effect on dye sensitization. In pursuit of covalently attached dyes to GaP(111)A, surface reactions were first shown on a model substrate (Si(111)) and cationic iminium dyes were tested for dye sensitization. Chemically modified Si(111) surfaces have been prepared through a series of wet chemical surface treatments that simultaneously show resistance towards surface oxidation, selective reactivity towards chemical reagents, and areal defect densities comparable to unannealed thermal oxides.

In Chapter 2, functionalization of crystalline GaP (111)B interfaces has been performed through the formation of P-O-*R* surface bonds. The approach described herein parallels classical Williamson ether synthesis, where hydroxyl groups on etched GaP(111)B surfaces were reacted with halogenated reactants. Grazing angle total internal reflectance infrared spectra showed increased intensities for -CH_2- and -CH_3 asymmetric and symmetric stretches after reaction with long alkyl halides. Changes in the X-ray photoelectron (XP) spectra collected before and after reaction separately corroborated surface attachment to GaP(111)B. Static sessile drop water contact angle measurements for GaP(111)B separately showed increased hydrophobicity following surface modification with long alkyl chains. The surface functionalization reaction rate was increased by the addition of non-nucleophilic bases, consistent with surface deprotonation as the rate limiting step. Separately, photoelectrochemical measurements conducted before and after reaction with alkyl halides at long wavelengths ($\lambda > 545$ nm) showed surface attachment decreased sub-band gap photocurrents, implying lowered activity of surface traps. Conversely, photoelectrochemical measurements performed after functionalization of p-GaP(111)B with Coomassie Blue sulfonyl chloride showed evidence of persistent sensitized hole injection from the dye into p-GaP.

In Chapter 3, the photoelectrochemical properties of p-type GaP(111)A electrodes before and after a two-step chlorination/Grignard reaction sequence have been assessed. Electrochemical impedance spectroscopy indicated both a change in the flat-band potential in water and decreased sensitivity of the band edge energetics towards pH for GaP(111)A surfaces following modification. Separate stability tests were performed to gauge the susceptibilities of unmodified and CH_3-terminated p-GaP(111)A

photoelectrodes towards reductive degradation under illumination. The steady-state photoelectrochemical results showed modification of GaP(111)A with -CH_3 groups significantly enhanced p-GaP stability. Separately, sub-bandgap photocurrent measurements were collected to assess relative changes in surface states acting as recombination centers. In the absence of any dye, the sub-bandgap photocurrent from trapping/de-trapping of charge carriers in surface states was higher for unmodified p-GaP photoelectrodes than for CH_3-terminated p-GaP(111)A. Further, sensitized photocurrents of p-GaP photoelectrodes with Brilliant Green were systematically higher after modification with -CH_3 groups, indicating a deactivation of a surface recombination pathway after surface modification. Collectively, this work illustrates a rational chemical strategy to modify and augment the pertinent interfacial properties of p-GaP photocathodes in an aqueous photoelectrochemical system.

In Chapter 4, chemically modified Si(111) surfaces have been prepared through a series of wet chemical surface treatments that simultaneously show resistance towards surface oxidation, selective reactivity towards chemical reagents, and areal defect densities comparable to unannealed thermal oxides. Specifically, grazing angle attenuated total reflectance infrared and XP spectroscopy were used to characterize allyl-, 3,4-methylenedioxybenzene-, or 4-[bis(trimethylsilyl)amino]phenyl-terminated surfaces and the subsequently hydroxylated surfaces. Hydroxylated surfaces were confirmed through reaction with 4-(trifluoromethyl)benzyl bromide and quantified by XP spectroscopy. Contact angle measurements indicated all surfaces remained hydrophilic, even after secondary backfilling with CH_3- groups. Surface recombination velocity measurements by way of microwave photoconductivity transients showed the relative defect-character of as-prepared and aged surfaces. The relative merits for each investigated surface type are discussed.

In Appendix A, additional work is presented that illustrates how these surface chemistries could be applied to GaP nanowires. Appendix B illustrates the influence of surface groups on sensitization trough band edge energy changes. Appendix C summarizes attempts to produce super hydrophobic Si(111) through termination with –CF_3 groups.

1.4 REFERENCES

(1) http://web.anl.gov/pse/solar/primer/primer1.html. Primer on Solar Energy. Date Accessed.

(2) In *Climate Change 2007: Synthesis Report. A Contribution of Working Groups I, II, and III to the Fourth Assessment Report of the Intergovernmental Panel on Climate Change (IPCC)* Geneva, Switzerland: IPCC, 2007; Vol. 6.1 Observed changes in climate and their effects, and their causes.

(3) Current Greenhouse Gas Concentrations. Date Accessed.

(4) http://energy.gov/eere/sunshot/about-sunshot-initiative. About SunShot Initiative. Date Accessed.

(5) Doyle, A.; Lewis, B. In *Reuters*; Thomson Reuters: 2015.

(6) Lewis, N. S. Powering the planet. *MRS Bull.* **2007**, *32*, 808-820.

(7) Dimroth, F.; Guter, W.; Schoene, J.; Welser, E.; Steiner, M.; Oliva, E.; Wekkeli, A.; Siefer, G.; Philipps, S. P.; Bett, A. W.; Ieee In *2009 34th Ieee Photovoltaic Specialists Conference, Vols 1-3* 2009, p 1933-1937.

(8) Green, M. A. The Path to 25% Silicon Solar Cell Efficiency: History of Silicon Cell Evolution. *Progress in Photovoltaics* **2009**, *17*, 183-189.

(9) Scrosati, B.; Garche, J. Lithium Batteries: Status, Prospects and Future. *Journal of Power Sources* **2010**, *195*, 2419-2430.

(10) Goodenough, J. B.; Park, K.-S. The Li-Ion Rechargeable Battery: A Perspective. *J. Am. Chem. Soc.* **2013**, *135*, 1167-1176.

(11) Lewis, N. S.; Nocera, D. G. Powering the Planet: Chemical Challenges in Solar Energy Utilization. *Proceedings of the National Academy of Sciences of the United States of America* **2006**, *103*, 15729-15735.

(12) Oregan, B.; Gratzel, M. A low-cost, high-efficiency solar-cell based on dye-sensitized colloidal TiO2 films. *Nature* **1991**, *353*, 737-740.

(13) Price, M. J.; Maldonado, S. Macroporous n-GaP in Nonaqueous Regenerative Photoelectrochemical Cells. *J. Phys. Chem. C* **2009**, *113*, 11988-11994.

(14) Aurianblajeni, B.; Halmann, M.; Manassen, J. Electrochemical Measurements on the Photoelectrochemical Reduction of Aqueous Carbon Dioxide on p-Gallium Phosphide and p-Gallium Arsenide Semiconductor Electrodes. *Solar Energy Materials* **1983**, *8*, 425-440.

(15) Barton, E. E.; Rampulla, D. M.; Bocarsly, A. B. Selective Solar-Driven Reduction of CO2 to Methanol Using a Catalyzed p-GaP Based Photoelectrochemical Cell. *J. Am. Chem. Soc.* **2008**, *130*, 6342-6344.

(16) Halmann, M. Photoelectrochemical Reduction of Aqueous Carbon Dioxide on p-type Gallium Phosphide in Liquid Junction Solar Cells. *Nature* **1978**, *275*, 115-116.

(17) Tomkiewicz, M.; Woodall, J. M. Photoassisted Electrolysis of Water by Visible Irradiation of a p-Type Gallium Phosphide Electrode. *Science* **1977**, *196*, 990-991.

(18) Sun, J. W.; Liu, C.; Yang, P. D. Surfactant-Free, Large-Scale, Solution-Liquid-Solid Growth of Gallium Phosphide Nanowires and Their Use for Visible-Light-

Driven Hydrogen Production from Water Reduction. *J. Am. Chem. Soc.* **2011**, *133*, 19306-19309.

(19) Hara, K.; Arakawa, H. In *Handbook of Photovoltaic Science and Engineering*; John Wiley & Sons, Ltd: 2005, p 663-700.

(20) Koops, S. E.; O'Regan, B. C.; Barnes, P. R. F.; Durrant, J. R. Parameters Influencing the Efficiency of Electron Injection in Dye-Sensitized Solar Cells. *J. Am. Chem. Soc.* **2009**, *131*, 4808-4818.

(21) He, J. J.; Lindstrom, H.; Hagfeldt, A.; Lindquist, S. E. Dye-sensitized nanostructured p-type nickel oxide film as a photocathode for a solar cell. *J. Phys. Chem. B* **1999**, *103*, 8940-8943.

(22) Daeneke, T.; Yu, Z.; Lee, G. P.; Fu, D.; Duffy, N. W.; Makuta, S.; Tachibana, Y.; Spiccia, L.; Mishra, A.; Baeuerle, P.; Bach, U. Dominating Energy Losses in NiO p-Type Dye-Sensitized Solar Cells. *Advanced Energy Materials* **2015**, *5*.

(23) Powar, S.; Daeneke, T.; Ma, M. T.; Fu, D.; Duffy, N. W.; Goetz, G.; Weidelener, M.; Mishra, A.; Baeuerle, P.; Spiccia, L.; Bach, U. Highly Efficient p-Type Dye-Sensitized Solar Cells based on Tris(1,2-diaminoethane)Cobalt(II)/(III) Electrolytes. *Angewandte Chemie-International Edition* **2013**, *52*, 602-605.

(24) Perera, I. R.; Daeneke, T.; Makuta, S.; Yu, Z.; Tachibana, Y.; Mishra, A.; Baeuerle, P.; Ohlin, C. A.; Bach, U.; Spiccia, L. Application of the Tris(acetylacetonato)iron(III)/(II) Redox Couple in p-Type Dye-Sensitized Solar Cells. *Angewandte Chemie-International Edition* **2015**, *54*, 3758-3762.

(25) Mathew, S.; Yella, A.; Gao, P.; Humphry-Baker, R.; Curchod, B. F. E.; Ashari-Astani, N.; Tavernelli, I.; Rothlisberger, U.; Nazeeruddin, M. K.; Graetzel, M. Dye-sensitized solar cells with 13% efficiency achieved through the molecular engineering of porphyrin sensitizers. *Nature Chemistry* **2014**, *6*, 242-247.

(26) Wen, W.; Carim, A. I.; Collins, S. M.; Price, M. J.; Peczonczyk, S. L.; Maldonado, S. Structural and Photoelectrochemical Properties of GaP Nanowires Annealed in NH3. *J. Phys. Chem. C* **2011**, *115*, 22652-22661.

(27) Wang, Z.; Brown, E. S.; Maldonado, S. Hybrid solar cells constructed of macroporous n-type GaP coated with PEDOT:PSS. *Chinese Chemical Letters* **2015**, *26*, 469-473.

(28) Stringfellow, G. B. Effect of Surface Treatment on Surface Recombination Velocity and Diode Leakage in GaP. *J. Vac. Sci. Technol.* **1976**, *13*, 908-913.

(29) Gershenzon, M.; Mikulyak, R. M. Radiative Pair Recombination and Surface Recombination in GaP Photoluminescence. *Appl. Phys. Lett.* **1966**, *8*, 245-247.

(30) Bansal, A.; Li, X. L.; Lauermann, I.; Lewis, N. S.; Yi, S. I.; Weinberg, W. H. Alkylation of Si Surfaces Using a Two-Step Halogenation Grignard Route. *J. Am. Chem. Soc.* **1996**, *118*, 7225-7226.

(31) Ciampi, S.; Eggers, P. K.; Le Saux, G.; James, M.; Harper, J. B.; Gooding, J. J. Silicon (100) Electrodes Resistant to Oxidation in Aqueous Solutions: An Unexpected Benefit of Surface Acetylene Moieties. *Langmuir* **2009**, *25*, 2530-2539.

(32) Hamann, T. W.; Lewis, N. S. Control of the stability, electron-transfer kinetics, and pH-dependent energetics of Si/H2O interfaces through methyl termination of Si(111) surfaces. *J. Phys. Chem. B* **2006**, *110*, 22291-22294.

(33) Loscutoff, P. W.; Bent, S. F. In *Annual Review of Physical Chemistry* 2006; Vol. 57, p 467-495.
(34) Hammond, C.; Back, A.; Lawrence, M.; Nebesny, K.; Lee, P.; Schlaf, R.; Armstrong, N. R. Growth of layered semiconductors by molecular-beam epitaxy. Formation and characterization of GaSe, MoSe2, and phthalocyanine ultrathin films on sulfur-passivated GaP(111). *J. Vac. Sci. Technol., A* **1995**, *13*, 1768-1775.
(35) Yuan, Z. L.; Ding, X. M.; Lai, B.; Hou, X. Y.; Lu, E. D.; Xu, P. S.; Zhang, X. Y. Neutralized (NH4)(2)S Solution Passivation of III-V Phosphide Surfaces. *Appl. Phys. Lett.* **1998**, *73*, 2977-2979.
(36) Flores-Perez, R.; Zernlyanov, D. Y.; Ivanisevic, A. Quantitative Evaluation of Covalently Bound Molecules on GaP (100) Surfaces. *J. Phys. Chem. C* **2008**, *112*, 2147-2155.
(37) Richards, D.; Zemlyanov, D.; Ivanisevic, A. Assessment of the Passivation Capabilities of Two Different Covalent Chemical Modifications on GaP(100). *Langmuir* **2010**, *26*, 8141-8146.
(38) Suzuki, Y.; Sanada, N.; Shimomura, A.; Fukuda, Y. High-Resolution XPS Analysis of GaP(001), (111)A, and (111)B Surfaces Passivated by (NH4)(2)S-x Solution. *Appl. Surf. Sci.* **2004**, *235*, 260-266.
(39) Mukherjee, J.; Erickson, B.; Maldonado, S. Physicochemical and Electrochemical Properties of Etched GaP(111)A and GaP(111)B Surfaces. *J. Electrochem. Soc.* **2010**, *157*, H487-H495.
(40) Richards, D.; Luce, P.; Zemlyanov, D.; Ivanisevic, A. Quantitative Analysis of the Functionalization of Gallium Phosphide With Organic Azides. *Scanning* **2012**, *34*, 332-340.
(41) Kim, H.; Colavita, P. E.; Metz, K. M.; Nichols, B. M.; Sun, B.; Uhlrich, J.; Wang, X. Y.; Kuech, T. F.; Hamers, R. J. Photochemical functionalization of gallium nitride thin films with molecular and biomolecular layers. *Langmuir* **2006**, *22*, 8121-8126.
(42) Flores-Perez, R.; Zemlyanov, D. Y.; Ivanisevic, A. DNA molecules on GaP (100) surfaces: Spectroscopic characterization and biospecificity assessment. *ChemPhysChem* **2008**, *9*, 1528-1530.
(43) Krawicz, A.; Yang, J.; Anzenberg, E.; Yano, J.; Sharp, I. D.; Moore, G. F. Photofunctional Construct That Interfaces Molecular Cobalt-Based Catalysts for H-2 Production to a Visible-Light-Absorbing Semiconductor. *J. Am. Chem. Soc.* **2013**, *135*, 11861-11868.
(44) Peczonczyk, S. L.; Mukherjee, J.; Carim, A. I.; Maldonado, S. Wet Chemical Functionalization of III-V Semiconductor Surfaces: Alkylation of Gallium Arsenide and Gallium Nitride by a Grignard Reaction Sequence. *Langmuir* **2012**, *28*, 4672-4682.
(45) Krawicz, A.; Cedeno, D.; Moore, G. F. Energetics and efficiency analysis of a cobaloxime-modified semiconductor under simulated air mass 1.5 illumination. *Phys. Chem. Chem. Phys.* **2014**, *16*, 15818-15824.
(46) Mukherjee, J.; Peczonczyk, S.; Maldonado, S. Wet Chemical Functionalization of III-V Semiconductor Surfaces: Alkylation of Gallium Phosphide Using a Grignard Reaction Sequence. *Langmuir* **2010**, *26*, 10890-10896.

(47) Peczonczyk, S. L.; Brown, E. S.; Maldonado, S. Secondary Functionalization of Allyl-Terminated GaP(111)A Surfaces via Heck Cross-Coupling Metathesis, Hydrosilylation, and Electrophilic Addition of Bromine. *Langmuir* **2014**, *30*, 156-164.
(48) Chitambar, M.; Wang, Z. J.; Liu, Y. M.; Rockett, A.; Maldonado, S. Dye-Sensitized Photocathodes: Efficient Light-Stimulated Hole Injection into p-GaP Under Depletion Conditions. *J. Am. Chem. Soc.* **2012**, *134*, 10670-10681.
(49) Choi, D.; Rowley, J. G.; Parkinson, B. A. Dye Sensitization of n and p Type Gallium Phosphide Photoelectrodes. *J. Electrochem. Soc.* **2012**, *159*, H846-H852.
(50) Maldonado, S., Fitch, A.G., Lewis, N.S. In *Nanostructured and Photoelectrochemical Systems for Solar Photon Conversion*; Archer, M. D., Nozik, A.J., Ed.; Imperial College Press: Covent Garden, 2008

CHAPTER 2

Wet Chemical Functionalization of GaP(111)B Through a Williamson Ether-type Reaction

2.1 INTRODUCTION

Gallium phosphide (GaP) is a potential photoelectrode material for solar energy to chemical fuel conversion/storage, with the capacity both to absorb an appreciable fraction of the solar spectrum and to generate a large (> 1 V) photovoltage.[1-7] Employing high aspect ratio photoelectrode form factors has proven effective in overcoming the intrinsically poor light-absorbing properties of GaP,[8] as both macroporous[3] and nanowire[9,10] GaP photoelectrodes have been demonstrated. However, such architectures do not address the two issues with the native surface chemistry of GaP, i.e., poor innate electrocatalytic activity for water splitting reactions and chemical instability.[4,11] Native oxides on GaP surfaces without large densities of electrical traps for charge recombination cannot be formed.[12-14] One possible strategy to ameliorate GaP surface issues is through deliberate chemical passivation/functionalization. Surface chemical strategies involving Lewis acid attack on atop Ga atoms have been shown in the form of thiols adsorbed on GaP(100)[15-19] and GaP(110)[20] and the reaction between GaP(111)A[21-23] and alkyl Grignard reagents. To date, no chemical strategies have been identified for P-rich surface planes such as GaP(111)B, representing a critical knowledge gap in functionalization strategies for nanostructured GaP photoelectrodes.

A previous report indicated that aqueous etching of GaP(111)B surfaces resulted in persistent oxide coverage,[14] in line with studies on other phosphide surfaces that reported the difficulty in obtaining P-rich surfaces that were rigorously oxide-free.[24-26] Nevertheless, functionalization of minimally oxidized phosphide surfaces should still be

possible. For metal oxides, a surface reaction analogous to the classical Williamson ether synthesis has been shown, where an ether-like surface bond is formed.[27,28]

Accordingly, we report here the viability of the Williamson ether-type reactions at GaP(111)B surfaces. We specifically show the reaction of halogenated organic reactants with freshly etched GaP(111)B under mild heating to demonstrate persistent adsorption through P-O-*R* surface bonds. Spectroscopic and electrochemical data are presented that demonstrate the resultant physicochemical and electrochemical properties of GaP(111)B after functionalization. In particular, data are shown that indicate this surface functionalization method is amenable for the preparation of dye-sensitized p-GaP photocathodes in water.

2.2 EXPERIMENTAL

2.2.1 Materials and Chemicals

Methanol (anhydrous >99.8%, Aldrich), acetone (HPLC grade, Fisher), doubly distilled H_2SO_4 (Fisher, 95 - 98%), hexanes (ACS grade, Macron Chemicals), acetonitrile (anhydrous >99.8%, Sigma-Aldrich), dichloromethane (anhydrous>99.8%, Sigma-Aldrich), borane-tetrahydrofuran (1 M, Aldrich), boron trichloride (1 M in heptane, Aldrich), 1-bromooctadecane (>97%, Aldrich), ether (anhydrous, Aldrich), europium (III) chloride hexahydrate (99.9%, Strem Chemicals), potassium chloride (ACS grade, Mallinckrodt), Coomassie Blue G (Sigma), phosphorus (V) oxychloride (Sigma-Aldrich) were used as received. 1-bromotetradecane (98%, Acros), 1-bromodecane (98%, Aldrich), *p*-(trifluoromethyl)benzyl bromide (98%, Aldrich), and *o*-(trifluoromethyl)benzenesulfonyl chloride (97%, Sigma-Aldrich) were outgassed by three freeze-pump-thawed cycles before use. Potassium bis(trimethylsilyl)amide (KHMDS), triethylamine (TEA), 1,8-diazabicycloundec-7-ene (DBU), and potassium butoxide (KBuO) were purchased from Aldrich. Water with a resistivity of > 18.2MΩ cm^{-1} (Barnsted Nanopure system) was used throughout. N-type GaP(111)B wafers (ITME) doped with S at 4 x 10^{14} cm^{-3} with a thickness of 400±25 μm were used throughout except for photoelectrochemical measurements. For photocurrent measurements, p-type

GaP(111)B (MTI Corp.) wafers doped with Zn at 2.1 $x10^{17}$ cm^{-3} with a thickness of 450±25 μm were used.

2.2.2 Etching

Prior to use, samples were cut into square ~0.5 cm^2 sections and degreased by two minute sequential sonication steps in water, methanol, acetone, methanol, and water. Samples were etched in concentrated $H_2SO_{4(aq)}$ for 30 s, rinsed with water, and dried with a stream of $N_{2(g)}$. We have previously determined that this protocol yields surfaces with root-mean-square roughness values of 0.28 ± 0.06 nm.[14]

2.2.3 X-ray Photoelectron Spectroscopy

All X-ray photoelectron (XP) spectra were collected with a PHI 5400 analyzer using an Al Kα (1486.6 eV) source without a monochromator. Spectra were collected without charge neutralization at a base pressure of < $2.5x10^{-9}$ Torr. A 6 mA current emission and a 12 kV anode high tension were used. Survey scans were recorded between 0 and 1350 eV at pass energy of 117.40 eV. High resolution spectra were collected at a pass energy of 23.5 eV. The binding energies of all spectra were corrected using the expected binding energy for adventitious carbon (284.6 eV).[29,30]

Spectra were fit and analyzed using CASAXPS 2.6.13 software. A Shirley background correction was used and all peaks were fit using a 80:20 Gaussian-Lorentzian line shape. The C 1s signatures were peak fitted using a singlet with FWHM constrained between 0.8 and 1.2. The P 2p signals were fit with two doublets with area ratio of 0.5 and a peak separation of 0.85 eV FWHM constrained between 0.8 and 2, with the first peak of each of the doublets centered at 128.5 and 129 eV, respectively; Ga 3d spectra were fit with a doublet with an area ratio of 0.66 and peak separation of 0.44 eV with FWHM constrained between 0.8 and 1.2; F 1s signals were fit two peaks with FWHM constrained between 1 and 3, one peak at 688 eV and an additional peak at 686.5 eV when present.[21] Oxide thickness and fractional monolayer coverage of the surface were calculated using either a single[31] or three-layer substrate overlayer model,[32] respectively.

For surface oxides, the thickness of oxide at the surface was calculated using the simplified substrate overlayer model:[31]

$$d = \lambda_{ov} \sin \varphi \left(ln \left(1 + \frac{I_{overlayer}}{I_{substrate}} \frac{I^0{}_{substrate}}{I^0{}_{overlayer}} \right) \right)$$

Equation 2.1 Simplified Overlayer Model Equation for Oxide Thickness.

where d is the thickness of the oxide overlayer in nanometer, λ_{ov} is escape depth of emitted electrons through the oxide layer, φ is the takeoff angle (54.6°) between the sample surface and the detector, I is the integrated area as follows: $I_{substrate}$ for bulk signal, $I_{overlayer}$ of oxide signals, $I^0_{substrate}$ for GaP freshly etched in NH_4F for 30s, $I^0_{overlayer}$ for a thick (>500 nm) thermal oxide layer on GaP. The escape depth for electrons was estimated with Equation 2.2,

$$\lambda = 0.41\, A^{3/2}\, E^{1/2}$$

Equation 2.2 Equation for Electron Escape Depth.

where A is the mean diameter of one unit in the overlayer (nm) and E is the kinetic energy of the ejected core electron (eV).

The mean diameter of one unit (A) can be calculated:

$$A = \sqrt[3]{\frac{MW}{\rho N_A}}$$

Equation 2.3 Equation for Mean Diameter.

where MW is mean atomic weight (g mol^{-1}), ρ is the density (g cm^{-3}), and N_A is Avogadro's number.

The surface coverage of molecules such as BF_3 and BCl_3, with a tag element, such as F or Cl, was calculated using the full substrate overlayer model[31]:

$$\frac{I_{ov}}{I_{sub}} = \left(\frac{SF_{ov}}{SF_{sub}}\right)\left(\frac{\rho_{ov}}{\rho_{sub}}\right)\left(\frac{1 - e^{(-d_{ov}/\lambda_{ov}sin\varphi)}}{e^{(-d_{ov}/\lambda_{sub}sin\varphi)}}\right)$$

Equation 2.4 Equation for Full Substrate Overlayer Model.

where SF_{sub} is the sensitivity factor for the element of interest in the substrate, SF_{ov} is the instrument sensitivity factor for the element of interest in the substrate (mol cm^{-3}), ρ_{ov} is the density of the element of interest in the overlayer (mol cm^{-3}). For GaP, ρ_{sub} is calculated from $GaPO_4$ (3.56g cm^{-3}).[33]

Monolayer coverage was calculated by dividing the overlayer thickness, or molecule length, by the escape depth of the molecule:

$$ML = \frac{d_{ov}}{t}$$

Equation 2.5 Equation for Monolayer Coverage.

Parameters for the various reactants are listed in Table 2.1. For larger molecules, such as *p*-(trifluoromethyl)benzyl bromide and Coomassie Blue sulfonyl chloride, a simple model of three-layer structure was used.[4] The topmost layer included the $–CF_3$ (t_1), the GaP substrate served as the bottom layer (*sub*), and the organic atoms in between served as t_2 (Figure 2.1).

To calculate overlayer coverage using the three layer model, the equation in Equation 2.6 was adopted from Asami, *et al*.[4]

$$\frac{I_{ov}}{I_{sub}} = \left(\frac{SF_{ov}}{SF_{sub}}\right)\left(\frac{\rho_{ov}}{\rho_{sub}}\right)\left(\frac{1 - e^{\frac{-t_1}{\lambda_{ov}cos\varphi}}}{e^{\frac{-(t_1+t_2)}{\lambda_{sub}cos\varphi}}}\right)$$

Equation 2.6 Monolayer Coverage Calculation Derived From Three-Layer Model.

Table 2.1 Monolayer Coverage Calculation Parameters for Various Reactants.

Reactant (Element Measured)	Density ($kg\ m^{-3}$)	A (nm)	P ($mol\ cm^{-3}$)	KE	λ_x	λ_P	SF	Length (nm) [a]
BCl_3 (Cl $2p^{3/2}$)	1326	0.527	0.01132	1287.1	5.627	5.779	0.891	0.35
$(C_2H_5)_2O{\bullet}BF_3$ (F 1s)	1150	0.59	0.02410	799.25	5.252	6.846	1	0.31

[a] Molecule lengths were estimated from tabulated bond length data.[34]

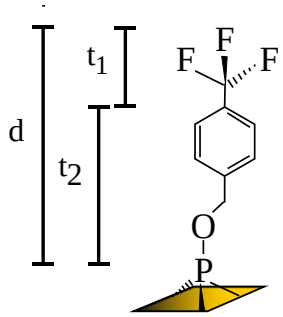

Figure 2.1 Illustration of Partial Layers t_1 and t_2 on GaP(111)B Reacted with *p*-(trifluoromethyl)benzyl bromide.

where parameters are the same as previously mentioned except those referring to *ov* are referencing the topmost layer containing F atoms in this situation. The value of I_{ov} was divided by 3 to account for 3 F atoms per molecule. The variable t_1 is the thickness of the second layer and t_2 is the thickness of the intermediate layer. The sum of the thicknesses is *d*, the total thickness of the organic overlayer. The following relationship also holds true:

$$t_1 = nt_2$$

Equation 2.7 Equation for Relationship Between Thickness of the Three Layers of the Overlayer.

where *n* is the ratio of thicknesses of the two layers. The relationship was entered into the equation in place of t_2 and subsequently t_1 was solved for. Total thickness of the organic layer was calculated using Equation 2.8

$$d = t_1 + t_2$$

Equation 2.8 Relationship Between Thickness of Three Layers and Total Overlayer Thickness.

Monolayer coverage was calculated:

$$ML = \frac{d}{a_m}$$

Equation 2.9 Monolayer Coverage Calculation.

where a_m is the atomic volume in nm. To obtain a_m, the density of the molecule was converted to atoms nm^{-3}, the value was divided by 3 to account for the 3 F atoms per molecule, and the cube root was taken. Parameters for each molecule of interest are listed in Table 2.2.

Table 2.2 Monolayer Coverage Calculation Parameters for Various Reactants.

Reactant (Element Measured)	Density (kg m^{-3})	N	ρ (mol cm^{-3})	a_m (nm^{-1})	λ_x	λ_p	SF	Length (nm) [b]
p-$CF_3C_6H_4CH_2Br$ (F 1s) [a]	1288	0.279	0.00731	1.136	5.522	7.197	1	0.87
o-$CF_3C_6H_4CH_2SO_2Cl$ (F 1s)	1585	0.396	0.00648	1.092	5.865	7.644	1	0.67
CB-I (S 2p)	5200	0.2/4.78[c]	0.00620	1.091	24.39	24.75	0.67	2.8

[a] Parameters for *p*-(trifluoromethyl)benzyl alcohol were used. [b] Molecule lengths were estimated from tabulated bond length data.[34] [c] Two *n* values reflect positions of both S atoms. In calculations, the *t* term became t_1*(0.5*(1 +1/0.2)+0.5*(1+1/4.78)).

For clarity, monolayer coverages are expressed as a function of expected loading if the adsorbates are oriented normal to the surface and are close-packed.

2.2.5 Infrared Spectroscopy

Infrared spectra were collected using a Thermo-Fisher 6700 FT-IR spectrometer equipped with a deuterated triglycerine sulfate (DTGS) detector and a Ge hemisphere grazing angle attenuated total reflectance (GATR) accessory. The incident light was p-polarized and fixed at an incident angle of 65°. GaP(111)B wafers were approximately 1.5 cm x 1.5 cm. Spectra were recorded with 4 cm^{-1} resolution and referenced to a background spectrum of the cleaned Ge hemisphere.

2.2.5 Static Sessile Drop Contact Angle Measurements

The contact angles formed between a droplet of distilled water (2.2 μL) and a GaP interface were recorded with a CAM 100 optical contact angle meter (KSV instrument, Helsinki, Finland) and analyzed using the KSV software analysis package.

2.2.6 Electrode Fabrication and Photoelectrochemical Cell Design

Ohmic contact to the backside of GaP wafers (0.5 cm^2) was prepared by etching with concentrated H_2SO_4 (aq), rinsing with distilled H_2O, soldering a thin, even film of In:Zn onto the surface, and annealing for 10 minutes at 400°C in forming gas. Electrodes were prepared by using silver print (GC Electronics) to attach the GaP section to a copper wire coil threaded through a glass tube and sealed with inert epoxy (Hysol C). Exposed epoxy was wrapped in Teflon tape to prevent absorption of reactants or solvent. Electrodes were degreased, etched, and reacted as mentioned previously. Photoelectrochemical measurements were acquired in an airtight glass cell with an optically flat bottom. A Pt counter electrode and Ag/AgCl reference electrodes were used. For all photoelectrochemical measurements, the distance between the optical window and the GaP photoelectrode face was ~1 mm. An aqueous solution of europium (III) chloride (0.002 M) and potassium chloride (0.1 M) was used as the background electrolyte for sub-bandgap photocurrent while concentrations of 0.002 M $EuCl_3$ and 1 M KCl were used as the background electrolyte for sensitization studies.

2.2.7 Photoelectrochemical Measurements

All measurements were performed at room temperature (23±3°C). Transmittance measurements were obtained with a Varian Cary 5000 ultraviolet-visible-near infrared (UV-Vis-NIR) photospectrometer. All photoelectrochemical measurements were performed in a three-electrode cell under potentiostatic control (Princeton Applied Research 267A) and with stirring. The net photocurrent collected per incident light intensity is reported here as an external quantum yield on a scale from 0 to 1. Wavelength-dependent external quantum yield measurements were taken with a setup described previously.[3] Illumination intensities ranged from ~0.1 to 1.0 mW cm^{-2}. Sub-bandgap light for surface state measurement was achieved using a long pass filter (Pyrex, Corning Glass Works) with absorption up to 553 nm.

2.3 RESULTS

2.3.1 Characterization of Etched GaP(111)B

High resolution P 2p XP spectra were collected for GaP(111)B and GaP(111)A immediately after etching with concentrated doubly distilled H_2SO_4 (Figure 2.2). Consistently, the spectra for GaP(111)B exhibited additional signal at 133.5 eV and 129.5 eV. The former signal suggested phosphate-type oxides.[14,25,35] The latter signal could be seen more definitively in the difference spectrum and was assigned to with P-OH surface moieties remaining on the surface after wet etching.[24,25] Still, in the context of the present study, we further wished to establish whether the predominant surface reactivity was more oxide-like rather than phosphine-like (i.e., bonding through bare atop P atoms). Freshly etched GaP(111)B surfaces were exposed to boranes (BH_3•THF, BCl_3, and BF_3•$O(C_2H_5)_2$) in a dry glovebox in analogy to formation of phosphinoborane adducts. All tested reaction parameters (Table 2.3) showed no evidence (XP or GATR-FTIR) of persistently adsorbed B-containing species, further indicating the surface reactivity of etched GaP(111)B did not follow the reactivity of phosphines.

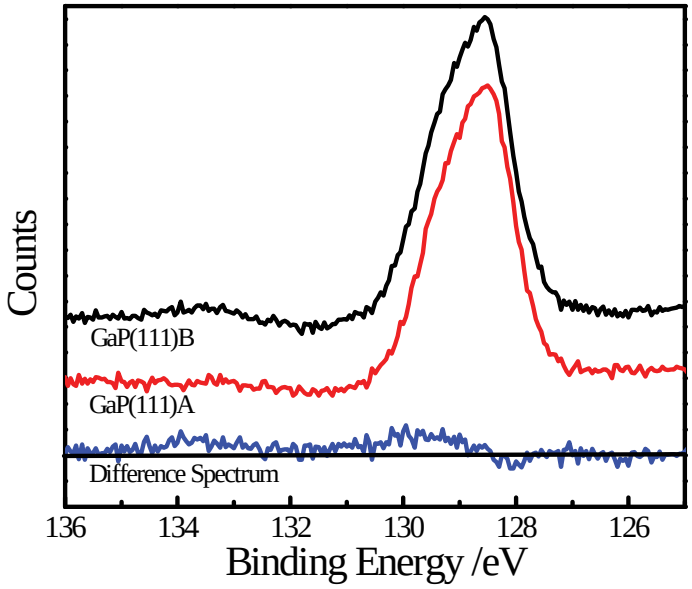

Figure 2.2 Difference spectra between high resolution P 2p XP spectra of (red) GaP(111)A etched with concentrated H_2SO_4 and (black) GaP(111)B etched with concentrated H_2SO_4. The difference between the two spectra is shown in blue.

Table 2.3 Reaction Parameters of GaP(111)B Surfaces.

Reagent [a]	Reagent Conc. (M)	Reaction Time (min)	Temp (°C)	Solvent
BH_3•THF	1.0	180	0	THF
BCl_3	1.0	60	22	Heptane
$(C_2H_5)_2O$•BF_3	0.4	30	40	10:1 hexane/ CH_2Cl_2

[a] Samples were etched in concentrated H_2SO_4(aq) prior to reaction. Samples were rinsed with THF and methanol and dried with a stream of N_2(g).

Specifically, after GaP(111)B was reacted with BH_3•THF for 3 h at 0° C, the B 1s (189 eV) XP spectra was convoluted by P 2s signal from the GaP substrate (186.1 eV) and signal corresponding to P-oxide (190.6 eV). Even when fitting was employed, no consistent B 1s signal was detected (Figure 2.3a). GATR-FTIR showed no evidence of B-H stretching at 2400 cm^{-1} (Figure 2.3b).

For the reaction of GaP(111)B with BCl_3, the Cl 2p spectrum could also be analyzed, as shown in Table 2.4, but monolayer coverage was low (~0.18).

2.3.2 Reaction of Etched GaP(111)B with Alkyl and Benzyl Halides

Williamson ether synthesis reactions were attempted with freshly etched GaP(111)B to graft organic groups through P-O-C bonds. The tested reaction conditions are listed in Table 2.5 and included *n*-alkyl bromides ($C_nH_{2n-1}Br$ where n = 10,14,18), *p*-(trifluoromethyl)benzyl bromide (*p*-$CF_3C_6H_4CH_2Br$), and *o*-(trifluoromethyl)benzenesulfonyl chloride (*o*-$CF_3C_6H_4CH_2SO_2Cl$). After reaction, sessile drop water contact angle measurements showed a consistent increase in hydrophobicity (Table 2.6). Figure 2.4 shows representative GATR-FTIR spectra before and after reaction of freshly etched GaP(111)B with $C_{18}H_{37}Br$ for 1 h at 60°C. The etched surface yielded spectra that were nominally devoid of any signatures between 2700 cm^{-1} and 3100 cm^{-1} (Figure 2.4a).

Conversely, intense symmetric -CH_2- and –CH_3 stretches were observed at 2854 and 2871 cm^{-1} and asymmetric -CH_2- and –CH_3 stretches were observed at 2923 and 2954 cm^{-1}, respectively (Figure 2.4a). The relative intensities of these modes was consistent with a flat orientation of the alkyl chains along the surface.[36] The asymmetric –CH_2- peak shifted to 2927 cm^{-1} for $C_{10}H_{21}Br$ (Figure 2.5). For reference, a methylene peak at 2920 cm^{-1} has been noted for ordered, crystalline alkyl chain packing whereas a methylene signal shifted to 2928 cm^{-1} is observed for liquid alkanes.[37-39] A separate signal at 965 cm^{-1} was observed only for the reacted surfaces (alkyl or benzyl halides, Figure 2.4b or Figure 2.6b, respectively) and was consistent with a P-O-C stretch.[40,41]

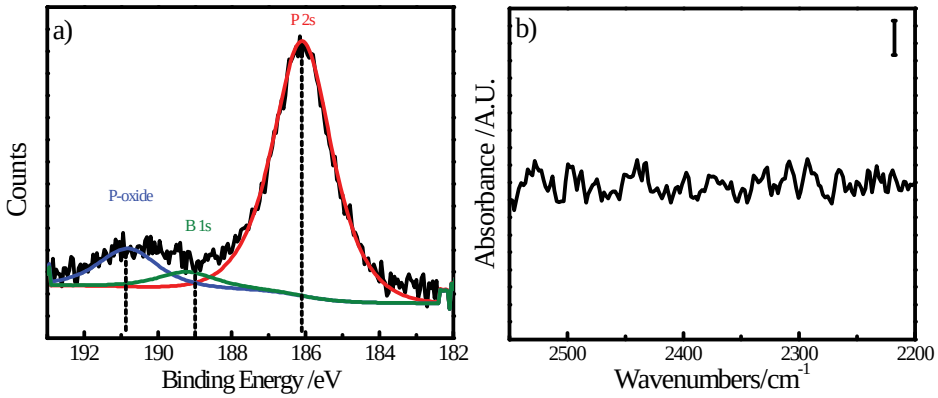

Figure 2.3 Representative spectra of reaction of GaP(111)B with BH_3•THF at 0°C for 3 h with (a) B 1s peak at 189 eV in XP spectra difficult to distinguish from the P 2s peak and corresponding P-oxide at 186.1 eV and 190.8 eV, respectively, and (b) no signal at 2400 cm^{-1} indicating B-H stretching in the GATR-FTIR spectrum. Vertical scale bar = 1.0 x 10^{-4} absorbance units.

Table 2.4 XPS Peak Positions and Intensities of Functionalized GaP(111)B.

Reagent [a]	P 2p BE [b]	*I* [c]	Ga 3d BE	X	BE	*I*	Oxide Thick-ness [d] (nm)	ML [d]
BCl_3	128.7	0.69 ± 0.15	19.25	Cl $2p^{3/2}$	198.5	0.041 ± 0.003	0.041	0.18
$(C_2H_5)_2O{\bullet}BF_3$	128.8	0.60 ± 0.01	19.4	F 1s	688.1	0.136 ± 0.009	0.054	0.20

[a] Samples were etched in H_2SO_4(aq) for 30s prior to reaction. [b] Peak positions were obtained at peak maximum and referenced to C 1s = 284.6 eV. Values are from repeated experiments and are listed as an average of binding energy (BE). Standard deviation for all BE was < 0.2 eV. [c] Intensities were referenced to Ga3d signal. [d] Oxide thickness and ML coverage were calculated using substrate-overlayer model as described in the Section 2.2.3. Standard deviations for oxide thickness were <0.03 nm and ML coverage were <0.03.

Table 2.5 Reaction Parameters of GaP(111)B Surfaces.

Reagent [a]		***Promoter***				
	Concentration /M		**Concentration /M**	**Reaction Time /min**	**Temperature / °C**	**Solvent**
$C_{18}H_{37}Br$	0.2	none	-	60	60	Hexanes
		TEA	0.02	60	60	Hexanes
		KBuO	0.02	60	60	Hexanes
		DBU	0.02	60	60	Hexanes
		KHMDS	0.02	60	60	Hexanes
$C_{14}H_{29}Br$	0.2	none	-	60	60	Hexanes
		KHMDS	0.02	60	60	Hexanes
$C_{10}H_{21}Br$	0.2	none	-	180	60	Hexanes
		TEA	0.02	180	60	Hexanes
		KBuO	0.02	180	60	Hexanes
		DBU	0.02	180	60	Hexanes
		KHMDS	0.02	180	60	Hexanes
p-$CF_3C_6H_4CH_2Br$	0.2	none	-	10, 15, 30, 45, 60, 75, 90, 105, 120	60	Hexanes
	0.2	TEA	0.02	60	60	Hexanes
	0.2	KBuO	0.02	60	60	Hexanes
	0.2	DBU	0.02	60	60	Hexanes
	0.2	KHMDS	0.02	5, 10, 15, 30, 45, 60	60	Hexanes
	0.2	none	0.02	60	60	CH_3CN
o-$CF_3C_6H_4CH_2SO_2Cl$	0.2	none	-	60	55	Hexanes
	0.2	none	-	60	55	CH_3OH
Coomassie Blue[b]	0.5	none	-	60	55	CH_3OH

[a] Samples were etched in concentrated H_2SO_4(aq) prior to reaction. After reaction, samples were rinsed with hexanes, sonicated in hexanes for 60 s, rinsed with diethyl ether, rinsed with methanol, and dried with a stream of N_2(g). [b]Reaction took place in the dark to avoid photoxidation of the dye. Samples were rinsed with methanol and allowed to dry in the glovebox. *TEA* = triethylamine; *KBuO* = potassium butoxide; *DBU* = 1,8-diazabicycloundec-7-ene; *KHMDS*= potassium bis(trimethylsilyl)amide.

Table 2.6 Contact Angle Data for Treated GaP(111)B.

Sample	Base Added	Reaction Time	n	Avg. Contact Angle /°	Std. Dev. /°
Etched	N/A	N/A	4	40.4	3
$C_{18}H_{37}Br$	None	1 h	3	76.3	4
$C_{18}H_{37}Br$	KBuO	1 h	6	78.7	3
$C_{18}H_{37}Br$	TEA	1 h	4	77.9	5
$C_{18}H_{37}Br$	DBU	1 h	5	68.5	6
$C_{18}H_{37}Br$	KHMDS	1 h	9	87.9	5
$C_{14}H_{29}Br$	None	1 h	2	63.6	10
$C_{14}H_{29}Br$	KHMDS	1 h	2	77.2	2
$C_{10}H_{21}Br$	None	24 h	7	66.3	11
$C_{10}H_{21}Br$	TEA	3 h	9	60.8	5
$C_{10}H_{21}Br$	KBuO	3 h	4	62.2	3
$C_{10}H_{21}Br$	DBU	3 h	6	72.8	1
$C_{10}H_{21}Br$	KHMDS	3 h	8	78.3	15
p-$CF_3C_6H_4CH_2Br$	None	1 h	4	54.2	9
p-$CF_3C_6H_4CH_2Br$	KHMDS	1 h	2	62.1	1

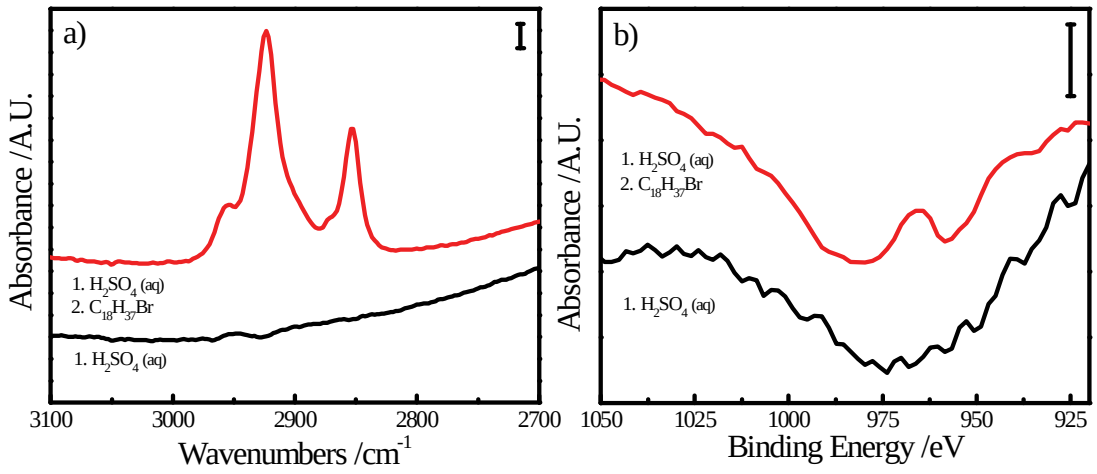

Figure 2.4 Representative GATR-FTIR spectra of the (a) $-CH_3/-CH_2$ stretching region and (b) P-O-C stretching region for etched GaP(111)B (black) and GaP(111)B reacted with $C_{18}H_{37}Br$ and KHMDS for 1 h at 60°C (red). Vertical scale bar = 5 x 10^{-4} absorbance units. Spectra are offset for clarity.

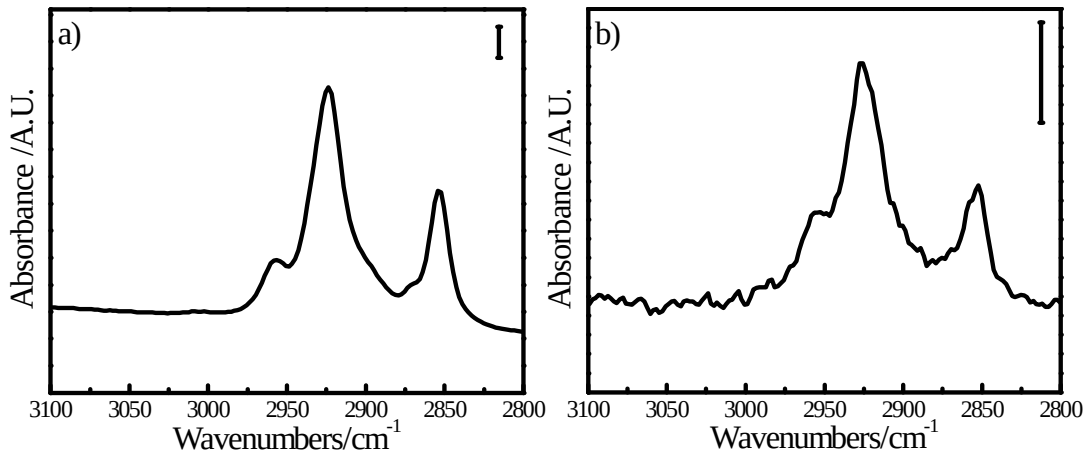

Figure 2.5 GATR-FTIR spectra showing the symmetric and asymmetric $–CH_2-$ and $–CH_3$ stretching modes of GaP(111)B after reaction with (a) $C_{14}H_{29}Br$ after 1 h and (b) $C_{10}H_{21}Br$ with KHMDS after 3 h. Vertical scale bar = 2.5 x 10^{-4} absorbance units. Spectra have been baseline corrected.

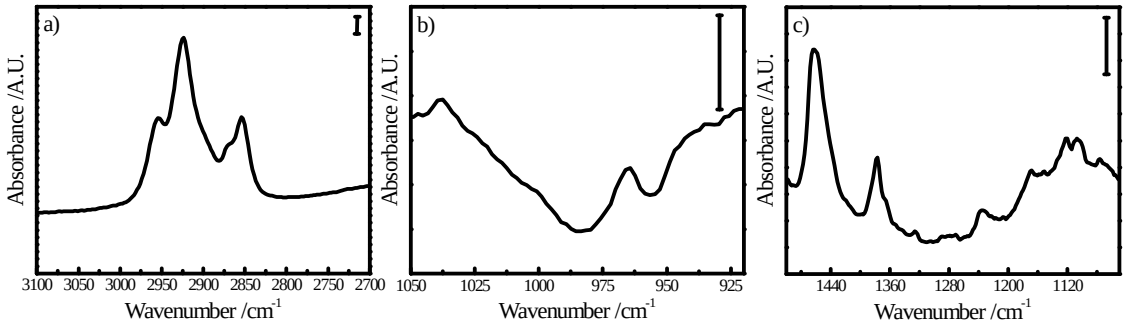

Figure 2.6 GATR-FTIR of GaP(111)B reacted with *p*-$CF_3C_6H_4CH_2Br$ showing (a) -CH_3/ -CH_2- stretches, (b) P-O-C stretches, and (c) several peaks for –CF_3 groups off of a benzene ring. Vertical scale bars = 1.0 x 10^{-3} absorbance units.

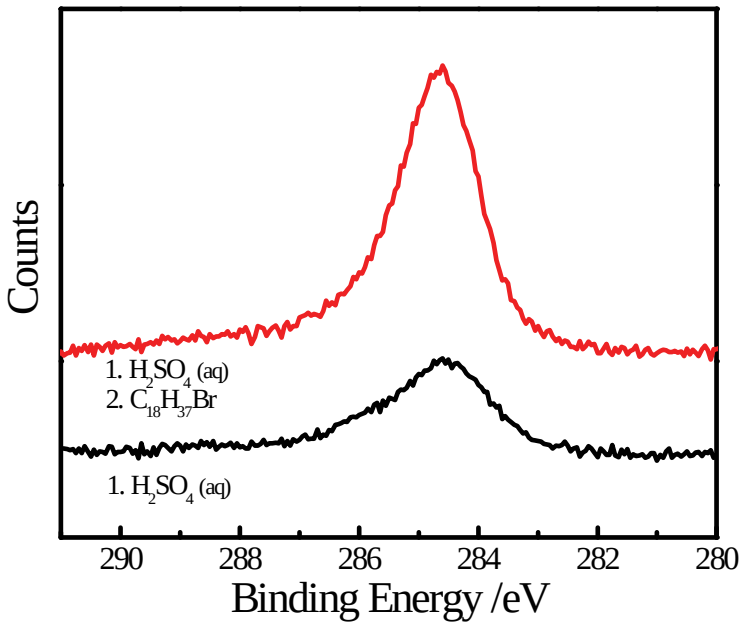

Figure 2.7 Increased signal intensity in the high resolution C 1s XP spectrum after reaction of GaP(111)B with $C_{18}H_{37}Br$ for 1 h.

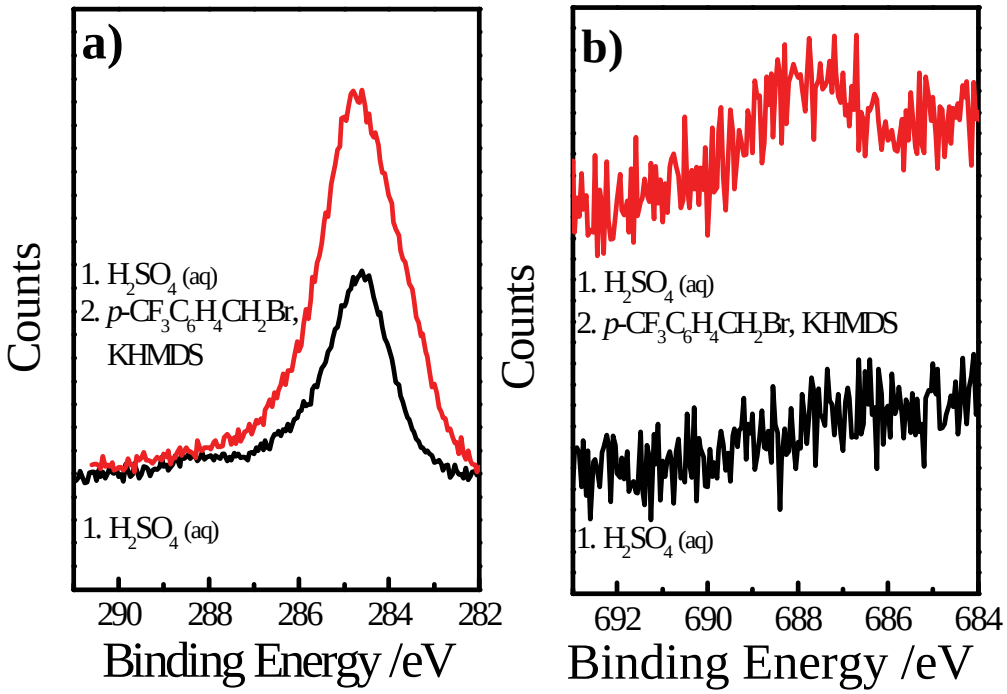

Figure 2.8 High-resolution XP spectra of (a) C 1s and (b) F 1s for GaP(111)B before and after reaction with *p*-$CF_3C_6H_4CH_2Br$ and KHMDS.

XP spectra were obtained for GaP(111)B surfaces after functionalization. After reaction of GaP(111)B with alkyl bromides, no Br 3d signatures were observed. Conversely, the total intensity of the C 1s signal increased systematically after reaction with $C_{18}H_{37}Br$ (Figure 2.7) and *p*-$CF_3C_6H_4CH_2Br$ (Figure 2.8a), however adventitious carbon[30] complicated direct analysis of the C 1s data. For GaP(111)B reacted with *p*-$CF_3C_6H_4CH_2Br$, the F 1s spectra was amenable to further analysis. Figure 2.8b displays the F 1s spectra of GaP(111)B before and after reaction with *p*-$CF_3C_6H_4CH_2Br$, where the peak at 688 eV was assigned to F-C bonding. The calculated monolayer coverages using a substrate-overlayer model[31] are summarized in Table 2.7. To further support a *p*-$CF_3C_6H_4CH_2$-terminated surface, GATR-FTIR spectra showed increased signal of $–CH_2$- and $-CH_3$ stretches and of modes ascribed to $–CF_3$ groups (Figure 2.6c).

The stability of the P-O-C linkage in aqueous solutions was assessed by prolonged immersion of GaP(111)B that had been reacted with *p*-$CF_3C_6H_4CH_2Br$. Under all conditions, the surfaces retained their increased hydrophobicity relative to unmodified GaP(111)B (Figure 2.9). The extent of oxide growth attack was monitored through P 2p XP spectra while removal of *p*-$CF_3C_6H_4CH_2$- groups from the surface was monitored through F 1s XP spectra (Figure 2.10). The highest coverage of *p*-$CF_3C_6H_4CH_2$- groups following prolonged immersion was observed in the *pH* range from 6 to 9, with the least oxidative degradation observed at *pH* = 8. For long chain alkyl groups, exposure to ambient conditions and aqueous environments for 30 h resulted in oxide thicknesses less than those measured for etched GaP(111)B (Figure 2.11).

2.3.3 Base Promoters

A set of non-nucleophilic, sterically hindered bases were used to determine whether surface derivitization of GaP(111)B is sensitive to the presence of a Bronsted-Lowry base. Figure 2.12 shows the monolayer coverage for GaP(111)B surfaces reacted with *p*-$CF_3C_6H_4CH_2Br$, calculated from high resolution F 1s XP spectra, with bases possessing varied Bronsted-Lowry base strength. At fixed reaction time (1 h) and temperature (60°C), inclusion of potassium bis(trimethylsilyl) amide (KHMDS, pK_A~25) yielded the highest monolayer coverage. The same sensitivity of monolayer coverage (as inferred from sessile drop contact angle) with base strength was also

Table 2.7 XPS Peak Positions and Intensities of Functionalized GaP(111)B.

Reagent [a]	*P 2p* Peak Position[b] /eV	Relative Intensity[c]	*F 1s* Peak Position /eV	Rel. Inten.	*Cl 2p* Peak Position /eV	Rel. Inten.	Oxide Thick-ness[d] /nm	Coverage[d] /ML
p-$CF_3C_6H_4CH_2Br$	128.7	0.68	687.7	0.24	*NA*	*NA*	0.034	0.22
p-$CF_3C_6H_4CH_2Br$ +KHMDS	128.6	0.49	687.9	0.08	*NA*	*NA*	0.053	0.94
p-$CF_3C_6H_4CH_2Br$ in acetonitrile	128.6	0.68	688.0	0.12	*NA*	*NA*	0.051	0.32
o-$CF_3C_6H_4CH_2SO_2Cl$	128.8	0.88	687.8	0.18	197.9	0.06	0.174	0.47
o-$CF_3C_6H_4CH_2SO_2Cl$ in CH_3OH	128.7	0.85	688.0	0.22	198.5	0.08	0.056	0.51
CB-I in CH_3OH[e]	128.5	0.53	*NA*	*NA*	198.1	0.10	0.043	0.69

[a] Samples were etched in H_2SO_4(aq) for 30s prior to reaction. Reactions were conducted at 60 ± 3°C for 60 min. [b] Peak positions were obtained at peak maximum and referenced to C 1s = 284.6 eV. Values are from repeated experiments and are listed as an average of binding energy (BE). Standard deviation for all BE was < 0.2 eV. [c] Intensities were referenced to Ga3d signal and averaged over all samples. Standard deviations were P 2p < 0.07, F 1s < 0.02, and Cl 2p < 0.04. Negligible Br 3d signal above background was observed after benzyl bromide reactions. [d] Oxide thickness and ML coverage were calculated using three-layer model as described in the experimental section. Standard deviations for oxide thickness were <0.02 nm and ML coverage were <0.05. [e] The S $2p^{3/2}$ peak at 168.0 eV (Avg. I = 0.049 ± 0.015) was used to calculate ML coverage.

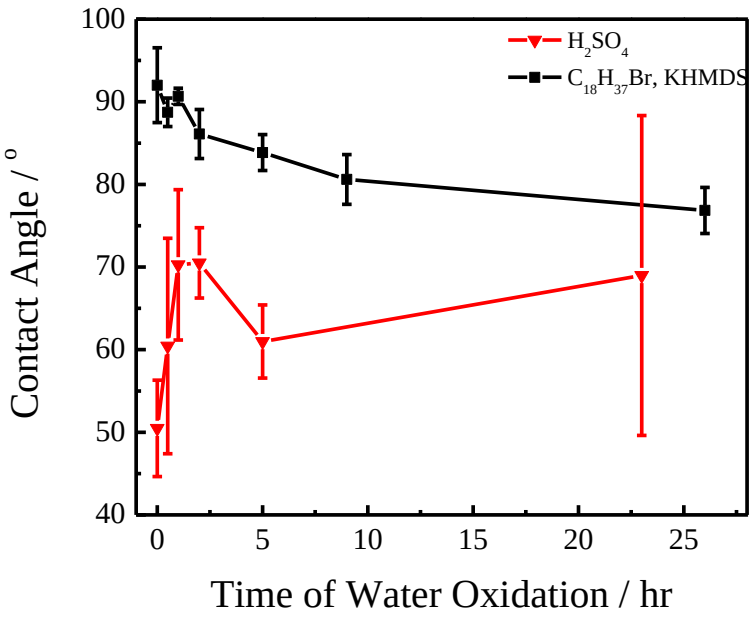

Figure 2.9 Water contact angle of etched (red triangles) and $C_{18}H_{37}$-terminated GaP(111)B (black squares) after time aging in water. Error bars indicate one standard deviation.

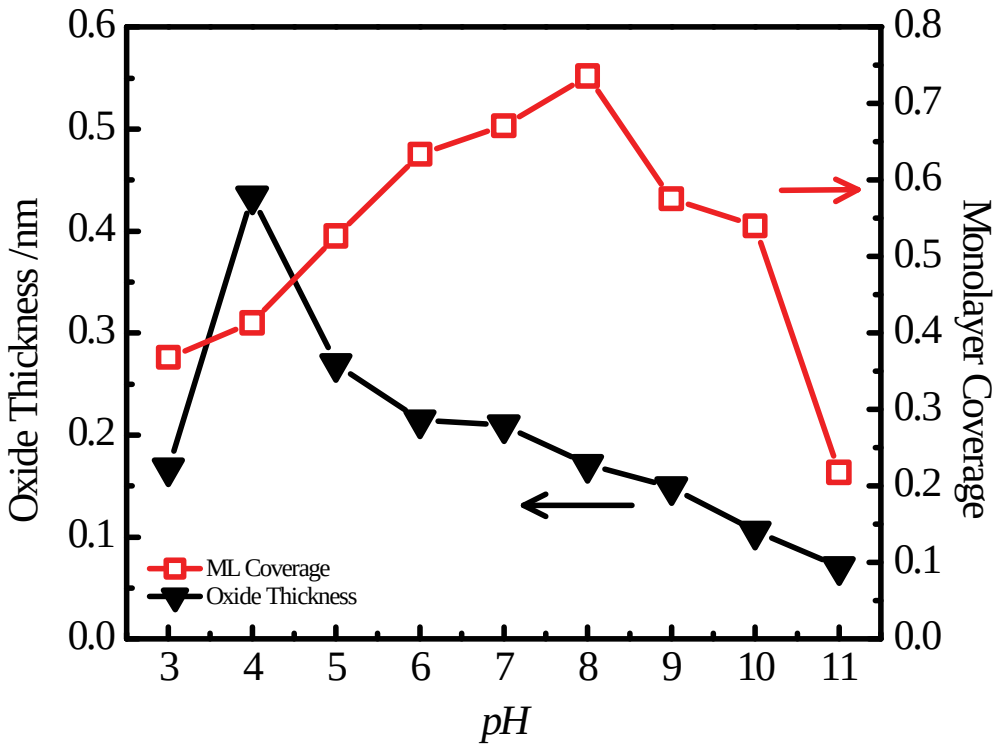

Figure 2.10 Measured oxide thickness (black triangles, left *y*-axis) and monolayer coverage (red squares, right *y*-axis) observed for GaP(111)B after reaction with *p*-$CF_3C_6H_4CH_2Br$ for 1 hour at T = 60°C followed by a 3 hour immersion in water with varying pH.

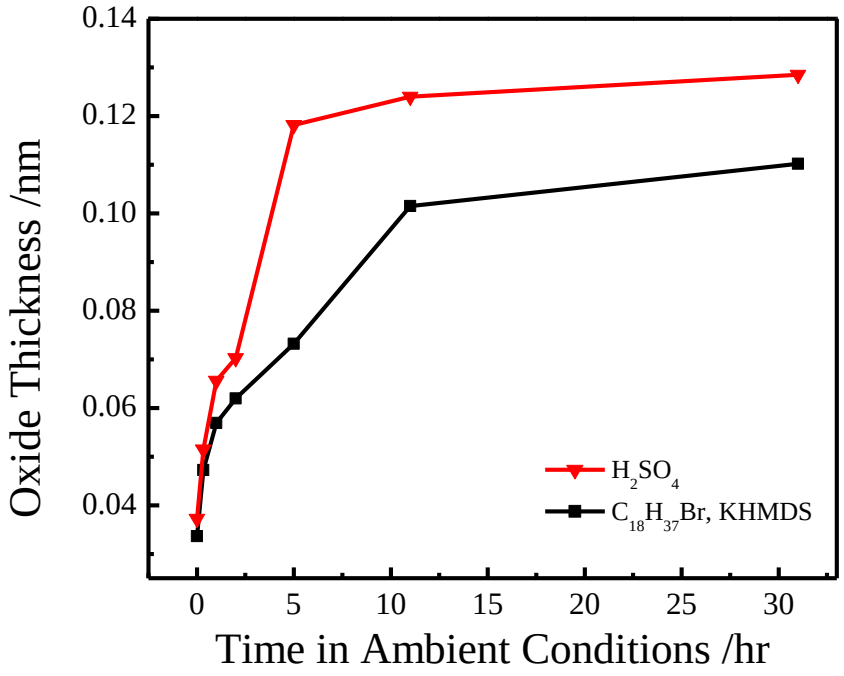

Figure 2.11 The calculated oxide thickness of etched (red triangles) and $C_{18}H_{37}$-terminated (black squares) GaP(111)B over time in ambient conditions.

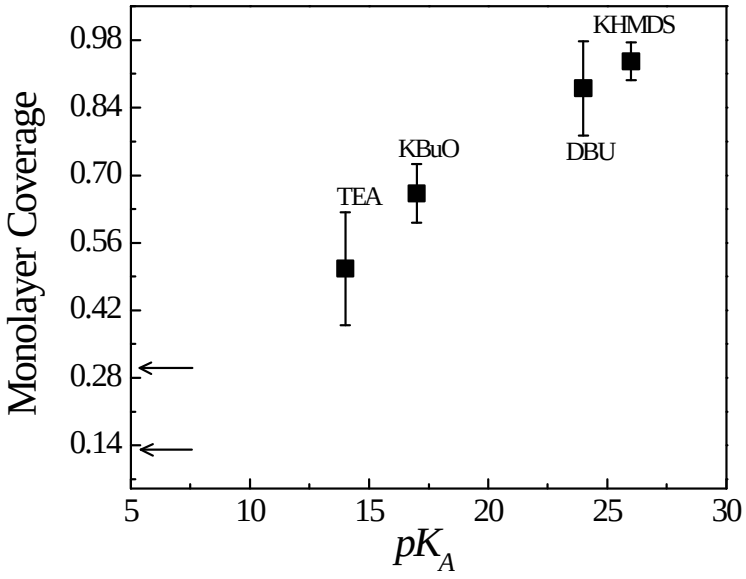

Figure 2.12 Monolayer coverages of p-$CF_3C_6H_4CH_2$- on GaP(111)B after reaction with p-$CF_3C_6H_4CH_2Br$ for 1 h at T = 60°C using several different base promoters (TEA = triethylamine; KBuO = potassium butoxide; DBU = 1,8-diazabicycloundec-7-ene; KHMDS= potassium bis(trimethylsilyl)amide). Arrows indicate the range of monolayer coverage values obtained under the same conditions in the absence of any base promoter.

observed for GaP(111)B reacted with $C_{18}H_{37}Br$ or $C_{10}H_{21}Br$ and the same series of bases (Figure 2.13).

The effect of base on reaction rate was also determined for the reaction between etched GaP(111)B and *p*-$CF_3C_6H_4CH_2Br$. Figure 2.14 presents the measured monolayer

coverage for a series of reactions without any added base promoter. Full monolayer coverage was obtained after 120 min. In contrast, inclusion of KHMDS in the reaction shortened the completion time to 60 min. The effect of base on reaction time was also noted for reactions of $C_{10}H_{21}Br$, where without base there was no spectroscopic or wetting evidence of reaction at times less than 24 h but inclusion of KHMDS facilitated reaction after just 3 h (Figure 2.5, Table 2.6).

2.3.4 Sub-Band Gap Photoelectrochemical Measurements

As described previously,[41] sub-band gap illumination can induce measureable photocurrents by excitation of charges to/from surface traps within the bandgap. The magnitude of the quantum yield for sub-band gap photocurrent has thus been used as a measure of surface state density.[42,43] Long wavelength ($\lambda > 545$ nm) photocurrent measurements were used to probe the impact on charge transfer through surface states on GaP(111)B following reaction with alkyl bromides. Etched p-type GaP(111)B exhibited higher photocurrent quantum yields at all sub-bandgap wavelengths than p-GaP(111)B reacted with $C_{18}H_{37}Br$, $C_{14}H_{29}Br$, or $C_{10}H_{21}Br$ (Figure 2.15). However, the supra-band gap photoresponse ($\lambda \leq 545$ nm) was nominally the same for all tested electrodes, illustrating that the adsorbed surface groups did not act completely like an insulating blocking layer that uniformally attenuated heterogeneous charge transfer. The attenuation of sub-band gap photocurrents at modified p-GaP(111)B was consistent with the premise that functionalization either directly passivated surface traps or sterically blocked access for charge transfer through those site(s).

2.3.5 Sensitization of GaP(111)B with Chemisorbed Coomassie Blue Dye

The premise of using the Williamson ether-type P-O-*R* surface bonding to attach purposefully a dye was explored. Coomassie Blue is a particularly attractive dye since it

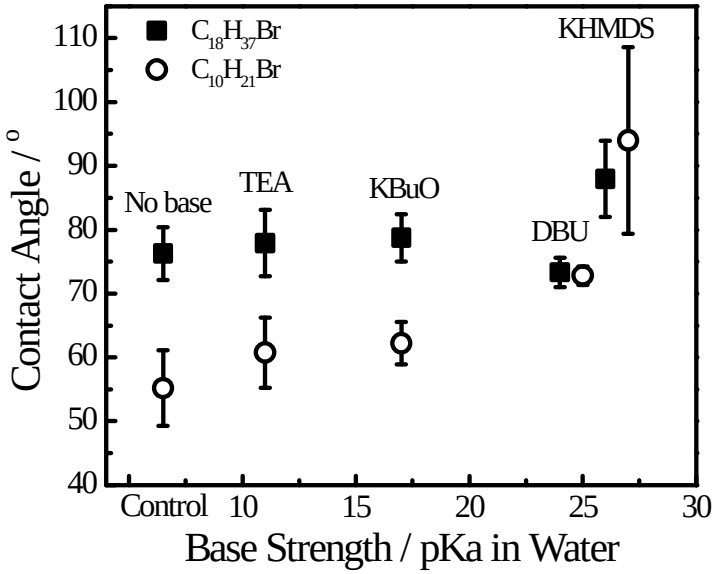

Figure 2.13 Contact angle data for GaP(111)B reaction with $C_{18}H_{37}Br$ (closed squares) or $C_{10}H_{21}Br$ (open circles) in the presence of a series of bases.

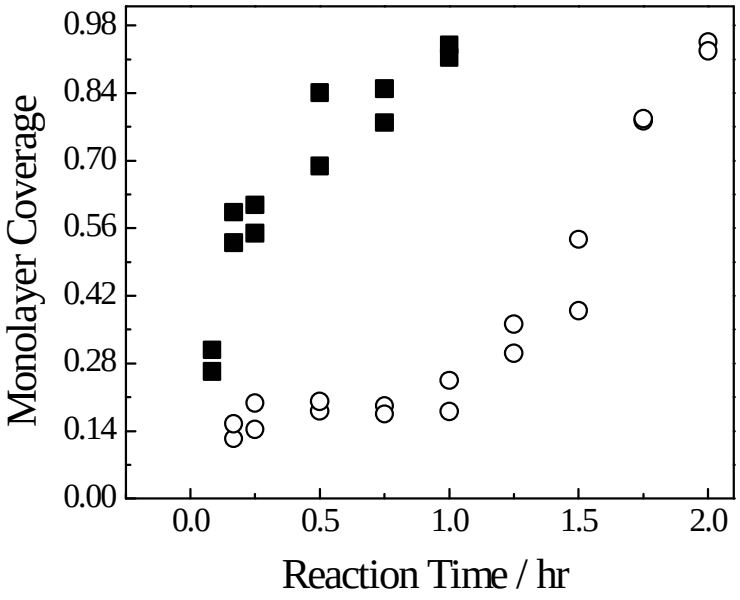

Figure 2.14 Monolayer coverage of *p*-$CF_3C_6H_4CH_2$- on GaP(111)B without (open circles) or with KHMDS (closed squares) at T = 60°C for different reaction times.

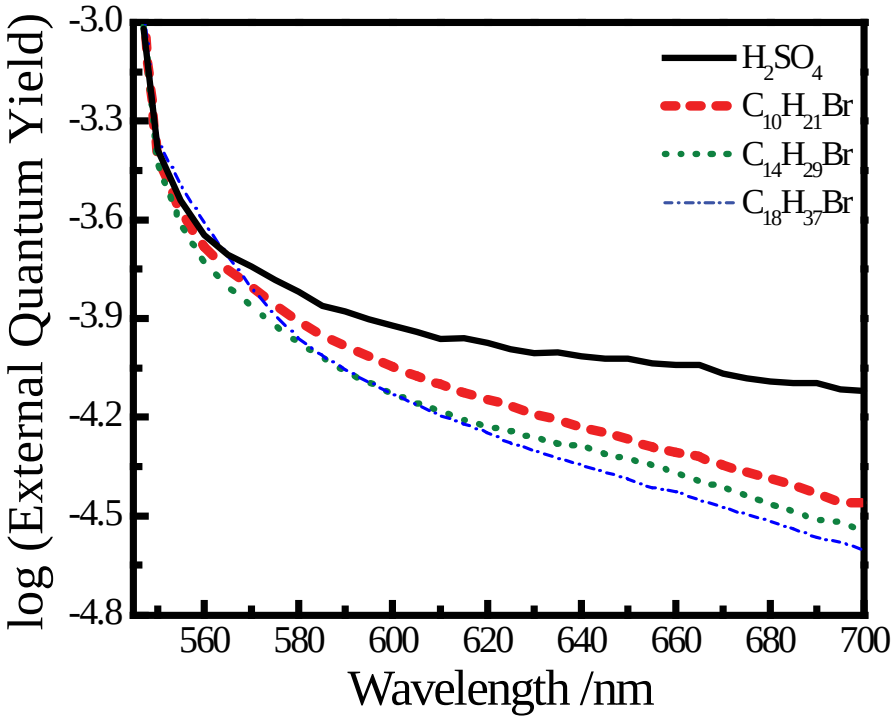

Figure 2.15 Wavelength-dependent external quantum yields for photocurrent for p-type GaP(111)B after reaction with concentrated H_2SO_4 and alkyl bromides ($C_nH_{2n+1}Br$, where n = 10, 14, 18).

absorbs strongly at $\lambda > 545$ nm and has a standard potential for oxidation that suggests it could sensitize GaP by injecting a hole.[44] To attach Coomassie Blue, a reaction between the surface hydroxyl groups on etched GaP(111)B and a sulfonyl chloride group on the dye was envisioned. A clear F 1s signal in the high resolution XP spectra after reaction of GaP(111)B with *o*-$CF_3C_6H_4CH_2SO_2Cl$ indicated that this strategy was viable (Table 2.7). A functionalized[45,46] form of Coomassie Blue dye featuring a terminal sulfonyl chloride was reacted with freshly etched p-GaP(111)B in methanol for 1 h at 55°C in the glovebox. XP spectra following functionalization showed evidence of surface-bound Coomassie Blue (Figure 2.16), with a monolayer coverage of 0.68. These functionalized p-GaP samples were then used as photoelectrodes in 1 M KCl(aq) containing 0.002 M $EuCl_3$. Illumination with sub-band gap light showed a persistent increase in steady-state photocurrent (Figure 2.17). The wavelength dependence of the measured quantum yield values did not change over time (Figure 2.18) and no dye was measured in solution after 120 min, consistent with persistent adsorption of Coomassie Blue.

2.4 DISCUSSION

The cumulative results indicate that etched GaP(111)B surfaces are readily modified by reaction with alkyl and benzyl halides, with a surficial P-O-C linkage formed through a base-promoted Williamson ether-type reaction. These results strongly imply that (*1*) surface reactions geared towards atop P atoms on freshly etched GaP follows P-OH reactivity rather than the reactivity of a dangling bond[26] and (*2*) this reaction scheme on GaP(111)B differs from the Williamson ether synthesis on hydroxyl-terminated metal oxides (e.g. TiO_2).

Two reaction pathways are possible for this functionalization of hydroxyl-terminated GaP(111)B. Surficial P-OH could react in a sequential two-step mechanism,

$$P-OH \rightarrow PO^- + H^+ \qquad \text{Reaction 2.1}$$

$$PO^- + RX \rightarrow PO-R + X^- \qquad \text{Reaction 2.2}$$

where the first deprotonation step is rate determining. Alternatively, the surface is already deprotonated prior exposure to the halide (i.e., *RX*), making Reaction 2.*2* the rate-limiting

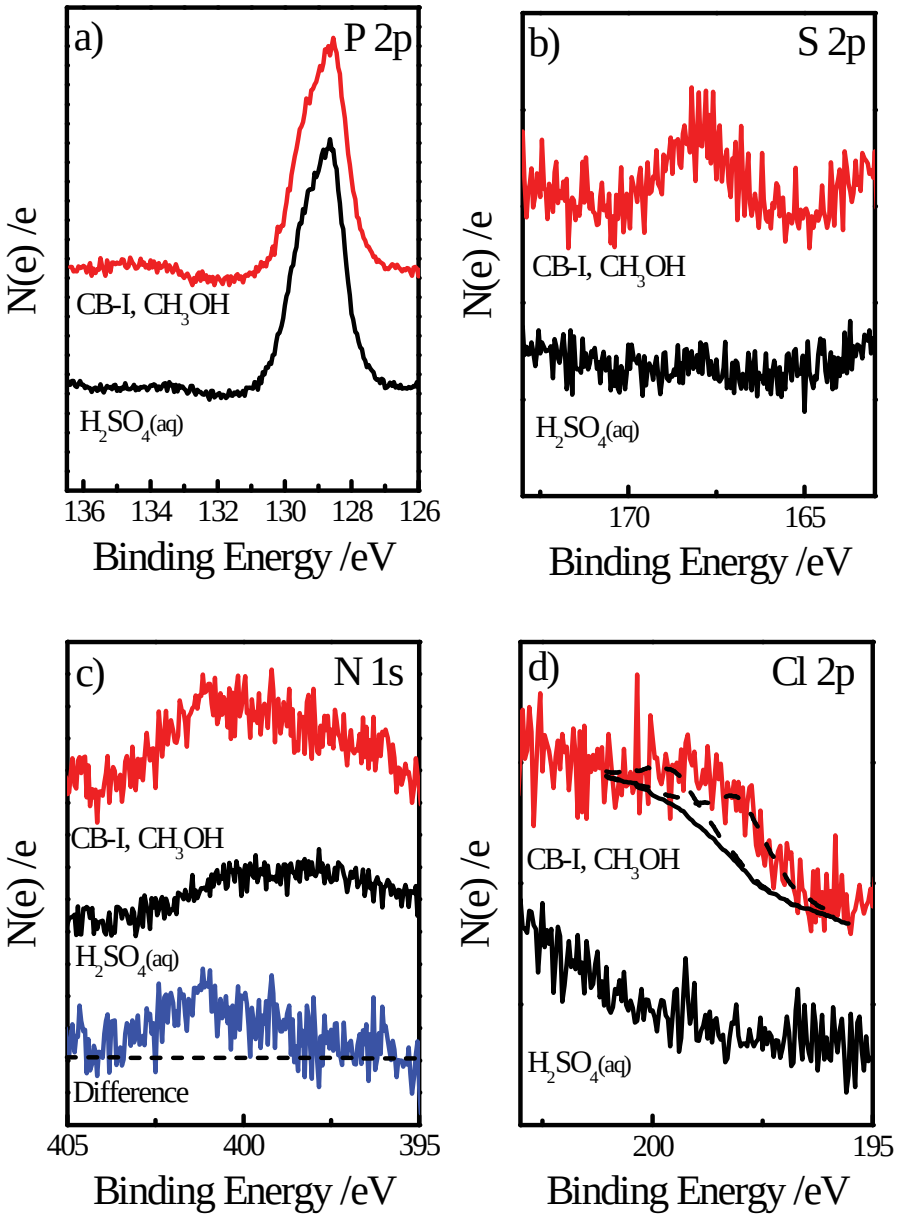

Figure 2.16 High resolution XP spectra of GaP(111)B after etching (black) and after reaction with CB-I in methanol in the dark. (a) Both P 2p spectra show negligible oxide formation at 133 eV. CB-I reacted GaP(111)B exhibited increased intensity at (b) 168.0 eV in the S 2p spectrum and at (c) ~400 eV in the N 1s spectrum. The difference spectrum (blue trace) is included for clarity. (d) Some Cl 2p signal remains after reaction.

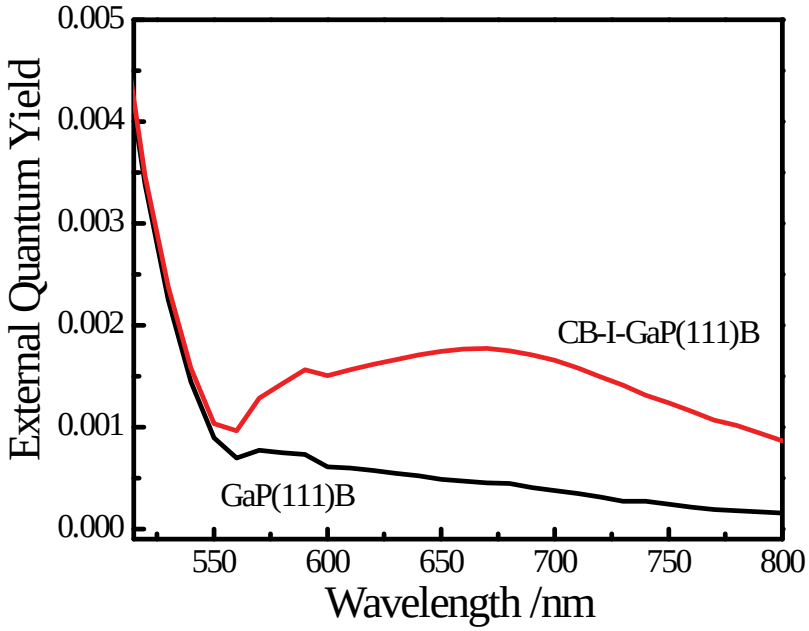

Figure 2.17 Wavelength-dependent external quantum yield for photocurrent at p-type GaP(111)B before and after attachment of Coommassie Blue dye.

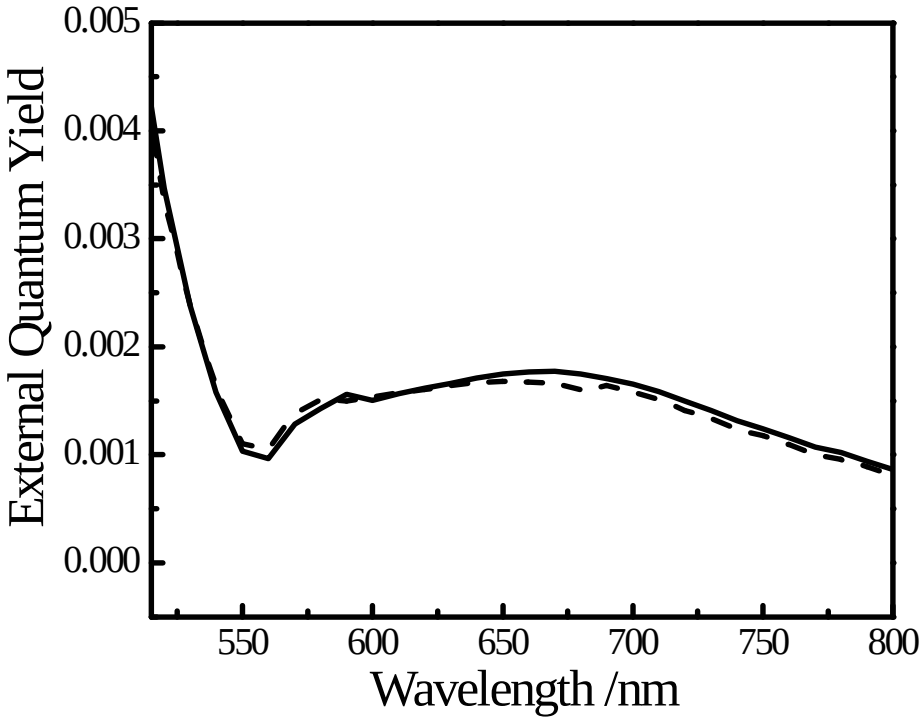

Figure 2.18 External QY response of p-type GaP(111)B reacted with CB-I (solid line) and the same electrode again after several measurements and one week under vacuum (dashed line).

process. The latter scenario describes the ether bond formation on TiO_2 surfaces, where the surface pK_A is sufficiently low to ensure that the addition of base promoters does not affect reaction rate or resultant monolayer coverage when reacted with *RX* reagents.[28,47] In contrast, the strong sensitivity of the reaction rates measured here for GaP(111)B implies that the surface etching step results in a protonated GaP(111)B surface oxide that must be deprotonated in order to form the P-O-C linkage at a high surface coverage. The activity of non-nucleophilic and sterically hindered base promoters for the surface bond formation further suggest that the S_N2 type reaction, i.e., *RX* reacting with PO^-, is the more efficient method for surface derivitization.

For GaP(111)B surfaces functionalized with straight alkyl chains, the collected spectroscopic and contact angle data were consistent with a disordered adsorbate layer, i.e., alkyl chains lying at shallow angles rather than at a sharp angle dictated by close-packing. In this context, the lack of order mirrors that seen for GaP(111)A surfaces modified with straight alkyl chains through reaction with Grignard reagents.[21,36] However, at the same nominal surface coverages, the surface layers produced here appeared to be less effective at eliminating further oxidation of the underlying GaP substrate.[21] This discrepancy suggests a difference in the stability of the surface bond occurring at GaP(111)B surfaces modified by the Williamson ether approach or GaP(111)A surfaces modified by Grignard reagents (i.e., P-O-C vs. Ga-C, respectively). Similarly, putative Ga-C bonds prepared on GaP(100) showed higher stability in aqueous solutions than the surfaces reported here.[16] Nevertheless, the oxide measurements performed on substrates immersed in solutions with varying *pH* showed that hydrolysis of the surficial P-O-C bonds were strongly *pH* dependent. That is, at extreme *pH* values, the organic adsorbates were removed from the GaP(111)B surface but at neutral/mildly basic *pH* the adsorbates remained on the surface. The eventual oxidation of the underlying surface implied that these persistently adsorbed organic groups were not sufficiently dense to block oxidative attack. However, if the packing density could be increased (e.g. using adsorbates with smaller footprints), perhaps the oxidation of underlying GaP could be further retarded.

In the context of photoelectrochemical cells, the susceptibility to oxidation is less critical for p-GaP since cathodic operation tends to naturally infer protection against further oxide formation. However, charge recombination at surficial structural defects is

detrimental.[48] The results here indicate that functionalization *via* the Williamson ether route has some mitigating effect on the number of electrically active surface traps. The data do not indicate whether adsorbate bonding specifically ameliorates specific surface traps or the presence of nearby organic groups blocks access to active surface traps. Unfortunately, the high density of bulk defects present in all commercially available GaP wafers[49] prevents the use of transient photoluminescence or photoconductivity measurements to deconvolute these possibilities. Nevertheless, the presented results show this chemistry as a possible means to gain control over the electrical properties of GaP photoelectrodes. With regards to sensitized p-GaP photocathodes,[50-52] the Williamson ether strategy has shown viable for persistent adsorption of a molecular chromophore. The sensitivity of the magnitude of the photocurrent quantum yield towards all possible factors was not tested. However, the clear observation of sensitized photocurrents at wavelengths far outside the bandgap energy confirms that attachment through P-O surface groups is a viable strategy for dye loading. The stability of the sensitized photoelectrodes (> 1 week) suggests that this binding method may be suitable in aqueous solutions at neutral *pH* values. Accordingly, applying the results presented here with other surface derivitization strategies developed for GaP affords a way to completely functionalize high aspect ratio/nanostructured GaP photoelectrodes.

A final comment should be made on the broad applicability of this surface chemistry tactic. These results, in conjunct with earlier findings on InP, suggest that the Williamson ether-type P-O-*R* surface bonding may not be specific to just InP or GaP. Rather, this surface modification strategy may be a general approach for other structurally related phosphide materials. Specifically, phosphide alloys (e.g. $GaInP_2$) and II-IV-V_2 phosphides (e.g. $ZnSnP_2$, $ZnGeP_2$, $ZnSiP_2$) also feature P atoms with tetrahedral coordination. Accordingly, surface atop P atoms with one available bonding orbital (as featured on GaP(111)B and InP(111)B) on these materials should also be reactive towards organic halides. Such surface chemistry may benefit the use of these materials in electrical/electrochemical technologies, as each of these materials have been explored as the light harvesting component in solar cell designs.[11,41,46,53-57] Since surface defects and corrosion/oxidation at the interfaces of the light harvesting component are detrimental to energy conversion/storage efficiencies, chemical methods that can ameliorate such

problems have value. The data presented here represent one new possible approach for phosphides in these applications.

2.5 SUMMARY

This work illustrates a facile, wet chemical strategy for the Williamson ether-type modification of acid-etched GaP(111)B surfaces with alkyl or benzyl halides through P-O-C bonds. Our results showed a strong sensitivity to the inclusion of strong base, implying a moderate basicity of the acid-etched GaP(111)B surface. The synthetic and operational features for the modified GaP(111)B surfaces illustrate design features for making chemically tailored GaP interfaces. Specifically, these initial sensitization measurements invite future fundamental studies and applied development of sensitized photocathodes based upon GaP. Work is ongoing in our group in this direction.

2.6 REFERENCES

(1) Barton, E. E.; Rampulla, D. M.; Bocarsly, A. B. Selective Solar-Driven Reduction of CO2 to Methanol Using a Catalyzed p-GaP Based Photoelectrochemical Cell. *J. Am. Chem. Soc.* **2008**, *130*, 6342-6344.

(2) McIntosh, D.; Zhou, Q. G.; Chen, Y. J.; Campbell, J. C. High Quantum Efficiency GaP Avalanche Photodiodes. *Opt. Express* **2011**, *19*, 19607-19612.

(3) Price, M. J.; Maldonado, S. Macroporous n-GaP in Nonaqueous Regenerative Photoelectrochemical Cells. *J. Phys. Chem. C* **2009**, *113*, 11988-11994.

(4) Gerischer, H. Electrolytic Decomposition and Photo-decomposition of Compound Semiconductors in Contact with Electrolytes *J. Vac. Sci. Technol.* **1978**, *15*, 1422-1428.

(5) Bard, A. J. Design of Semiconductor Photo-electrochemical Systems for Solar Energy Conversion *J. Phys. Chem.* **1982**, *86*, 172-177.

(6) Tomkiewicz, M.; Woodall, J. M. Photoassisted Electrolysis of Water by Visible Irradiation of a p-Type Gallium Phosphide Electrode. *Science* **1977**, *196*, 990-991.

(7) Turner, J. A. A Realizable Renewable Energy Future. *Science* **1999**, *285*, 687-689.

(8) Aspnes, D. E.; Studna, A. A. Dielectric Functions and Optical Parameters of Si, Ge, GaP, GaAs, GaSb, InP, InAs, and InSb from 1.5 to 6.0 eV. *Phys. Rev. B: Condens. Matter* **1983**, *27*, 985-1009.

(9) Sun, J. W.; Liu, C.; Yang, P. D. Surfactant-Free, Large-Scale, Solution-Liquid-Solid Growth of Gallium Phosphide Nanowires and Their Use for Visible-Light-Driven Hydrogen Production from Water Reduction. *J. Am. Chem. Soc.* **2011**, *133*, 19306-19309.

(10) Wen, W.; Carim, A. I.; Collins, S. M.; Price, M. J.; Peczonczyk, S. L.; Maldonado, S. Structural and Photoelectrochemical Properties of GaP Nanowires Annealed in NH3. *J. Phys. Chem. C* **2011**, *115*, 22652-22661.

(11) Khaselev, O.; Turner, J. A. Electrochemical Stability of p-GaInP2 in Aqueous Electrolytes Toward Photoelectrochemical Water Splitting. *J. Electrochem. Soc.* **1998**, *145*, 3335-3339.

(12) Gershenzon, M.; Mikulyak, R. M. Radiative Pair Recombination and Surface Recombination in GaP Photoluminescence. *Appl. Phys. Lett.* **1966**, *8*, 245-247.

(13) Stringfellow, G. B. Effect of Surface Treatment on Surface Recombindation Velocity and Diode Leakage Current in GaP. *J. Vac. Sci. Technol.* **1976**, *13*, 908-913.

(14) Mukherjee, J.; Erickson, B.; Maldonado, S. Physicochemical and Electrochemical Properties of Etched GaP(111)A and GaP(111)B Surfaces. *J. Electrochem. Soc.* **2010**, *157*, H487-H495.

(15) Flores-Perez, R.; Zernlyanov, D. Y.; Ivanisevic, A. Quantitative Evaluation of Covalently Bound Molecules on GaP (100) Surfaces. *J. Phys. Chem. C* **2008**, *112*, 2147-2155.

(16) Richards, D.; Zemlyanov, D.; Ivanisevic, A. Assessment of the Passivation Capabilities of Two Different Covalent Chemical Modifications on GaP(100). *Langmuir* **2010**, *26*, 8141-8146.
(17) Li, F.; Basile, V. M.; Pekarek, R. T.; Rose, M. J. Steric Spacing of Molecular Linkers on Passivated Si(111) Photoelectrodes. *ACS Appl. Mater. Interfaces* **2014**, *6*, 20557-20568.
(18) Yuan, Z. L.; Ding, X. M.; Lai, B.; Hou, X. Y.; Lu, E. D.; Xu, P. S.; Zhang, X. Y. Neutralized (NH4)(2)S Solution Passivation of III-V Phosphide Surfaces. *Appl. Phys. Lett.* **1998**, *73*, 2977-2979.
(19) Liu, K. Z.; Suzuki, Y.; Fukuda, Y. Surface Analysis of (NH2)(2)CS-Treated GaP(001) by AES and XPS. *Surf. Interface Anal.* **2004**, *36*, 966-968.
(20) Zerulla, D.; Chasse, T. Structure and Self-Assembly of Alkanethiols on III-V Semiconductor (110) Surfaces. *J. Electron Spectrosc. Relat. Phenom.* **2009**, *172*, 78-87.
(21) Mukherjee, J.; Peczonczyk, S.; Maldonado, S. Wet Chemical Functionalization of III-V Semiconductor Surfaces: Alkylation of Gallium Phosphide Using a Grignard Reaction Sequence. *Langmuir* **2010**, *26*, 10890-10896.
(22) Peczonczyk, S. L.; Brown, E. S.; Maldonado, S. Secondary Functionalization of Allyl-Terminated GaP(111)A Surfaces via Heck Cross-Coupling Metathesis, Hydrosilylation, and Electrophilic Addition of Bromine. *Langmuir* **2014**, *30*, 156-164.
(23) Suzuki, Y.; Sanada, N.; Shimomura, A.; Fukuda, Y. High-Resolution XPS Analysis of GaP(001), (111)A, and (111)B Surfaces Passivated by (NH4)(2)S-x Solution. *Appl. Surf. Sci.* **2004**, *235*, 260-266.
(24) Sturzenegger, M.; Lewis, N. S. An X-ray Photoelectron Spectroscopic and Chemical Reactivity Study of Routes to Functionalization of Etched InP Surfaces. *J. Am. Chem. Soc.* **1996**, *118*, 3045-3046.
(25) Sturzenegger, M.; Prokopuk, N.; Kenyon, C. N.; Royea, W. J.; Lewis, N. S. Reactions of Etched, Single Crystal (111)B-Oriented InP to Produce Functionalized Surfaces with Low Electrical Defect Densities. *J. Phys. Chem. B* **1999**, *103*, 10838-10849.
(26) Spool, A. M.; Daube, K. A.; Mallouk, T. E.; Belmont, J. A.; Wrighton, M. S. Reaction of the (111) Faces of Single-Crystal Indium-Phosphide with Alkylating Agents. Evidence for Selective Reaction of the P-Rich Face. *J. Am. Chem. Soc.* **1986**, *108*, 3155-3157.
(27) Chen, J. X.; Franking, R.; Ruther, R. E.; Tan, Y. Z.; He, X. Y.; Hogendoorn, S. R.; Hamers, R. J. Formation of Molecular Monolayers on TiO2 Surfaces: A Surface Analogue of the Williamson Ether Synthesis. *Langmuir* **2011**, *27*, 6879-6889.
(28) English, C. R.; Bishop, L. M.; Chen, J. X.; Hamers, R. J. Formation of Self-Assembled Monolayers of pi-Conjugated Molecules on TiO2 Surfaces by Thermal Grafting of Aryl and Benzyl Halides. *Langmuir* **2012**, *28*, 6866-6876.
(29) Haber, J. A.; Lewis, N. S. Infrared and X-ray Photoelectron Spectroscopic Studies of the Reactions of Hydrogen-Terminated Crystalline Si(111) and Si(100) Surfaces with Br-2, I-2, and Ferrocenium in Alcohol Solvents. *J. Phys. Chem. B* **2002**, *106*, 3639-3656.

(30) Barr, T. L.; Seal, S. Nature of the Use of Adventitious Carbon as a Binding-Energy Standard. *J. Vac. Sci. Technol., A* **1995**, *13*, 1239-1246.
(31) *Practical Surface Analysis*; Briggs, D.; Seah, M. P., Eds.; John Wiley & Sons: Chichester, 1983.
(32) Asami, K.; Hashimoto, K.; Shimodaira, S. XPS Determination of Compositions of Alloy Surfaces and Surface Oxides on Mechanically Polished Iron-Chromium Alloys. *Corros. Sci.* **1977**, *17*, 713-723.
(33) Pies, W., Weiss, A. *Crystal Structure Data of Inorganic Compounds*; Springer-Verlag: Berlin, 1979.
(34) Laibinis, P. E.; Bain, C. D.; Whitesides, G. M. Attenuation of Photoelectrons in Monolayers of Normal-Alkanethiols Adsorbed on Copper, Silver, and Gold. *J. Phys. Chem.* **1991**, *95*, 7017-7021.
(35) Segar, P. R.; Koval, C. A.; Koel, B. E.; Gebhard, S. C. A Comprehensive Investigation of HCl and Br2/NH3(aq) Etched p-InP Interfaces. *J. Electrochem. Soc.* **1990**, *137*, 544-552.
(36) Lummerstorfer, T.; Kattner, J.; Hoffmann, H. Monolayers at Solid-Solid Interfaces Probed with Infrared Spectroscopy. *Analytical and Bioanalytical Chemistry* **2007**, *388*, 55-64.
(37) Snyder, R. G.; Strauss, H. L.; Elliger, C. A. C-H Stretching Modes and the Sturcture of Normal-Alkyl Chains. 1. Long, Disordered Chains. *J. Phys. Chem.* **1982**, *86*, 5145-5150.
(38) Porter, M. D.; Bright, T. B.; Allara, D. L.; Chidsey, C. E. D. Spontaneously Organized Molecular Assemblies. Part 4: Structural Characterization of Normal-Alkyl Thiol Monolayer on Gold by Optical Ellipsometry, Infrared Spectroscopy, and Electrochemistry. *J. Am. Chem. Soc.* **1987**, *109*, 3559-3568.
(39) Seitz, O.; Bocking, T.; Salomon, A.; Gooding, J. J.; Cahen, D. Importance of Monolayer Quality for Interpreting Current Transport Through Organic Molecules: Alkyls on Oxide-Free Si. *Langmuir* **2006**, *22*, 6915-6922.
(40) Daasch, L. W.; Smith, D. C. Infrared Spectra of Phosphorus Compounds. *Anal. Chem.* **1951**, *23*, 853-868.
(41) Wei, W.; Huang, X. B.; Zhao, X. L.; Zhang, P.; Tang, X. Z. A Rapid and Efficient Strategy for Preparation of Super-Hydrophobic Surface with Cross-Linked Cyclotriphosphazene/6F-bisphenol A Copolymer Microspheres. *Chem. Commun.* **2010**, *46*, 487-489.
(42) Butler, M. A.; Ginley, D. S. Surface-Treatment Induced Sub-Band Gap Photoresponse of GaP Photoelectrodes. *J. Electrochem. Soc.* **1981**, *128*, 712-714.
(43) Brown, E. S.; Peczonczyk, S. L.; Wang, Z. J.; Maldonado, S. Photoelectrochemical Properties of CH3-Terminated p-Type GaP(111)A. *J. Phys. Chem. C* **2014**, *118*, 11593-11600.
(44) Parkinson, B. A. Dye Sensitization of van der Waals Surfaces of SnS2 Photoanodes. *Langmuir* **1988**, *4*, 967-976.
(45) Seker, F.; Meeker, K.; Kuech, T. F.; Ellis, A. B. Surface Chemistry of Prototypical Bulk II-VI and III-V Semiconductors and Implications for Chemical Sensing. *Chem. Rev.* **2000**, *100*, 2505-2536.
(46) Nie, G. C.; Hah, H. J.; Kim, G.; Lee, Y. E. K.; Qin, M.; Ratani, T. S.; Fotiadis, P.; Miller, A.; Kochi, A.; Gao, D.; Chen, T.; Orringer, D. A.; Sagher, O.; Philbert, M.

A.; Kopelman, R. Hydrogel Nanoparticles with Covalently Linked Coomassie Blue for Brain Tumor Delineation Visible to the Surgeon. *Small* **2012**, *8*, 884-891.
(47) Kosmulski, M. Compilation of PZC and IEP of Sparingly Soluble Metal Oxides and Hydroxides From Literature. *Advances in Colloid and Interface Science* **2009**, *152*, 14-25.
(48) Fonash, S. J. *Solar Cell Device Physics, 2nd Edition*, 2010.
(49) Gershenzon, M.; Mikulyak, R. M. Structural Defects in GaP Crystals and Their Electrical and Optical Effects. *J. Appl. Phys.* **1964**, *35*, 2132-2141.
(50) Chitambar, M.; Wang, Z. J.; Liu, Y. M.; Rockett, A.; Maldonado, S. Dye-Sensitized Photocathodes: Efficient Light-Stimulated Hole Injection into p-GaP Under Depletion Conditions. *J. Am. Chem. Soc.* **2012**, *134*, 10670-10681.
(51) Choi, D.; Rowley, J. G.; Parkinson, B. A. Dye Sensitization of n and p Type Gallium Phosphide Photoelectrodes. *J. Electrochem. Soc.* **2012**, *159*, H846-H852.
(52) Memming, R.; Tributsch, H. Electrochemical Investigations on Spectral Sensitization of Gallium Phosphide Electrodes. *J. Phys. Chem.* **1971**, *75*, 562-570.
(53) Kocha, S. S.; Turner, J. A. Displacement of the Bandedges of GaInP2 in Aqueous Electrolytes Induced by Surface Modification. *J. Electrochem. Soc.* **1995**, *142*, 2625-2630.
(54) Ajmera, P. K.; Shin, H. Y.; Zamanian, B. Vacuum Growth of Thin Films of $ZnSnP_2$. *Solar Cells* **1987**, *21*, 291-299.
(55) Yokoyama, T.; Oba, F.; Seko, A.; Hayashi, H.; Nose, Y.; Tanaka, I. Theoretical Photovoltaic Conversion Efficiencies of $ZnSnP_2$, $CdSnP_2$, and $Zn_{1-x}Cd_xSnP_2$ Alloys. *App. Phys. Express* **2013**, *6*, 061201-061204.
(56) van Schilfgaarde, M.; Coutts, T. J.; Newman, N.; Peshek, T. Thin Film Tandem Photovoltaic Cell From II-IV-V Chalcopyrites. *Appl. Phys. Lett.* **2010**, *96*, 143503.
(57) Prochukhan, V. D.; Rud, Y. V. Potential Practical Applications of II-IV-V2 Semiconductors. *Soviet Physics Semiconductors* **1978**, *12*, 121-135.

CHAPTER 3

Photoelectrochemical Properties of CH_3-Terminated P-type GaP(111)A

3.1 INTRODUCTION

No known semiconductor electrode material natively possesses both sufficiently good bulk and surface properties for driving fuel-forming reactions in photoelectrochemical energy conversion/storage cells. Although the possibility remains that some heretofore unknown semiconductor exists that intrinsically has all the right attributes,[1-6] a prudent strategy for advancing water-splitting photoelectrochemical technologies is to correct the deficiencies of known semiconductors with the capacity to supply large photovoltages and meaningful photocurrent densities under solar insolation. For III-V semiconductors like gallium phosphide (GaP) and related alloys (e.g. $GaInP_2$, $GaAs_xP_{1-x}$), the bulk optoelectronic properties are naturally suited for generating the large electromotive forces needed for driving complex redox transformations.[7-13] However, these semiconductors suffer from severe chemical instability of their surface properties both in air and in water,[9,14-18] leading to either a substantial deterioration of their interfacial electronic quality and/or catastrophic chemical corrosion. In principle, interfacial chemistry deficiencies can be ameliorated through deliberate covalent chemical modification of the surface. For example, although silicon (Si) also suffers from deleterious surface reactivity, an extensive precedent now exists for protecting, functionalizing, and augmenting Si surfaces in photoelectrochemical systems through covalent attachment of chemical functionalities.[19-28] In comparison, few covalent surface modification strategies have been developed for these III-V semiconductors.

Our group recently proposed a new protection strategy for GaP, GaAs, and GaN through the introduction of putative Ga-C surface bonds following a two-step chlorination/Grignard reaction sequence.[29-31] The cumulative data showed the chemical durability and electrical quality of these Ga-containing semiconductor interfaces could be substantially improved through this modification strategy. To date, the effects that alkylation *via* reaction with Grignard reagents have on the photoelectrochemical properties specifically of GaP have not been assessed. Accordingly, in this work we report experiments on the effect that CH_3-termination has on the photoelectrochemical properties of single-crystalline p-type GaP acting as a photocathode in aqueous electrolyte. This study focuses on -CH_3 groups since these moieties have the smallest areal footprint for an alkyl group and the shortest length so as to minimize current attenuation by tunneling. The use of single-crystalline planar GaP(111)A electrodes further affords well-defined platforms to make direct inferences on the reactivity of atop Ga atoms that should be similarly operative on nanostructured GaP photoelectrodes.[15,32] Specifically, data are presented and discussed that relate to the surface energetics, resistance to cathodic degradation, and density of electronic surface defects before and after covalent grafting of -CH_3 groups *via* a two-step chlorination/Grignard reaction sequence.

3.2 EXPERIMENTAL

3.2.1 Materials and Chemicals

All chemicals were purchased from Aldrich unless otherwise noted. Methanol (anhydrous, 99.8%), acetone (HPLC-grade, Fisher), tetrahydrofuran (anhydrous, ≥ 99.9%), CH_3MgCl (2.0 M solution in THF), PCl_5 (95%), chlorobenzene (anhydrous, 99.8%), dichloromethane (anhydrous, ≥ 98.7%), doubly distilled H_2SO_4 (95-98%), H_3PO_4 (Mallinckrodt, ACS grade), europium (III) chloride hexahydrate (99.9%, Strem Chemicals), europium (II) chloride (99.9%, Strem Chemicals), Brilliant Green (98%) and potassium chloride (ACS grade, Mallinckrodt) were all used as received. Benzoyl peroxide (≥ 97%, Fluka) was dried under a vacuum of < 200 mTorr for at least 24 h. Water with a resistivity of >18 MΩ cm (Barnsted Nanopure system) was used throughout.

Polished p-type GaP(111)A wafers doped with zinc at 2.7 x 10^{18} cm^{-3} with a thickness of 350 ± 25 μm were purchased from ITME.

3.2.2 Electrode Fabrication

P-type GaP(111)A wafers were diced into 0.5 cm x 0.5 cm sections. Ohmic contacts were prepared by soldering In onto the scratched back of the wafers and subsequently annealing for 10 min at 400°C in forming gas. Electrodes were prepared using silver print (GC Electronics) to attach the GaP sections to a tinned copper wire coil threaded through a glass tube and sealing with inert epoxy (Hysol C). Geometric areas of the electrodes were determined through analysis of digital optical photographs. Electrode areas were nominally between 0.1 and 0.2 cm^2 for all investigated samples. Immediately before use, electrodes were etched in doubly distilled H_2SO_4 for 30 seconds, rinsed with water, and dried with $N_{2(g)}$.[16]

3.2.3 Chlorination and Grignard Reaction Sequence of Electrodes

Before modification, the epoxy was covered with Teflon tape to prevent chemical degradation. In a N_2-purged glovebox, the electrodes were reacted in a saturated solution of PCl_5 in chlorobenzene at 90-95°C for 50 minutes as previously described.[30] The sample was thoroughly rinsed with chlorobenzene and dried in the glovebox. The electrodes were alkylated with CH_3MgCl in a closed reaction vessel over 3 h at 150-160°C. After reaction, electrodes were prepared by removal of Teflon tape, thorough rinsing with THF and subsequently anhydrous methanol, and drying in the glovebox. All samples were stored in the glovebox until use.

3.2.4 Experimental Surface Characterization

The coverage of methyl groups on GaP(111)A electrodes was evaluated by XP spectra. X-ray photoelectron (XP) spectra were collected with a PHI 5400 analyzer using an Al Kα (1486.6 eV) source without a monochromator. Emitted photoelectrons were collected at 54.6° from the sample surface. Spectra were recorded without charge neutralization at a base pressure of < 2.5 x 10^{-9} Torr. A 6 mA emission current and a 10 kV anode HT were used. High-resolution C 1s, Ga 3d, and P 2p spectra were recorded at

a pass energy of 23.5 eV. The binding energies of all spectra were corrected using the expected binding energy for adventitious carbon (284.6 eV).[33]

Samples did not undergo observable degradation during spectra acquisition. In Figure 3.1a, a representative XP survey spectra of a CH_3-terminated GaP(111)A electrode showed no evidence of leftover reagents from the chlorination /Grignard reaction sequence. There is no observable oxidation in the high-resolution P 2p XP spectrum around ~133 eV after ten minutes in ambient conditions (Figure 3.1b). This lack of oxidation is consistent with covalently terminated GaP surface and with previous reports of this reaction on GaP(111)A.[30] The high-resolution C 1s XP spectrum in Figure 3.1c shows a shoulder at lower binding energies than adventitious carbon (284.6 eV). The shoulder at 282.7 eV is consistent with Ga-C bonding.

3.2.5 Electrochemical Impedance Spectroscopy

Impedance measurements were performed using a Schlumberger SI1286 electrochemical interface and a Schlumberger SI1250 frequency response analyzer modulated by CorrWare and ZPlot software. Frequency responses were measured with a sinusoidal AC potential waveform (10 mV amplitude) on top of a dc bias that was stepped to increasingly more negative potentials. Impedance measurements were made in the dark in a three-electrode electrochemical with nitrogen-purged electrolyte solutions (1 M KCl, 2 mM $EuCl_2$, 2 mM $EuCl_3$, and acetate/acetic acid buffer to control pH). The standard potential of the $Eu^{3+/2+}$ redox couple (-0.55 V vs Ag/AgCl)[34,35] was expected to promote strong depletion within GaP without fear of surface inversion that could complicate interpretation of impedance measurements.[36] At intermediate frequencies, *f*, a strongly frequency-dependent total impedance, *Z*, can be expected when a semiconductor electrode has a large space-charge capacitance, C_{SC}, in parallel with an interfacial charge-transfer resistance, R_{ct}. Assuming a small solution resistance, R_s, in series with R_{CT} and C_{SC}, R_{ct} can be measured from the imaginary and real (*Z*') components of the total impedance:[37]

$$R_{CT} = Z'(f) - R_s + \frac{Z''(f)^2}{Z'(f) - R_s}$$

Equation 3.1 Equation for Impedance of Photoelectrochemical Cell with Small Solution Resistance.

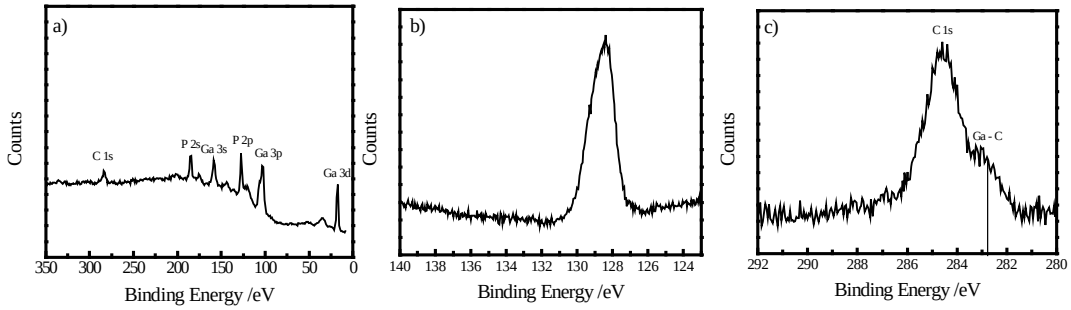

Figure 3.1 XP (a) survey spectrum and (b) high-resolution P 2p or (c) C 1s spectra of p-GaP(111)A electrode after subsequent reaction with PCl_5 in chlorobenzene and CH_3MgCl in THF. In (a), no signature of excess reagents was observed. In (b), no oxidation of the electrode was observed at 133 eV. In (c), the shoulder at 282.7 eV was present after reaction of the electrode with CH_3MgCl.

Similarly, the imaginary component of the total impedance, Z'', can be related to the space-charge capacitance:[24,37-39]

$$C_{SC} = \frac{1}{4\pi f Z''}\left(1+\sqrt{1-\frac{4Z''^2}{R_{CT}^2}}\right)$$

Equation 3.2 Relationship Between Total Impedance and Space-Charge Capacitance.

Fitting measured impedance data with Equations 3.1 and 3.2 is appropriate when the frequency-dependence of the total impedance is in accord with an equivalent circuit composed of a solution resistance, R_s, in series with a parallel RC network.[37] Data were assessed for consistency with Equations 3.1 and 3.2 through analyses of Bode plots, where a Bode slope of -1 is expected for an equivalent circuit network of a resistor in series with a network of a resistor and capacitor in parallel. Average Bode slope measurements from plots of log Z vs. log f more negative than -0.95 were used to validate calculations of the space-charge capacitance from the impedance data. For consistency across all electrodes, data collected between 413 Hz to 16 Hz was used.

Plots of the squared reciprocal space-charge capacitance, C_{SC}^{-2}, as a function of applied electrochemical bias, E, were used to calculate the flat-band potential (E_{FB}) for modified p-type GaP electrodes through the Mott-Schottky relation,[40]

$$C_{SC}^{-2} \times A^2 = \frac{2}{q\varepsilon\varepsilon_0 N_D}\left(E - E_{FB} + \frac{k_B T}{q}\right)$$

Equation 3.3 Mott-Schottky Relation.

where A is the electrode area, q is the unsigned charge of an electron, ε and ε_0 describe the semiconductor dielectric properties, N_D is the semiconductor dopant density, E is the applied potential, k_B is Boltzmann's constant, and T is the temperature. For a non-degenerately doped p-type electrode, the valence band edge potential can be estimated from the flat-band potential through Equation 3.4,

$$E_{vb} = E_{FB} + \frac{k_B T}{q} \ln \frac{N_{vb}}{N_D}$$

Equation 3.4 Relationship Between Flat-Band Potential and Valence Band Potential.

where E_{vb} is the valence band edge and N_{vb} is the effective density of states in the valence band. For the non-degenerately doped GaP used in this study, the second term on the right in Equation 3.4 is 0.049 V at T = 25 C.

3.2.6 Photoelectrochemical Measurements

Photoelectrochemical measurements were made in an airtight Pyrex cell with an optically flat bottom. A Pt counter electrode and a Ag/AgCl reference electrode were used. For all optical measurements, the distance between the optical window and the GaP face was nominally 1 mm. For stability tests, p-GaP(111)A electrodes were immersed under illumination in 0.1 M H_3PO_4 aqueous solution while continuously purging with $N_{2(g)}$ and a bias of -2.5 V was applied for ~15 hours. Each electrode was periodically agitated to dislodge $H_{2(g)}$ bubbles. White light illumination was provided by a tungsten halogen lamp light source (ELH, Osram) with a quartz diffuser. The illumination intensity was set to 100 mW/cm^2 using a thermopile (S302A, Thorlabs). The bottom of the photoelectrochemical cell was cooled with a stream of $N_{2(g)}$. The counter and reference electrodes were placed behind a Vycor frit. A Schlumberger SI1250 Frequency Response Analyzer and SI 1286 Electrochemical Interface were used for potentiostatic control.

Sensitized photocurrent measurements were carried out shortly after electrodes were submerged in a nitrogen-purged 0.1 M KCl solutions, both with and without dissolved Brilliant Green dye. Wavelength-dependent external quantum yield measurements were obtained with an Oriel 150 W Xe arc lamp (Newport) and a quarter-turn single-grating monochromator (Model 74125, Newport). Sample measurements were recorded with chopped illumination (20 Hz). A quartz beam-splitter was used to simultaneously record the light output intensity with a separate Si photodiode (Model 70316NS, Newport) to adjust for fluctuations in lamp intensity. Absolute photocurrents were measured by a digital PAR 273 potentiostat at -0.6 V vs. Ag/AgCl. The output

current signal was connected to a Stanford Instruments SR830 lock-in amplifier. The output signals from the lock-in amplifier and the reference Si photodiode were relayed to a computer controlled by custom-written LabVIEW software. For sub-bandgap photoresponse measurements in the absence of a dye, a long pass filter (Corning Glass Works) was placed in the beam path between the monochromator and the photoelectrochemical cell to block wavelengths shorter than 553 nm.

3.3 RESULTS

3.3.1 Impedance Characteristics of p-GaP(111)A Electrodes in Aqueous Solution

Impedance measurements in the absence of illumination were obtained for N = 5 etched and N = 6 CH_3-terminated p-GaP(111)A electrodes. A comparison of representative impedance response characteristics for p-GaP electrodes with the two surface types immersed in an aqueous electrolyte (pH = 4) is shown in Figure 3.2. Both electrode types showed a strong frequency dependence on the total impedance measured for the semiconductor/electrolyte junction, consistent with operation in strong depletion at reverse bias. Linear slopes between -0.95 and -1.0 were routinely acquired at frequencies below 10^4 Hz. Impedance-frequency responses acquired at higher frequencies showed deviations from linearity, with the two GaP(111)A electrode types showing slightly different high frequency response characteristics. Although not investigated here, the discrepancies at high frequencies were broadly consistent with complications arising from the small geometric sizes of the electrodes and the use of a redox couple with slow charge-transfer kinetics.[38,39] Nevertheless, the impedance responses at $f < 10^4$ Hz allowed reasonably consistent estimation of the value of the space charge capacitance at every potential more negative than the rest potential (i.e., $E(Eu^{3+}/Eu^{2+})$)

3.3.2 Band Edge Energetics of Native and CH_3-terminated p-GaP(111)A Electrodes in Aqueous Solution

The potential-dependent space-charge capacitance values for modified and native GaP(111)A surface types allowed for determination of the respective flat band conditions through the Mott-Schottky relation. Figure 3.3a shows a representative Mott-Schottky

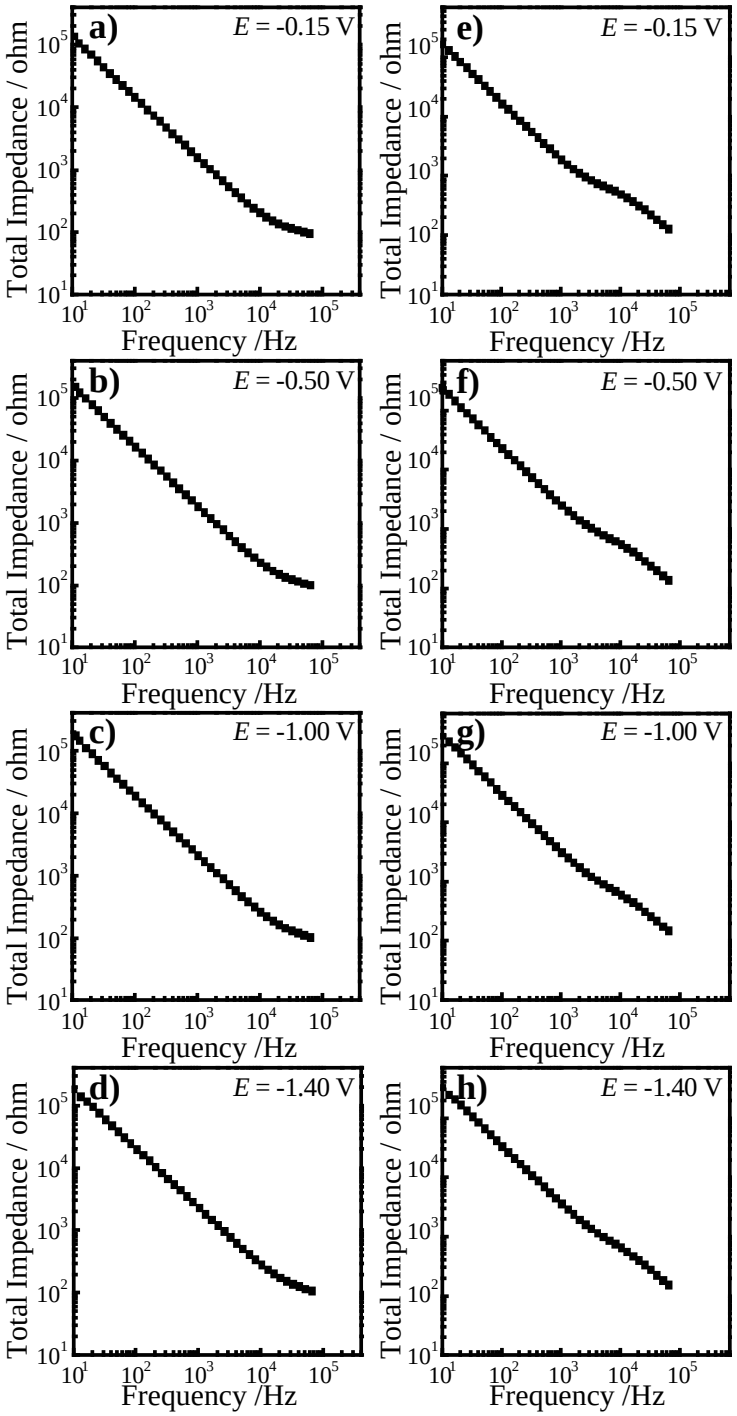

Figure 3.2 Bode plots for (a-d) a representative acid etched and (e-h) a representative CH_3-terminated GaP(111)A electrodes immersed in N_2-purged aqueous solution containing 1 M KCl, 0.002 M $EuCl_2$, 0.002 M $EuCl_3$, and acetate buffer (pH = 4).

plot for the two p-GaP(111)A electrode types at pH = 4. At this pH value, CH_3-terminated GaP(111)A electrodes showed a distinct *x*-axis intercept relative to the acid-etched GaP(111)A electrodes. The difference between the two intercepts was well outside the sample standard deviation of the measurements and thus directly implicated a 0.52 V difference in the flat band potentials and (by extension) in the valence band edge potentials of GaP before and after modification with -CH_3 groups.

Impedance measurements across a range of pH values highlighted two separate points. First, within a pH range of 4 to 7.5, the valence band edge potentials of GaP(111)A were statistically different for CH_3-terminated electrodes. Second, as reported previously,[31,41,42] the flat band potentials of etched GaP electrodes showed a strong dependence on solution pH, changing by roughly 0.060 V per pH unit (Figure 3.3b). Since the solution redox potential was independent of pH, the results were consistent with the valence band edge potential of etched GaP(111)A shifting with pH by the 0.060 V per pH unit. In contrast, the flat band potentials of CH_3-terminated GaP(111)A electrodes showed no dependence with solution pH over the range tested, indicating an invariance of the valence band edge of CH_3-terminated GaP(111)A towards pH change. In effect, the extent of depletion within GaP electrodes and the interfacial charge-transfer barrier height at the GaP/electrolyte junction were not affected by the acidity of the electrolyte for CH_3-terminated p-GaP(111)A.

3.3.3 Cathodic Stability of p-GaP Photoelectrodes

Although cathodic operation is generally perceived to be less corrosive towards semiconductor photoelectrodes in water,[43] reductive degradation of semiconductor surfaces through the formation of metallic clusters/particles is possible.[41] Specifically, since native GaP surfaces are not electrocatalytic towards H^+ reduction in water, photogenerated electrons in p-GaP that reach the electrode/electrolyte interface may participate in the reduction of atop Ga atoms which form metallic Ga clusters/particles (Figure 3.4). Depending on the Pourbaix diagram of the electrolyte, the newly formed elemental Ga either can leach into solution (e.g. in NaOH, H_2SO_4)[41] or accumulate on the surface (H_3PO_4).[41] Either scenario results in a catastrophic attenuation/elimination of photocurrent. Figure 3.5a shows the results of linear sweep experiments that detail the photocurrent stability of native p-GaP(111)A acting as a photocathode in H_3PO_4(aq). The

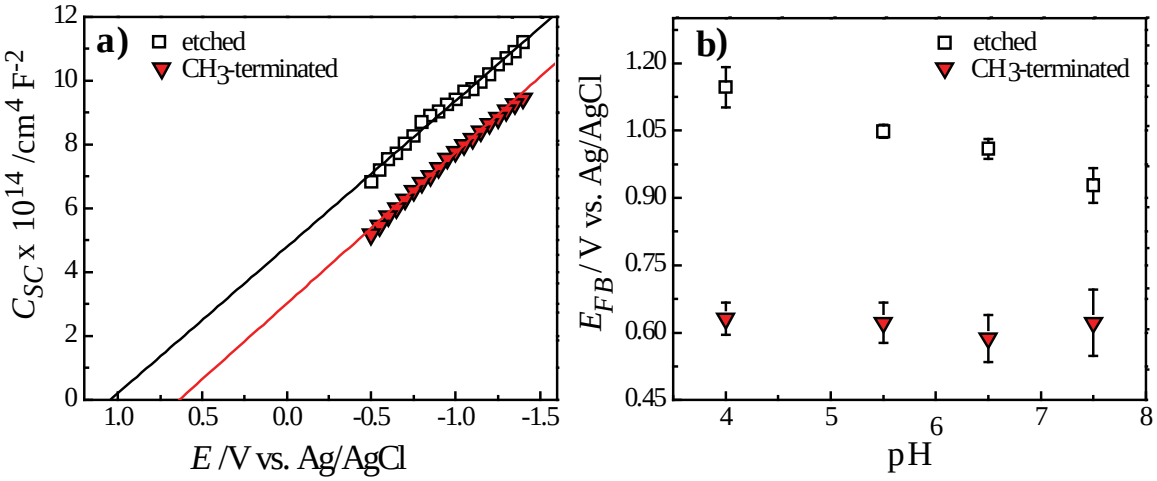

Figure 3.3 a) Representative plots of the squared reciprocal capacitance values at f = 103 Hz as a function of electrochemical potential for etched and CH_3-terminated p-type GaP(111)A electrodes in N_2-saturated solution containing 1 M KCl, 0.002 M $EuCl_2$, 0.002 M $EuCl_3$, and acetate buffer (pH = 4). Measurements were performed in the dark and plots are normalized to electrode area. b) Flat-band potentials of etched and CH_3-terminated p-GaP(111)A as a function of pH. Error bars indicate the standard error mean over five etched and six CH_3-terminated electrodes.

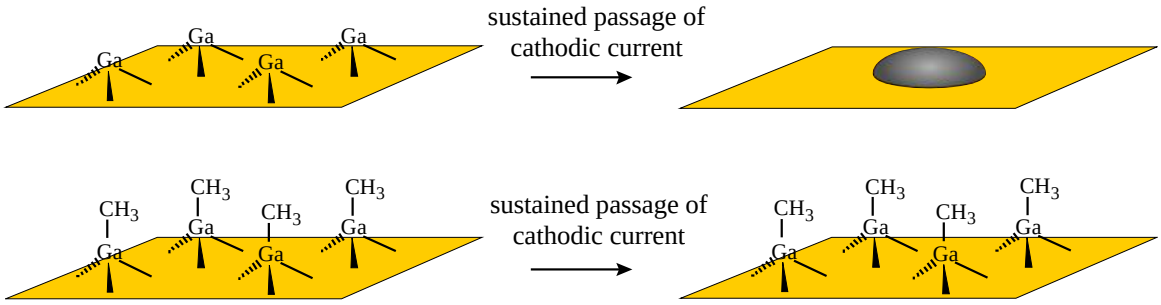

Figure 3.4 Idealized schematic depiction of the stabilities of native and CH_3-terminated p-GaP(111)A photoelectrode interfaces after sustained passage of cathodic current.

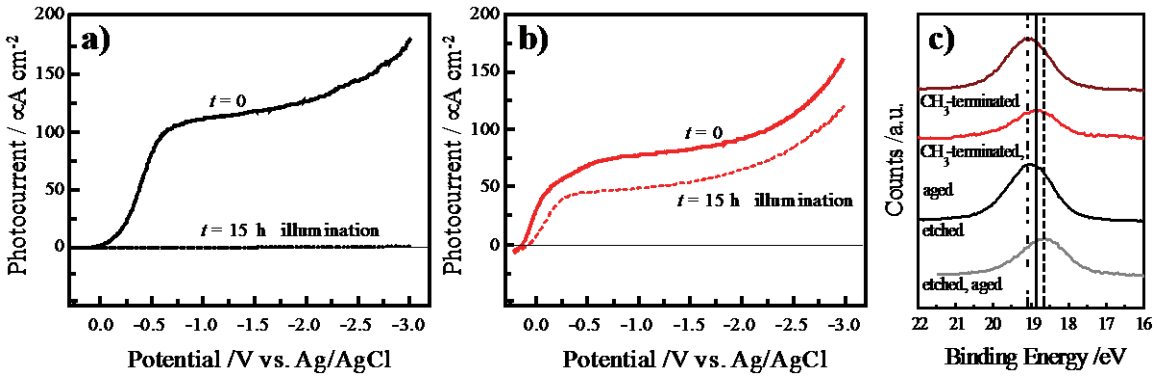

Figure 3.5 The current-voltage characteristics for p-type GaP(111)A photoelectrodes in N_2-purged aqueous solution containing 0.1 M H_3PO_4 while illuminated with 100 mW cm $^{-2}$. (a) Photoresponses for an etched p-GaP(111)A photoelectrode (solid line) at the start and (dashed line) after 15 h of continuous illumination at E = -2.5 V vs Ag/AgCl. (b) Photoresponses for a CH_3-terminated p-GaP(111)A photoelectrode (solid line) at the start and (dashed line) after 15 h of continuous illumination at E = -2.5 V vs Ag/AgCl. (c) High resolution Ga 3d XP spectra of etched (bottom) and CH_3-terminated (top) p-GaP(111)A photoelectrodes before and after continuous illumination at E = -2.5 V vs Ag/AgCl for 15 h. The Ga 3d peak shift is highlighted by a dashed line (18.65 eV) for aged etched electrodes, a dot-dashed line for both before electrodes (19.0 eV), and a solid line for aged CH_3-terminated electrode (18.9 eV).

photocurrent passed at the start of the experiment (*i.e.*, $t = 0$) corresponds to the reduction of H^+ in solution and atop Ga atoms. The respective faradaic efficiencies for the two processes were not calculated but the latter was inferred to be small as repetitive cycling at short times did not change appreciably and a substantial amount of bubbling was observed. However, after 15 hours of illumination and passage of 1.1 C of charge, photocurrent was no longer observed upon cycling and the GaP electrode surfaces were slightly discolored, showing a metallic gray tone. When the same stability experiments were repeated with CH_3-terminated GaP(111)A electrodes, a markedly different result was obtained (Figure 3.5b). Following 15 hours of illumination and net cathodic current passage, the CH_3-terminated GaP(111)A electrodes retained 66% of the photocurrent passed at $t = 0$. Further, these surfaces still exhibited the same orange tint observed at the start of the experiments. High-resolution Ga 3d XP spectra (Figure 3.5c) were collected from both GaP electrode types after the 15 hour stability test. The limited resolution of the XP spectrometer inhibited detail convolution of the Ga $3d_{3/2}$ and $3d_{5/2}$ doublets. However, a perceptible shift of the Ga 3d peak for the etched GaP(111)A electrode after the stability experiment was observed. The peak center at 18.65 eV was consistent with a GaP surface containing a high content of reduced (metallic) Ga.[44] The peak position of aged CH_3-terminated GaP remains largely unchanged from the pristine CH_3-terminated surface, as the difference (0.1 eV) is within the resolution of our XP spectrometer.

3.3.4 Non-sensitized Sub-bandgap Photoresponse of Etched and CH_3-terminated p-GaP(111)A

The predominant mode for photocurrent generation in a semiconductor photoelectrode under illumination is through absorption of supra-bandgap light, i.e., promotion of excited electrons and holes into the conduction and valence bands, respectively (Figure 3.6a). However, sub-bandgap light can also induce measurable photocurrent if there is an appreciable density of mid-gap states in which charge-carriers can be promoted to/from.[45,46] For the commercial grade crystalline GaP used in this study, the prevalence of mid-gap states in the bulk and surface of GaP has been identified previously[41] and shown to induce detectable levels of photocurrent.[47] Since both the absorption cross-section and the total density of such defects are small, the expected sub-

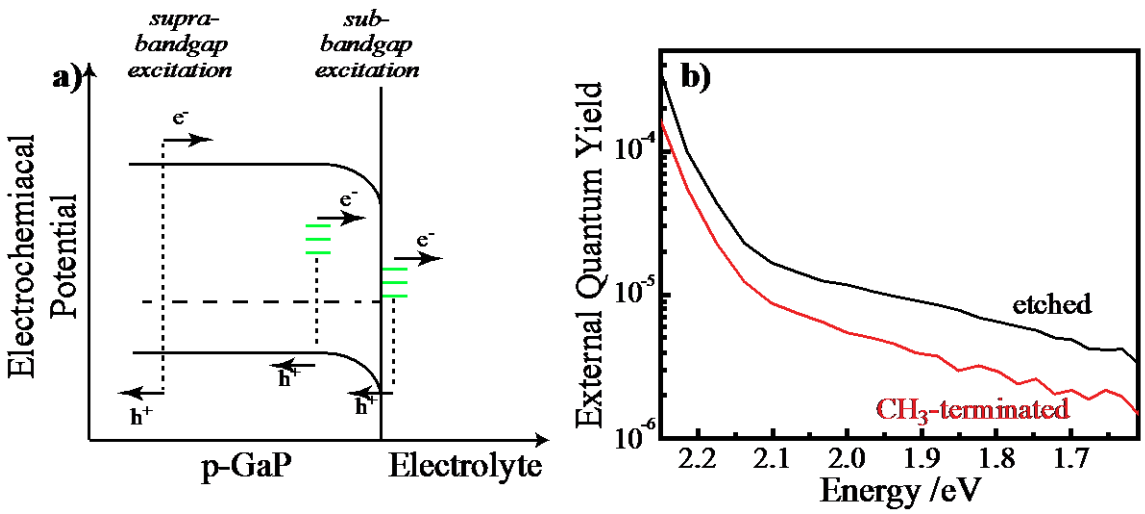

Figure 3.6 a) Schematic depiction of a p-type GaP photoelectrode under depletion conditions in contact with an electrolyte. Photoexcitation is shown for band-to-band transition from the absorption of supra-bandgap light and for band-to-state transition for sub-bandgap light. The dotted lines show excitation from supra-bandgap or sub-bandgap light. b) Wavelength-dependent external quantum yields measured at E = -0.6 V vs. Ag/AgCl bias in deaerated 0.1 M KCl solution for etched and CH_3-terminated p-GaP(111) photoelectrodes.

bandgap photocurrents can be vanishingly small. However, with chopped light and lock-in photocurrent detection, sub-bandgap photocurrents for p-GaP can be readily detected. Figure 3.6b highlights the measured external quantum yield (i.e., the total number of charge-carriers collected per incident photon) for sub-bandgap photocurrent at E = -0.6 V vs. Ag/AgCl for both etched and CH_3-terminated GaP(111)A. Both electrode types showed detectable levels of photocurrent consistent with photoexcitation involving mid-gap states in the bulk.[41] However, CH_3-terminated GaP(111)A photoelectrodes consistently yielded uniformly lower external quantum yield values. For reference, the external quantum yield measured for etched GaP(111)A photoelectrodes at 645 nm was 8 $\pm$ 1 x 10^{-6} but only 3 $\pm$ 2 x 10^{-6} for CH_3-terminated GaP(111)A electrodes (Table 3.1).

3.3.5 Sensitized Sub-bandgap Photoresponse of Etched and CH_3-terminated p-GaP(111)A

Photocurrent at sub-bandgap wavelengths can also be induced in p-GaP photoelectrodes through the addition of a sensitizer.[48-50] Recent studies indicate many triphenylmethane dyes are well suited to inject photoexcited holes into the valence band of etched GaP(111)A, thereby inducing a net cathodic current.[48,49] Brilliant Green, a triphenylmethane dye, is a positively charged sensitizer that readily sensitizes etched p-GaP(111)A without the need for a formal covalent attachment with the surface, i.e., Brilliant Green spontaneously physisorbs on etched GaP surfaces. Figure 3.7a shows a sensitized isotherm of the measured external quantum yield for sub-bandgap photocurrent for an etched p-GaP(111)A photoelectrode immersed in an aqueous electrolyte containing dilute amounts of Brilliant Green. The overall external quantum yield is low since the sensitized response represents injected charge from adsorbed dye on a flat planar interface. The data nominally show a typical adsorption profile, where the sensitized photocurrent plateaus at higher concentrations due to a ‘saturation’ of dye near the surface. Results for equivalent measurements using CH_3-terminated p-GaP(111)A photoelectrodes are also shown in Figure 3.7a. These data also showed a saturation of the measured external quantum yield for photocurrent at higher dye concentrations, albeit at a lower overall value than for etched GaP(111)A.

Table 3.1 Average External Quantum Yield of GaP(111)A at 650 nm.

Sample Treatment	Average External Quantum Yield at 650 nm[a]
H_2SO_4(aq)	8 ± 1 x 10^{-6}
CH_3MgCl	3 ± 2 x 10^{-6}

[a] N = 3 for each reported value

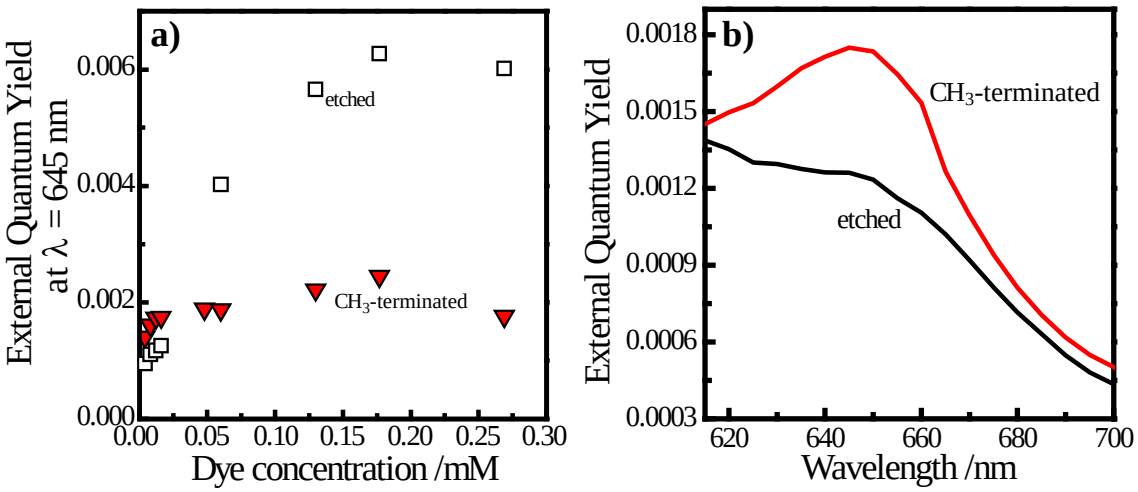

Figure 3.7 a) The measured external quantum yield at 645 nm for etched and CH_3-terminated GaP(111)A photoelectrodes at E = -0.6 V vs. Ag/AgCl in 0.1 M KCl as a function of dye (Brilliant Green) concentration. b) Wavelength-dependent external quantum yields measured for etched and CH_3-terminated GaP(111)A photoelectrodes. Measurement conditions were as in (a) with [Brilliant Green] = 16 μM.

In the absence of any change in surface roughness, the measured external quantum yields are a function of both the total amount of sensitizing dye at the electrode surface to inject charge and/or the net efficiency for charge-injection from an individual dye molecule into the electrode. The total surface coverages were not measured but should be most influential at high dye concentrations where the sensitized signal has reached a plateau. A lower surface coverage of the charged Brilliant Green dye under these conditions on CH_3-terminated GaP(111)A relative to etched GaP(111)A is broadly consistent with the more hydrophobic character of CH_3-terminated GaP(111)A.[30] Separately, the intrinsic external quantum yield for sensitized injection from individual dye molecules is more directly reflected in the data acquired for very low dye concentration. Under these conditions, the sensitized external quantum yield values were actually *higher* on CH_3-terminated p-GaP(111)A. Figure 3.7b further emphasizes this point, illustrating the spectral profile for the photocurrent responses with a very dilute concentration of dye in solution. The photoresponse for CH_3-terminated was uniformly higher, implying that sensitized hole injection from Brilliant Green into CH_3-terminated GaP(111)A was subject to fewer deleterious loss mechanisms. That is, the net efficiency for sensitization increases when the competing recombination pathways are minimized.[48] Since all the available recombination pathways involving either bulk traps or species dissolved in solution were the same in the experiments in Figure 3.7, the data thus argue that loss mechanisms at the GaP/electrolyte interface were specifically attenuated by introduction of $-CH_3$ groups.

3.4 DICUSSION

The presented data highlight three notable aspects of the impact of covalent modification of GaP by $-CH_3$ groups. In relation to unmodified GaP, CH_3-terminated GaP photoelectrodes (*1*) have substantially altered and more stable surface energetics in solution, (*2*) are significantly more resistant towards degradation pathways under passage of current, and (*3*) possess a measurably lower density of electronic defects/traps relevant to photocathode operation in water.

3.4.1 Surface Energetics of CH_3-terminated GaP

Two photoelectrochemical phenomena were observed here after modification of GaP with -CH_3 groups that follow previous reports on the photoelectrochemical behavior of Si after -CH_3 modification. Specifically, for Si electrodes, introduction of -CH_3 groups systematically shifted the band edge potentials to more negative values[23,51,52] and eliminated their pH-dependence.[21] A comparison of the magnitude of the shift of the band edge potentials between GaP and Si is difficult to ascertain unambiguously since etched GaP rapidly forms a native oxide upon exposure to the ambient.[14,16] Further, the specific packing and homogeneity of surface groups substantially impact the measurable surface energetics of a modified semiconductor interface.[53] Thus, precise measures of the energetics of etched GaP interfaces are not feasible in water. Still, the data presented here indicate that, as with Si, the effective band edge potentials of unmodified GaP surfaces immersed in aqueous acidic solutions are at much more positive values (> 0.2 V) than the CH_3-terminated surface, implying a net negative surface dipole imparted by -CH_3 groups.[19,21-23,28,53] Accordingly, covalent attachment of a well-ordered monolayer of -CH_3 groups is expected to shift the apparent band edge potentials of related semiconductors GaAs and GaN (alloys thereof) in a similar manner. Further, since the valence band edge potential is a critical parameter that affects whether a dye can act as a sensitizer of GaP,[48] modification with -CH_3 groups could increase the possible dye choices for GaP-based dye sensitized systems.

3.4.2 Stability of Surface Bonds at CH_3-terminated GaP

The invariance of the band edge potentials of CH_3-terminated GaP(111)A towards pH suggests a surface that has little/no Bronsted-Lowry acid/base character. Since -CH_3 groups are compact enough to fit on every atop site on the (111) surface, one interpretation is that the use of Grignard reagents to add -CH_3 groups is efficient enough to result in a monolayer coverage. Previous XP results separately indicated such a high surface coverage.[30] On other III-V surfaces where the spacing between atop sites is not enough to support a full monolayer or on this GaP surface with larger alkyl groups too large to pack densely, the insensitivity towards pH may not be as pronounced. The extant literature on Si electrodes modified with larger alkyl groups suggests that the sensitivity towards pH increases.[22] More experiments are needed to test this point for III-V

semiconductor surfaces of interest. Still, measurement of the dependence of the band edge energetics with [H^+] may prove useful as a simple diagnostic of surface coverage.

The observation that CH_3-terminated GaP(111)A surfaces are significantly more resistant against cathodic degradation *via* atop Ga atom reduction indicates a strong, inert surficial Ga-C bonds. One possible competing hypothesis for the observed stability after modification with -CH_3 groups is an increased electrocatalytic activity for H^+ reduction. However, the photocurrent-potential data shown here highlight an identical cathodic current breakdown for increased H^+ reduction at E < - 2.0 V vs Ag/AgCl for both electrode types (i.e., increased reduction current at extreme negative applied bias), indicating a comparable inactivity of both surfaces towards H^+. Further, since H^+ reduction in water is facilitated by favorable adsorption/desorption,[54] addition of an inert -CH_3 group is unlikely to participate in H^+ binding. Rather, the increased stability is a direct indication that the atop Ga atoms on CH_3-terminatd GaP(111)A are in a stable tetrahedral coordination environment, i.e., they behave more like fully bonded Ga atoms in the bulk rather than surface Ga atoms susceptible to chemical attack. The data shown here do not allow a quantitative measure of the Ga-C bond strength. However, as noted previously,[30] the observed stability enhancement imparted by covalently grafted -CH_3 groups suggests a stronger Ga-C bonding than found in simple trialkylgallium compounds. Similarly, Si surface studies have separately indicated that surface groups introduced by Grignard reagents translate into measurably better surface properties as compared to the same surface groups grafted through other chemistries.[55] Quantitative comparison between these surface Ga-C bonds, molecular Ga-C bonds, and surficial Si-C bonds would help better understand the surface bonding that results from the use of Grignard reagents.

3.4.3 Surface Defect Density of CH_3-terminated GaP

Precise estimates of surface defect density require the use of GaP substrates with much higher bulk charge-carrier lifetimes than those commercially available.[56] Still, the separate non-sensitized and sensitized sub-bandgap photoresponse measurements reported here directly implicate a lower level of deleterious surface traps on GaP(111)A following reaction with CH_3MgCl. On both Si[27] and GaAs,[29] decreased charge-carrier

recombination at surface states has been observed after alkylation *via* reaction with Grignard reagents. Accordingly, the observations here for GaP are in line with the premise that nucleophilic attack of the surface by Grignard reagents results in strongly chemisorbed -CH_3 groups that substantially change the bonding/anti-bonding orbitals of the semiconductor surface atoms. A key consequence is a shift of surface state energies away from the mid-gap point, decreasing their capacity as Shockley-Read-Hall recombination centers.[57,58]

3.5 SUMMARY

This work described photoelectrochemical properties of chemically modified p-type GaP in aqueous solutions. CH_3-terminated GaP(111)A photoelectrodes were found to have a flat-band potential that did not shift with solution pH, in contrast to bare (unmodified) GaP(111)A photoelectrodes. Under illumination, photocurrent-potential profiles for native and CH_3-terminated p-GaP photoelectrodes after prolonged cycling also showed a difference in stability. Grafting of the -CH_3 groups to the surface of GaP imparted a markedly enhanced chemical resistance against reductive degradation under illumination at negative applied bias. Further, a lowering of the active surface defect density was noted after modification of GaP(111)A with -CH_3 groups. In conjunction with earlier reports on the physicochemical properties of alkyl-terminated GaP surfaces, the collective data argue that wet chemical functionalization *via* Grignard chemistry is potent method for mediating the intrinsic surface chemistry deficiencies of GaP.

3.6 REFERENCES

(1) Woodhouse, M.; Herman, G. S.; Parkinson, B. A. Combinatorial Approach to Identification of Catalysts for the Photoelectrolysis of Water. *Chem. Mat.* **2005**, *17*, 4318-4324.

(2) Woodhouse, M.; Parkinson, B. A. Combinatorial Approaches for the Identification and Optimization of Oxide Semiconductors for Efficient Solar Photoelectrolysis. *Chemical Society Reviews* **2009**, *38*, 197-210.

(3) Woodhouse, M.; Parkinson, B. A. Combinatorial Discovery and Optimization of a Complex Oxide with Water Photoelectrolysis Activity. *Chem. Mat.* **2008**, *20*, 2495-2502.

(4) Parkinson, B. A. *Combinatorial Identification and Optimization of New Oxide Semiconductors*, 2012.

(5) Seley, D.; Ayers, K.; Parkinson, B. A. Combinatorial Search for Improved Metal Oxide Oxygen Evolution Electrocatalysts in Acidic Electrolytes. *Acs Combinatorial Science* **2013**, *15*, 82-89.

(6) He, J.; Parkinson, B. A. Combinatorial Investigation of the Effects of the Incorporation of Ti, Si, and Al on the Performance of alpha-Fe2O3 Photoanodes. *Acs Combinatorial Science* **2011**, *13*, 399-404.

(7) Tomkiewicz, M.; Woodall, J. M. Photoassisted Electrolysis of Water by Visible Irradiation of a p-Type Gallium Phosphide Electrode. *Science* **1977**, *196*, 990-991.

(8) Kocha, S. S.; Turner, J. A. Displacement of the Bandedges of GaInP2 in Aqueous Electrolytes Induced by Surface Modification. *J. Electrochem. Soc.* **1995**, *142*, 2625-2630.

(9) Khaselev, O.; Turner, J. A. Electrochemical Stability of p-GaInP2 in Aqueous Electrolytes Toward Photoelectrochemical Water Splitting. *J. Electrochem. Soc.* **1998**, *145*, 3335-3339.

(10) Hilal, H. S.; Turner, J. A. Controlling Charge-Transfer Processes at Semiconductor/Liquid Junctions. *Electrochimica Acta* **2006**, *51*, 6487-6497.

(11) Bansal, A.; Turner, J. A. Suppression of Band Edge Migration at the p-GaInP2/H2O Interface Under Illumination via Catalysis. *J. Phys. Chem. B* **2000**, *104*, 6591-6598.

(12) Dare-Edwards, M. P.; Hamnett, A.; Goodenough, J. B. The Efficiency of Photogeneration of Hydrogen at p-type III-V Semiconductors. *J. Electroanal. Chem.* **1981**, *119*, 109-123.

(13) Gronet, C. M.; Lewis, N. S. Design of a 13-Percent Efficient n-GaAs1-xPx Semiconductor-Liquid Junction Solar-Cell. *Nature* **1982**, *300*, 733-735.

(14) Gerischer, H. Electrolytic Decomposition and Photo-decomposition of Compound Semiconductors in Contact with Electrolytes *J. Vac. Sci. Technol.* **1978**, *15*, 1422-1428.

(15) Price, M. J.; Maldonado, S. Macroporous n-GaP in Nonaqueous Regenerative Photoelectrochemical Cells. *J. Phys. Chem. C* **2009**, *113*, 11988-11994.

(16) Mukherjee, J.; Erickson, B.; Maldonado, S. Physicochemical and Electrochemical Properties of Etched GaP(111)A and GaP(111)B Surfaces. *J. Electrochem. Soc.* **2010**, *157*, H487-H495.

(17) Gershenzon, M.; Mikulyak, R. M. Radiative Pair Recombination and Surface Recombination in GaP Photoluminescence. *Appl. Phys. Lett.* **1966**, *8*, 245-247.
(18) Stringfellow, G. B. Effect of Surface Treatment on Surface Recombination Velocity and Diode Leakage in GaP. *J. Vac. Sci. Technol.* **1976**, *13*, 908-913.
(19) Bansal, A.; Li, X. L.; Lauermann, I.; Lewis, N. S.; Yi, S. I.; Weinberg, W. H. Alkylation of Si Surfaces Using a Two-Step Halogenation Grignard Route. *J. Am. Chem. Soc.* **1996**, *118*, 7225-7226.
(20) Bansal, A.; Lewis, N. S. Stabilization of Si Photoanodes in Aqueous Electrolytes Through Surface Alkylation. *J. Phys. Chem. B* **1998**, *102*, 4058-4060.
(21) Hamann, T. W.; Lewis, N. S. Control of the stability, electron-transfer kinetics, and pH-dependent energetics of Si/H2O interfaces through methyl termination of Si(111) surfaces. *J. Phys. Chem. B* **2006**, *110*, 22291-22294.
(22) Johansson, E.; Boettcher, S. W.; O'Leary, L. E.; Poletayev, A. D.; Maldonado, S.; Brunschwig, B. S.; Lewis, N. S. Control of the pH-Dependence of the Band Edges of Si(111) Surfaces Using Mixed Methyl/Allyl Monolayers. *J. Phys. Chem. C* **2011**, *115*, 8594-8601.
(23) Maldonado, S.; Plass, K. E.; Knapp, D.; Lewis, N. S. Electrical Properties of Junctions Between Hg and Si(111) Surfaces Functionalized with Short-Chain Alkyls. *J. Phys. Chem. C* **2007**, *111*, 17690-17699.
(24) Bansal, A.; Lewis, N. S. Electrochemical Properties of (111)-Oriented n-Si Surfaces Derivatized with Covalently-Attached Alkyl Chains. *J. Phys. Chem. B* **1998**, *102*, 1067-1070.
(25) Boukherroub, R.; Morin, S.; Bensebaa, F.; Wayner, D. D. M. New Synthetic Routes to Alkyl Monolayers on the Si(111) Surface. *Langmuir* **1999**, *15*, 3831-3835.
(26) Plass, K. E.; Liu, X. L.; Brunschwig, B. S.; Lewis, N. S. Passivation and Secondary Functionalization of Allyl-Terminated Si(111) Surfaces. *Chem. Mat.* **2008**, *20*, 2228-2233.
(27) Royea, W. J.; Juang, A.; Lewis, N. S. Preparation of Air-Stable, Low Recombination Velocity Si(111) Surfaces through Alkyl Termination. *Appl. Phys. Lett.* **2000**, *77*, 1988-1990.
(28) O'Leary, L. E.; Johansson, E.; Brunschwig, B. S.; Lewis, N. S. Synthesis and Characterization of Mixed Methyl/Allyl Monolayers on Si(111). *J. Phys. Chem. B* **2010**, *114*, 14298-14302.
(29) Peczonczyk, S. L.; Mukherjee, J.; Carim, A. I.; Maldonado, S. Wet Chemical Functionalization of III-V Semiconductor Surfaces: Alkylation of Gallium Arsenide and Gallium Nitride by a Grignard Reaction Sequence. *Langmuir* **2012**, *28*, 4672-4682.
(30) Mukherjee, J.; Peczonczyk, S.; Maldonado, S. Wet Chemical Functionalization of III-V Semiconductor Surfaces: Alkylation of Gallium Phosphide Using a Grignard Reaction Sequence. *Langmuir* **2010**, *26*, 10890-10896.
(31) Peczonczyk, S. L.; Brown, E. S.; Maldonado, S. Secondary Functionalization of Allyl-Terminated GaP(111)A Surfaces via Heck Cross-Coupling Metathesis, Hydrosilylation, and Electrophilic Addition of Bromine. *Langmuir* **2014**, *30*, 156-164.

(32) Wen, W.; Carim, A. I.; Collins, S. M.; Price, M. J.; Peczonczyk, S. L.; Maldonado, S. Structural and Photoelectrochemical Properties of GaP Nanowires Annealed in NH3. *J. Phys. Chem. C* **2011**, *115*, 22652-22661.

(33) Barr, T. L.; Seal, S. Nature of the Use of Adventitious Carbon as a Binding-Energy Standard. *J. Vac. Sci. Technol., A* **1995**, *13*, 1239-1246.

(34) Gierst, L.; Cornelissen, P. Linfluence de la Nature et de la Concentration de Lelectrolyte-Support dur la Morphologie des ondes Polarographiques du Systeme EuII-EuIII. *Collection of Czechoslovak Chemical Communications* **1960**, *25*, 3004-3015.

(35) Timmer, B.; Sluyters.M; Sluyters, J. H. On Impedance of Galvanic Cells. 19. Potential Dependence of Faradaic Impedance in Case of an Irreversible Electrode Reaction--Experimental Verification for Redox Couple Eu3+/Eu2+ in 1M NaClO4 and Mechanism of Zn2+/Zn(Hg) Reaction in KCl. *J. Electroanal. Chem.* **1967**, *14*, 181-&.

(36) Green, M. A. Capacitance of Large Barrier Schottky Diodes. *Solid-State Electronics* **1976**, *19*, 421-422.

(37) Bard, A. J., Faulkner, L.R. *Electrochemical Methods: Fundamentals and Applications*; 2nd ed. ed.; John Wiley & Sons, Inc.: Hoboken, NJ, 2001.

(38) Pomykal, K. E.; Fajardo, A. M.; Lewis, N. S. Theoretical and Experimental Upper Bounds on Interfacial Charge-Transfer Rate Constants Between Semiconducting Solids and Outer-Sphere Redox Couples. *J. Phys. Chem.* **1996**, *100*, 3652-3664.

(39) Fajardo, A. M.; Lewis, N. S. Free-Energy Dependence of Electron-Transfer Rate Constants at Si/Liquid Interfaces. *J. Phys. Chem. B* **1997**, *101*, 11136-11151.

(40) Morrison, S. R. *Electrochemistry at Semiconductor and Oxidized Metal Electrodes*; Plenum: New York, 1980.

(41) Butler, M. A.; Ginley, D. S. P-type GaP as a Semiconducting Photoelectrode. *J. Electrochem. Soc.* **1980**, *127*, 1273-1278.

(42) Horowitz, G. Flatband Potential of a p-type Phosphide Electrode *J. Appl. Phys.* **1978**, *49*, 3571-3573.

(43) Tan, M. X.; Laibinis, P. E.; Nguyen, S. T.; Kesselman, J. M.; Stanton, C. E.; Lewis, N. S. Principles and Applications of Semiconductor Photoelectrochemistry. *Progress in Inorganic Chemistry, Vol 41* **1994**, *41*, 21-144.

(44) Leonhard.G; Berndtss.A; Hedman, J.; Klasson, M.; Nilsson, R.; Nordling, C. ESCA Studies of Some A-IIIB-V Compounds with Ga and A. *Physica Status Solidi B-Basic Research* **1973**, *60*, 241-248.

(45) Chazalviel, J. N.; Stefenel, M.; Truong, T. B. Surface-States Induced by Metal Atoms at the Si Electrolyte Interface. *Surf. Sci.* **1983**, *134*, 865-885.

(46) Chazalviel, J. N. Photocurrent Spectroscopy of Interface States at a Semiconductor-Electrolyte Junction. *J. Electrochem. Soc.* **1980**, *127*, 1822-1826.

(47) Butler, M. A.; Ginley, D. S. Surface-Treatment Induced Sub-Band Gap Photoresponse of GaP Photoelectrodes. *J. Electrochem. Soc.* **1981**, *128*, 712-714.

(48) Chitambar, M.; Wang, Z. J.; Liu, Y. M.; Rockett, A.; Maldonado, S. Dye-Sensitized Photocathodes: Efficient Light-Stimulated Hole Injection into p-GaP Under Depletion Conditions. *J. Am. Chem. Soc.* **2012**, *134*, 10670-10681.

(49) Choi, D.; Rowley, J. G.; Parkinson, B. A. Dye Sensitization of n and p Type Gallium Phosphide Photoelectrodes. *J. Electrochem. Soc.* **2012**, *159*, H846-H852.

(50) Memming, R.; Tributsch, H. Electrochemical Investigations on Spectral Sensitization of Gallium Phosphide Electrodes. *J. Phys. Chem.* **1971**, *75*, 562-570.
(51) Li, Y.; O'Leary, L. E.; Lewis, N. S.; Galli, G. Combined Theoretical and Experimental Study of Band-Edge Control of Si through Surface Functionalization. *J. Phys. Chem. C* **2013**, *117*, 5188-5194.
(52) Maldonado, S.; Lewis, N. S. Behavior of Electrodeposited Cd and Pb Schottky Junctions on CH3-Terminated n-Si(111) Surfaces. *J. Electrochem. Soc.* **2009**, *156*, H123-H128.
(53) Makinen, A. J.; Kim, C. S.; Kushto, G. P. Monolayer-Induced Band Shifts at Si(100) and Si(111) Surfaces. *Appl. Phys. Lett.* **2014**, *104*.
(54) Norskov, J. K.; Bligaard, T.; Logadottir, A.; Kitchin, J. R.; Chen, J. G.; Pandelov, S. Trends in the Exchange Current for Hydrogen Evolution. *J. Electrochem. Soc.* **2005**, *152*, J23-J26.
(55) Webb, L. J.; Lewis, N. S. Comparison of the Electrical Properties and Chemical Stability of Crystalline Silicon(111) Surfaces Alkylated using Grignard Reagents or Olefins with Lewis Acid Catalysts. *J. Phys. Chem. B* **2003**, *107*, 5404-5412.
(56) Orton, J. W., Blood, P. *Measurement of Minority Carrier Properties*; Academic Press: London, 1990.
(57) Fonash, S. J. *Solar Cell Device Physics, 2nd Edition*, 2010.
(58) Heller, A. In *Photoeffects at Semiconductor-Electrolyte Interfaces*; Nozik, A. J., Ed.; American Chemical Society: Washington, D.C., 1981; Vol. 146, p 55-77.

CHAPTER 4

Chemically Modified Si(111) Surfaces Simultaneously Demonstrating Hydrophilicity, Resistance Against Oxidation, and Low Trap State Densities

Reprinted from Surface Science, Vol. 645, Chemically Modified Si(111) Surfaces Simultaneously Demonstrating Hydrophilicity, Resistance Against Oxidation, and Low Trap State Densities, Brown, E.S.; Hlynchuk, S.; Maldonado, S., 49-55, Copyright 2016, with permission from Elsevier.

4.1 INTRODUCTION

This chapter discusses chemically modified Si(111) surfaces through a series of wet chemical surface treatments that simultaneously show resistance towards surface oxidation, selective reactivity towards chemical reagents, and areal defect densities comparable to unannealed thermal oxides. These reaction strategies were targeted for eventual transfer to GaP(111)A for cationic iminium dye attachment, which are known to sensitize p-GaP.[1] With no Ga LMM Auger peak interference in the N 1s spectrum, Si(111) was a model substrate for determining reactions and strategies while simultaneously having novel merit for processed optoelectronic technologies.

Three features are highly desirable in semiconductor interfaces when used to construct optoelectronic technologies. First, the chemical integrity of the semiconductor surface must be both compatible with all device fabrication/metallurgical steps. Second, the electrical quality of each semiconductor interface must be sufficiently good so as not to present an operational bottleneck or otherwise adversely affect the device. Third, the semiconductor surface should be (and remain) either highly conducting or insulating (depending on the application) with respect to heterogeneous charge transfer. No native semiconductor surface perfectly and simultaneously demonstrates these aspects, motivating

the development of new and improved chemical modification strategies of semiconductor interfaces.

Vapor phase atomic layer deposition (ALD)[2,3] and spin casting of aqueous metal oxo cluster solutions[4,5] are highly advantageous for rapidly and simply constructing high quality semiconductor heterojunctions. However, they are best suited for hydrophilic semiconductor interfaces that can withstand elevated temperatures and have proton donating/accepting character. The majority of technologically relevant Groups IV and III-V have native interfaces that do not possess these attributes in addition to retaining a low defect density. Although native oxides on such semiconductors are generally hydrophilic,[6,7] they possess deleterious levels of trap states. Of the few high quality oxides (e.g. annealed thermal oxide Si(100)[8]), they are naturally insulating. Chemical methods to eliminate electrically active surface states on Groups IV and III-V surfaces (e.g. etching with NH_4F;[9] lattice matched AlGaAs epilayers[10]) render surfaces that have too few nucleation sites for ALD[11] and/or are neither wettable nor stable towards exposure to aqueous solutions.[12-20]

This report focuses on the potential of wet chemical surface modification to yield semiconductor surfaces that are jointly hydrophilic, resistant against oxidation, and possesses a low level of surface defects. Using single crystalline Si(111) as a model surface, we demonstrate organically modified interfaces prepared through a sequence of reactions involving Grignard reagents[21,22] and subsequent activation steps. Specifically, we show the preparation of Si(111) surfaces decorated with either a terminal primary alcohol, a terminal diol, or a terminal amine group (Figure 4.1). Distinctions between the surfaces prepared here and the prior art in organically-modified Si surfaces[23-34] are drawn through measurements of oxide growth via X-ray photoelectron spectroscopy, contact angle wetting measurements, reactivity towards model test reagents, and surface recombination velocities, *S*, of photogenerated carriers. The purpose of the work is to not only identify the attainable physicochemical properties of these modified Si interfaces but more generally to show that semiconductor surfaces that are reactive towards modification by Grignard reagents can be deterministically tailored as needed.

4.2 EXPERIMENTAL

4.2.1 Materials and Chemicals

All chemicals were purchased from Sigma-Aldrich and used as received unless noted. Methanol (anhydrous >99.8%,), chlorobenzene (Acros, 99.8%), tetrahydrofuran (THF) (anhydrous ≥ 99.9%, inhibitor free), acetone (Fisher, HPLC grade), hexanes (Macron Chemicals, ACS grade), dichloromethane (anhydrous > 99.8%), phosphorus (V) oxychloride, borane-tetrahydrofuran (1 M), diethyl ether (anhydrous), potassium bis(trimethylsilyl)amide (KHMDS), 40% ammonium fluoride (Transene Electronic Chemicals, semiconductor grade), sodium hydroxide (Fisher, 95.0 to 100.5% FCC grade), 30wt% in H_2O hydrogen peroxide (ACS grade), trifluoroacetic acid (TFA) (99%), 2,2,3,3,4,4,5,5-octafluoro-1-pentanol (98%), and 37% hydrochloric acid (ACS grade) were used as received. Methylmagnesium chloride (3.0 M), allyl magnesium chloride (2.0 M), and 4-[bis(trimethylsilyl)amino]phenyl magnesium bromide (0.5 M) were used as received. 3,4-(methylenedioxy)phenylmagnesium bromide (1.0 M) was diluted to 0.5 M with THF to help prevent polymerization during reaction. 4-(trifluoromethyl)benzyl bromide (Sigma-Aldrich, 98%) was outgassed by three freeze-pump-thaw cycles before use. Benzoyl peroxide (Fluka, ≥ 97%) was dried under a vacuum of < 200 mTorr for at least 24 h and placed in the nitrogen-atmosphere glovebox. Water with a resistivity of 18.2MΩ cm^{-1} (Barnsted Nanopure system) was used throughout. For surface characterization studies, one-side polished, n-type Si (111) wafers doped with As were purchased from Wafer Works Corp. and had thickness of 525 ± 15 μm. For SRV measurements, float-zone (FZ), intrinsically-doped Si(111) (El-Cat) wafers with a resistivity equal to 16500 ± 3500 Ω·cm, a thickness of 460 ± 15 μm, and both sides polished were used.

4.2.2 Sample Preparation

Samples were diced into 0.5 cm by 0.5 cm squares for surface characterization and into 1 cm by 1.5 cm rectangles for SRV measurements. Si(111) samples were etched prior to use in 40% NH_4F solution for 5 minutes while continuously purging with nitrogen gas, rinsed with water, and dried in a stream of nitrogen gas. Immediately after etching, wafers were transferred to a nitrogen-purged glove box. Freshly etched wafers were chlorinated at 90°C for 50 minutes using a saturated solution of phosphorous (V) pentachloride in chlorobenzene, to which a few grains of benzoyl peroxide were added.[35] Following the chlorination step, samples were washed with THF, dried in the glovebox, and transferred to reaction vessels to which designated Grignard reagents were added (Figure 4.1).

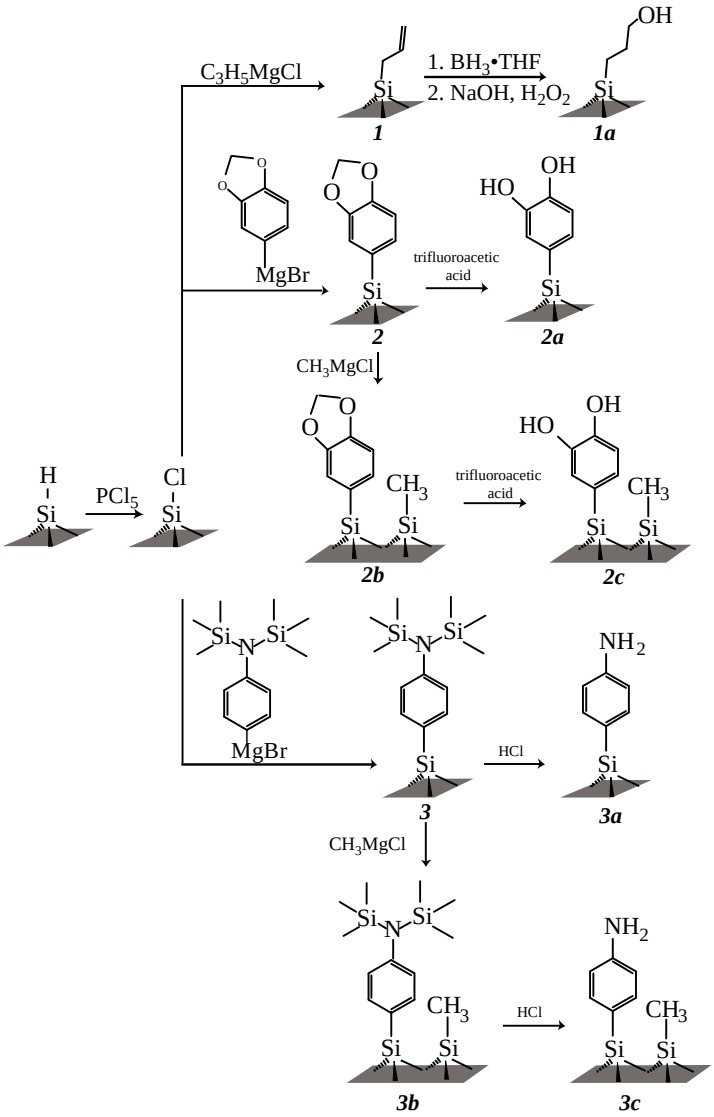

Figure 4.1 Chemical modification routes for Si surfaces outlined in this work.

4.2.3 Preparation of *1* and *1a*

Chlorinated wafers were transferred to closed reaction vessels to which a solution of allylmagnesium chloride was added. Reaction solution was heated for 13 h at 110 ± 5°C. Samples were rinsed with THF and methanol (**1**). To prepare ***1a*** surfaces, ***1*** surfaces were hydroborated and hydroxylated with a procedure modified from Toledano, *et al.*[31] In a nitrogen-purged glove box, ***1*** wafers were immersed in a solution of BH_3 •THF complex at room temperature for 5 h , rinsed with THF and allowed to dry, and transferred to a round bottom flasks, sealed with a rubber stopper and taken out of the glove box. To the flask, 1 mL 3 M NaOH and 1 mL 30% H_2O_2 injected through a rubber septum via syringe were added stepwise. After 20 min at room temperature, the wafers were removed from the flask, washed with water and methanol, and dried under a stream $N_{2(g)}$.

4.2.4 Preparation of *2, 2a, 2b* and *2c*

Chlorinated wafers were transferred to closed reaction vessels to which a solution of 3,4-(methylenedioxy)phenylmagnesium bromide was added and diluted to 0.5 M. Reaction temperature was reduced to 90 ± 5°C to prevent polymerization of the reagent. Upon completion, samples were rinsed with THF and methanol (***2***). Samples were either backfilled with methylmagnesium chloride in a new reaction vessel for additional 13 h at 110 ± 5°C, rinsed with THF and methanol, and dried in the glovebox (***2b***) or deprotected with a solution of TFA:THF:H_2O (1:20:5) for 4 h at room temperature outside of the glovebox (***2a*** and ***2c***).[36]

4.2.5 Preparation of *3, 3a, 3b* and *3c*

Chlorinated wafers were transferred to closed reaction vessels to which a solution of 4-[bis(trimethylsilyl)amino]phenyl magnesium bromide was added. Reaction vessel was heated to 110 ± 5°C for 12-16 h, samples were rinsed with THF and methanol, and allowed to dry in the glovebox (***3***). Samples were either backfilled with methylmagnesium chloride in a new reaction vessel for additional 3 h at 90 ± 5°C, rinsed with THF and methanol, and dried in the glovebox (***3b***) or deprotected with a 20% v/v HCl solution for 1 h at room temperature outside of the glovebox (***3a*** and ***3c***).

4.2.6 Nucleophilic Reaction with 4-(trifluoromethyl)benzyl bromide.

In the glovebox, samples were reacted with 0.02 M TFB with <1 mg KHMDS in hexanes at 60°C for 1 h. Samples were rinsed with hexanes, diethyl ether, and methanol, sonicated in methanol for 2 min, and dried with a stream of nitrogen gas.

4.2.7 X-ray Photoelectron Spectroscopy

Elemental composition of functionalized Si(111) surfaces was collected using a PHI 5400 analyzer equipped with Al K α(1486.6 eV) source, without a monochromator. Acquisition took place at a pressure of < 2.5×10^{-9} torr, without the need for charge neutralization due to the natural conductivity of the samples. A 6 mA current emission and a 12 kV anode high tension were used. For each sample survey scans were recorded between 0 and 1350 eV at pass energy of 117.40 eV. While high resolution spectra were collected at pass energy of 23.5 eV. All binding energies were referenced to the expected binding energy for adventitious carbon (284.6 eV).[37] Spectrum analysis was performed with CASA XPS 2.3.13 software. Further characterization of the surfaces were performed by calculating oxide thickness using a simplified substrate/overlayer model[38] and calculating fractional monolayer coverage of the surface using three-layer model.[39]

For surface oxides, the thickness of oxide at the surface was calculated using the simplified substrate overlayer model,[38]

$$d = \lambda_{ov} \sin\varphi \left(\ln\left(1 + \frac{I_{overlayer}}{I_{substrate}} \frac{I^{0}{}_{substrate}}{I^{0}{}_{overlayer}} \right) \right)$$

Equation 4.1 Simplified Substrate Overlayer Equation.

where d is the thickness of the oxide overlayer in nanometer, λ_{ov} is escape depth of emitted electrons through the oxide layer, φ is the takeoff angle (54.6°) between the sample surface and the detector, I is the integrated area as follows: $I_{substrate}$ for bulk signal, $I_{overlayer}$ of oxide signals, $I^{0}{}_{substrate}$ for Si freshly etched in NH_4F for 1 min, $I^{0}{}_{overlayer}$ for a thick (>500 nm) thermal oxide layer on Si. The escape depth for electrons was estimated:

$$\lambda = 0.41 A^{3/2} E^{1/2}$$

Equation 4.2 Electron Escape Depth Calculation.

where A is the mean diameter of one unit in the overlayer (nm) and E is the kinetic energy of the ejected core electron (eV).

The mean diameter of one unit, *A*, is

$$A = \sqrt[3]{\frac{MW}{\rho N_A}}$$

Equation 4.3 Mean Diameter Calculation.

where *MW* is mean atomic weight (g mol^{-1}), ρ is the density (g cm^{-3}), and N_A is Avogadro's number.

Due to the larger size of all molecules tested here, a simple model of three-layer structure was used for monolayer coverage calculations.[39] For calculations of coverage of ***3a***, the high resolution N 1s XP spectrum was used. Aniline was used as a model molecule and parameters of interest are listed in Table 4.1. The topmost layer included the $-NH_2$ (t_1), the Si substrate served as the bottom layer (*sub*) and the linker in between t_1 and the substrate served as t_2 (Figure 4.2).

To calculate overlayer coverage using the simple three-layer model, Equation 4.4 was adopted from Asami, *et al*.[4]

$$\frac{I_{ov}}{I_{sub}} = \left(\frac{SF_{ov}}{SF_{sub}}\right)\left(\frac{\rho_{ov}}{\rho_{sub}}\right)\left(\frac{1-e^{\left[\frac{-t_1}{\lambda_{ov}\cos\varphi}\right]}}{e^{\left[\frac{-(t_1+t_2)}{\lambda_{sub}\cos\varphi}\right]}}\right)$$

Equation 4.4 Three-Layer Model for Monolayer Calculation.

where SF_{sub} is the sensitivity factor for the element of interest in the substrate, SF_{ov} is the instrument sensitivity factor for the element of interest in the substrate, ρ_{ov} is the density of the element of interest in the overlayer. For Si, ρ_{sub} is 2.32 g cm^{-3} and SF_{sub} is 0.339.[42] Parameters referring to *ov* are referencing the topmost layer containing an *N* atom in this situation. The variable t_1 is the thickness of the second layer and t_2 is the thickness of the intermediate layer. Values of t_1 and t_2 were approximated using known data from model molecules, which are listed in Table 4.1, and using previously reported data on bond lengths and molecule size.[40,41,43] The sum of the thicknesses is *d*, the total thickness of the organic overlayer. The following relationship also holds true:

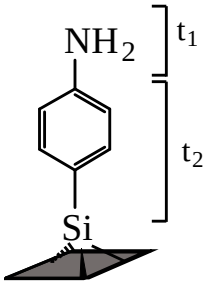

Figure 4.2 Surface Labeled with t_1 and t_2.

Table 4.1 Monolayer Coverage Calculation Parameters for Various Reactants.

Surface Type (Element Measured)	ρ (g cm^{-3})	n	a_m (nm)	λ_x	λ_{Si}	SF[a]	Length (nm) [b]	No. Density (atoms cm^{-2})
3a (N 1s)[c]	1.20	0.40	0.502	5.26	5.94	0.477	0.70	4.22 x 10^{14}
***1a*+TFB** (F 1s)[d]	1.30	0.18	0.641	5.95	7.83	1.0	1.08	2.44 x 10^{14}
***2a*+TFB** (F 1s)[e]	1.30	0.14	0.815	8.53	11.23	1.0	1.51	1.52 x 10^{14}
***3a*+TFB** (F 1s)[f]	1.32	0.14	0.672	6.38	8.41	1.0	1.38	2.22 x 10^{14}

[a]*SF* values from Asami, *et al*.[39] [b]Molecule lengths were estimated from tabulated bond length values.[40,41] [c]Parameters for aniline were used. [d]Parameters for methyl 4-(trifluoromethyl)benzyl ether were used. [e]MW and density were obtained from Chemdraw approximation since data could not be found for analogous structures. Values were also used for ***2c***+TFB. [f]Parameters for N-phenyl-3-(trifluoromethy)aniline were used. Values were also used for ***3c***+TFB.

$$t_1 = nt_2$$

Equation 4.5 Relationship Between Two Sub-Layers in Three-Layer Model.

where *n* is the ratio of thicknesses of the two layers. The relationship was entered into the equation in place of t_2 and subsequently t_1 was solved for. Total thickness of the organic layer was calculated:

$$d = t_1 + t_2$$

Equation 4.6 Relationship Between Total Overlayer Thickness and Two Sub-Layers.

Monolayer coverage was calculated:

$$ML = \frac{d}{d_{lit}}$$

Equation 4.7 Monolayer Coverage Relationship.

where d_{lit} is the sum of expected lengths t_1 and t_2 published in the literature.[43,44] This value indicates the amount of total possible aniline molecules on the surface. Fractional monolayer coverage, θ, was calculated to determine the number of aniline molecules per atop Si atom. Converting the density of aniline to number density (atoms cm^{-2}) and multiplying by the monolayer coverage, we divide by the number of unreconstructed atop atoms on Si(111) (7.83×10^{-14} atoms cm^{-2}) to get θ.[45]

For calculations of surface coverage after etherification, the topmost layer included the $-CF_3$ (t_1), the Si substrate served as the bottom layer (*sub*), and the linker in between t_1 and the substrate served as t_2 (Figure 4.3). Here, *ov* is referencing the topmost layer containing F atoms and the value of I_{ov} was divided by 3 to account for three F atoms per molecule. The F 1s intensities of ***2a*** and ***2c*** surfaces reacted with TFB were divided by 6 to account for attachment of more than one TFB molecule. Parameters of interest are tabulated in Table 4.1.

Tabulated ML coverage and θ values for surface reactions on Si(111) quantified by XP spectra are shown in Table 4.2.

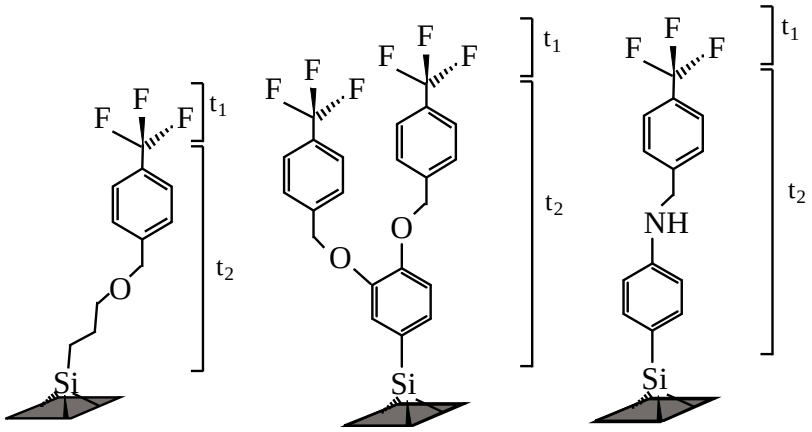

Figure 4.3 Modified Si(111) surfaces after reaction with 4-(trifluoromethyl)benzyl bromide.

Table 4.2 Monolayer Coverage and Fractional Coverage (θ) of Modified Si(111) Surfaces.

Surface	ML Coverage	θ
***1a*+TFB**	0.60	0.19
***2a*+TFB**	1.13	0.22
***2c*+TFB**	1.03	0.21
***3a*[a]**	0.91	0.49
***3a*+TFB**	0.78	0.22
***3c*[a]**	0.93	0.50
***3c*+TFB**	0.63	0.18

[a]Calculated with N 1s XP spectra. All other ML values calculated with F 1s spectra.

4.2.8 Infrared Spectroscopy

Infrared spectra were acquired using a Thermo- Fisher 6700 FT-IR spectrometer equipped with a deuterated triglycerine sulfate (DTGS) detector and a Ge hemisphere grazing angle attenuated total reflectance (GATR) accessory. P-polarized light at an incident angle of 65^{o} was applied and spectra were recorded with 4 cm^{-1} resolution and referenced to spectrum of clean Ge hemisphere.

4.2.9 Static Sessile Drop Contact Angle Measurements

Surface wettability was determined by recording the contact angles of water droplets formed on functionalized surfaces. CAM 100 optical contact angle meter (KSV instrument, Helsinki, Finland) and KSV software analysis package were utilized during data collection and analysis.

4.2.10 Surface Recombination Velocity Measurement

A custom-built microwave photoconductivity system[39,46] was used to measure the minority carrier lifetime in Si wafer sections after various surface treatments. Float-grown Si with low resistivity (R > 13000 ohm cm) and a thickness of 0.046 cm was used exclusively for these measurements. A Continuum Minilite Nd:YAG laser operating at λ = 1064 nm was used to produce excitation pulses with a full-width at half-maximum of < 10 ns. Photoexcitation was performed on the sample side opposite of where microwave radiation was incident. The microwave source was a HP 8350B Sweep Oscillator with a 83570A module operating at a frequency of 18.670 GHz and a nominal output power of 3.16 mW. The reflected signal was measured with an Advanced Control Devices diode (ACSP2644NZ, rise time < 1 ns) connected to a Tektronix TDS 1002B digital oscilloscope. The transient responses were normalized by the reflected signal at t = 0 and plotted as '$\Delta P/P_0$'. The apparent photoconductivity lifetime, τ, was then determined from plots of $\Delta P/P_0$ vs t through a fit with a single exponential function. The explicit relation between τ and the surface recombination velocity, S, is given in Equation 4.8,[47]

$$\frac{1}{\tau} = \frac{1}{\tau_b} + \left(\frac{2S\pi^2 D}{W\pi^2 D + 2SW^2} \right)$$

Equation 4.8 Relationship Between Lifetime and Surface Recombination Velocity.

where τ_b is the bulk lifetime of the Si wafer section, D is the ambipolar diffusion constant in crystalline Si (10 cm^2 s^{-1} at T = 300 K)[48], and W is the wafer thickness. Equation 4.8 defines several important bounds. The shortest time constant (= $W^2\pi^{-2}D^{-1}$) occurs when S is infinitely large. For the materials used here, the shortest measurable value of τ is 2 x 10^{-5} s. The largest possible value of τ occurs when S = 0 cm s^{-1} and corresponds exactly to τ_b. According to the manufacturer, τ_b > 2 x 10^{-3} s for the wafers used here. All values of τ measured between these two bounds thus report on S. Since $\pi^2 D >> 2SW$ for S <10^3 cm s^{-1} for all measured samples, the following approximation was used to estimate S.

$$\frac{1}{\tau} = \frac{1}{\tau_b} + \frac{2S}{W}$$

Equation 4.9 Relationship Between Lifetime and Surface Recombination Velocity when Wafer Thickness Is Small.

4.3 RESULTS

Three different surface terminations were evaluated for achieving a hydrophilic, stable, and electronically passivated surface (Figure 4.1). After etching with NH_4F(aq) and then chlorination with PCl_5 in chlorobenzene, samples were reacted with one of three Grignard reagents to achieve surfaces decorated by either an allyl group, a cyclic diether, or a bis(trimethylsilyl)amino group. We henceforth refer to these surfaces as types ***1***, ***2***, and ***3*** (Figure 4.1). These surfaces were subsequently modified by introducing Bronsted-Lowry functionality without affecting the underlying putative Si-C bond. The resultant surfaces were selectively decorated with primary alcohols, diols, and amine groups. These surfaces are henceforth denoted as types ***1a***, ***2a***, and ***3a***. The characterization and properties of each surface are described individually below.

4.3.1. Passivated Surfaces Featuring Chemisorbed Primary Alcohols (1a)

The preparation of Si surfaces decorated with allyl groups was first described by Lewis and co-workers.[49] In this work, we specifically set out to selectively oxidize the terminal olefin to a primary alcohol, i.e. the anti-Markovnikov addition of an alcohol across the '-C=C-' group. A hydroboration/hydroxylation method was employed, similar to an approach used to oxidize surface-grafted 1-decene reported previously by Cahen and co-workers.[31] That procedure was modified for surface ***1*** by extending both hydroboration times (>5 h) and subsequent hydroxylation (20 min) as long as possible without inducing surface oxidation, as monitored by high resolution Si 2p XP spectra. These surfaces are denoted as type ***1a***. The oxide thickness inferred from the integrated intensity of the shoulder centered at 103 eV was below <0.09 nm (Figure 4.4a). Before reaction, a peak for the C=C-H stretch at 3051 cm^{-1} was observable in the infrared spectrum but was absent after reaction (Figure 4.4b). Further, analysis of GATR-IR spectra of ***1a*** resulted in a peak at 1265 cm^{-1} ascribed to COH bend of primary alcohols (Figure 4.5) and no signatures at 2500-3000 cm^{-1} that indicated oxidation to a terminal carboxylic acid group (Figure 4.6). The wetting properties of type ***1*** and ***1a*** surfaces were decidedly different, with the sessile contact angles with water of 75 ± 5° to 42 ± 3°, respectively (Table 4.3). This contact angle value for type ***1a*** surfaces is broadly in agreement with the value of 50° demonstrated by Zhong and Bernasek for Si surfaces decorated with long primary alcohols.[50] The reactivity of type ***1a*** surfaces was probed with test reagents so as to identify the predominant surface group (e.g. alcohol, carboxylic acid). Specifically, we attempted to perform both an etherification reaction with an organic halide and an esterification reaction with a primary alcohol. The hypothesis was that a surface decorated with primary alcohols is only reactive (under the employed reactions) towards organic halides for ether bond formation and wholly unreactive towards molecular alcohols. Upon reaction of ***1a*** with 4-(trifluoromethyl)benzyl bromide (TFB) as shown in Figure 4.7, a new signal was observed in the F 1s XP spectrum (Figure 4.4c). Fractional coverage was calculated to be 0.19 molecules per Si atom (Table 4.2). Conversely, exposure to 2,2,3,3,4,4,5,5-octafluoro-1-pentanol (OFP) yielded no change in the recorded F 1s XP spectra (Figure 4.8). These cumulative observations strongly suggest that type ***1a*** surfaces were populated by terminal alcohol groups.

The presence of surface-based electrical traps on these two surfaces was assessed through contactless microwave photoconductivity transients (Figure 4.4d). The measured value of *S* for type ***1*** surfaces was 40 ± 30 cm s^{-1}, consistent with prior estimates of *S* for

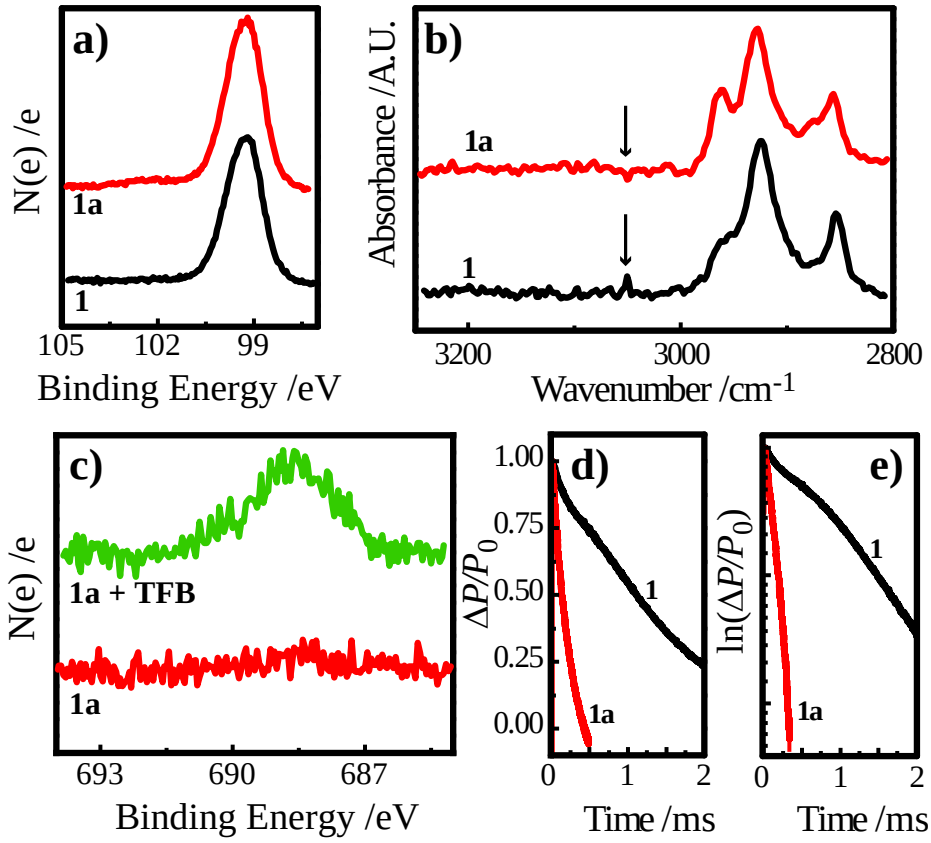

Figure 4.4 Comparison of (*a*) Si 2p XP and (*b*) infrared spectra for freshly prepared type *1* and *1a* surfaces. (*c*) Comparison of F 1s XP spectra before and after reaction of a type *1a* surface with 4-(trifluoromethyl)benzyl bromide. All spectra offset vertically for clarity. Representative microwave photoconductivity transients presented as (*d*) normalized and (*e*) natural log signal vs time.

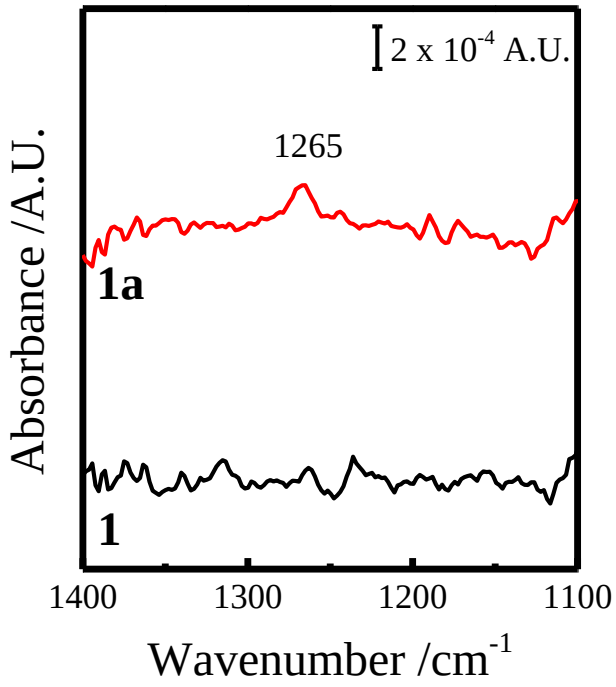

Figure 4.5 GATR-FTIR of ***1*** and ***1a*** surfaces in the COH bend region. Scale bar indicates 2 x 10^{-4} A.U. Spectra were baseline corrected and offset for clarity.

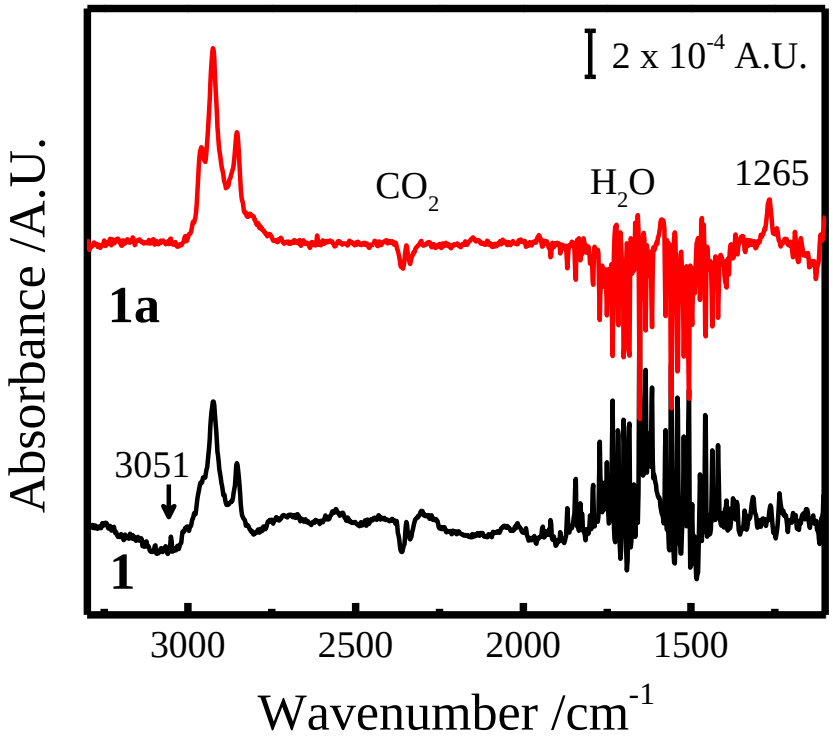

Figure 4.6 GATR-FTIR of ***1*** and ***1a*** surfaces. Scale bar indicates 2 x 10^{-4} A.U. Spectra were baseline corrected and offset for clarity.

Table 4.3 Contact Angle Data for Modified Si(111) Surfaces.

Surface Type	Number of Samples Measured	Contact Angle /°
1	10	75±5
1a	16	42±3
2	10	64±2
2a	7	57±3
2b	10	57±3
2c	4	53±4
3	11	70±6
3a	7	57±4
3b	3	76±1
3c	3	64±2

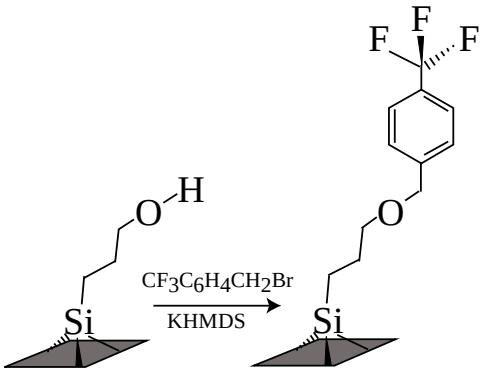

Figure 4.7 Representative etherification reaction, showing reaction *1a* with TFB with base promotor (KHMDS).

.

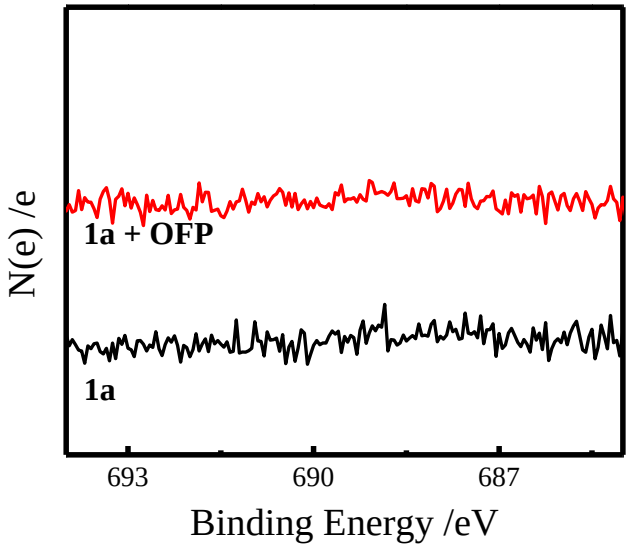

Figure 4.8 High resolution F 1s XP spectra of pristine ***1a*** (bottom) and after reaction with OFP (top). Spectra offset for clarity.

Table 4.4 Calculated SRV Values in cm s^{-1} Over Time in Ambient Conditions for N=3.

Time/hr	1	1a	2	2a	2b	2c	3	3a	3b	3c
0	40 ± 30	200 ± 150	150 ± 120	170 ± 40	75 ± 2	110 ± 40	140 ± 90	190 ± 50	190 ± 80	180 ± 90
1	40 ± 30	210 ± 170	110 ± 70	190 ± 60	82 ± 3	90 ± 20	170 ± 60	170 ± 40	140 ± 20	180 ± 100
4	40 ± 10	220 ± 150	110 ± 90	170 ± 50	130 ± 40	130 ± 60	400 ± 200	170 ± 50	210 ± 70	200 ± 120
24	70 ± 60	160 ± 120	170 ± 120	120 ± 50	120 ± 10	110 ± 50	210± 120	170 ± 70	200 ± 110	220 ±110
48	40 ± 40	150 ± 90	220 ± 170	140 ± 50	90 ± 20	100 ± 40	--	300 ± 140	160 ± 40	180 ± 80
96	70 ± 70	90 ± 50	180 ± 110	110 ± 30	100 ± 2	80 ± 40	--	350 ± 100	170 ± 80	173 ± 130

Table 4.5 Average Oxide Thickness of Modified Si(111) Surfaces in nm**.**

Surface	Initial	Aged 48 h
1	0.025	0.361
1a	0.050	0.550
2	0.171	0.454
2a	0.135	0.382
2b	0.051	0.045
2c	0.011	0.020
3	0.016	0.210
3a	0.018	0.033
3b	0.038	0.181
3c	0.031	0.011

allyl-terminated Si.[49,51] The values of *S* for ***1*** slightly increased over the course of 4 days (Table 4.4). After conversion to ***1a***, the value of *S* increased significantly to 220 ± 150 cm s^{-1},well above any *S* value measured for ***1***. However, for type ***1a*** surfaces, the values of *S* slightly *decreased* to 90 ± 50 cm s^{-1} after 4 days. Concurrently, the measured oxide thickness over the same time frame increased substantially to 0.55 nm (Table 4.5).

4.3.2 Passivated Surfaces Featuring Chemisorbed Diols

H-terminated Si(111) was converted to a surface decorated with 3,4-(methylenedioxy)phenyl groups (type ***2*** surfaces). These surfaces could be reacted with trifluoroacetic acid without substantially increasing the surface oxide content (Figure 4.9a). However, the wetting character became slightly more hydrophilic, decreasing from 64 ± 2° to 57 ± 3° (Table 4.3). Further, after reaction with trifluoroacetic acid, new modes corresponding to a CO stretch at 1288 cm^{-1}, an OH bend at 1198 cm^{-1}, and a CH bend at 1076 cm^{-1} in the GATR-IR spectra were observed (Figure 4.9b), consistent with deprotection of the 3,4-(methylenedioxy)phenyl groups to a 3,4-benzenediol. These type ***2a*** surfaces were then reactive towards 4-(trifluoromethyl)benzyl bromide. F1s XP spectra of these surfaces showed a clear signature indicative of grafted trifluoromethyl groups (Figure 4.9c). The integrated intensity of these spectra corresponded to a total fractional surface coverage of 0.22 per atop Si atom (assuming no surface roughness and each 3,4-benzenediol was functionalized with two 4-(trifluoromethyl)benzyl groups).

Because these surface groups have a large areal footprint (0.8 nm^2, assuming phenyl ring plane is perpendicular to the surface plane and freely rotates about the putative Si-C bond), a significant fraction of the available atop Si atoms remain unreacted. A mixed monolayer approach based on the premise of using CH_3- groups to occupy unreacted sites was established previously.[51-54] We sought to apply this premise on type ***2*** surfaces. Reaction of ***2*** with CH_3MgCl yielded surface ***2b.*** The measured water contact angles for ***2b*** were only slightly changed relative to ***2*** (Table 4.3). Reaction of type ***2b*** surfaces with trifluoroacetic acid (yielding type ***2c*** surfaces) and then 4-(trifluoromethyl)benzyl bromide yielded signal in the F1s the XP spectrum (Figure 4.10a) comparable to that for type ***2a***, corresponding to a fractional coverage of 0.21 surface groups per atop Si atom.

The photoconductivity transients for type ***2, 2a, 2b,*** and ***2c*** surfaces exposed to the laboratory ambient are shown in Figures 4.9e,f. Type ***2*** surfaces showed slightly larger initial *S* values

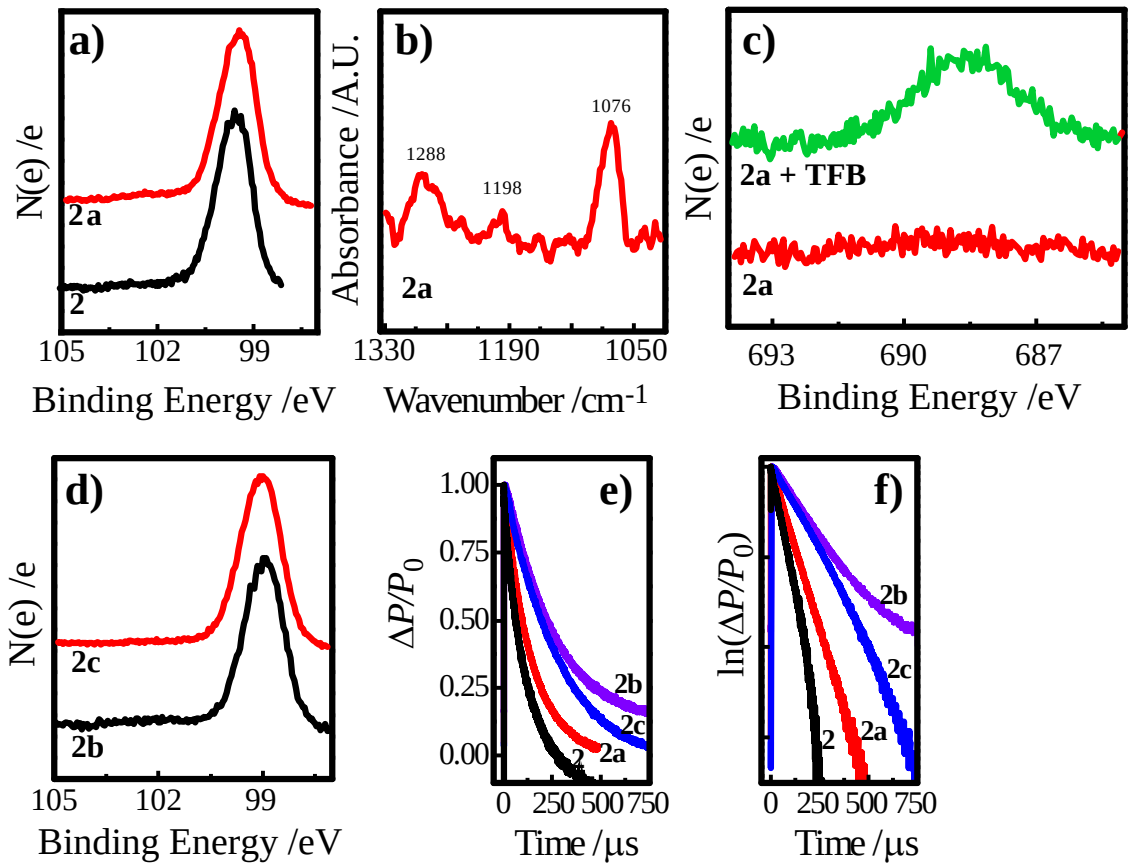

Figure 4.9 (*a*) Comparison of Si 2p XP spectra for freshly prepared type ***2*** and ***2a*** surfaces. (*b*) Infrared spectra showing the CO stretches, -OH bend, and CH bend for type ***2a*** surfaces. (*c*) Comparison of F 1s XP spectra before and after reaction of a type ***2a*** surface with 4-(trifluoromethyl)benzyl bromide. (*d*) Comparison of Si 2p XP spectra for freshly prepared type ***2b*** and ***2c*** surfaces. All spectra offset vertically for clarity. Representative microwave photoconductivity transients presented as (*e*) normalized and (*f*) natural log signal vs time.

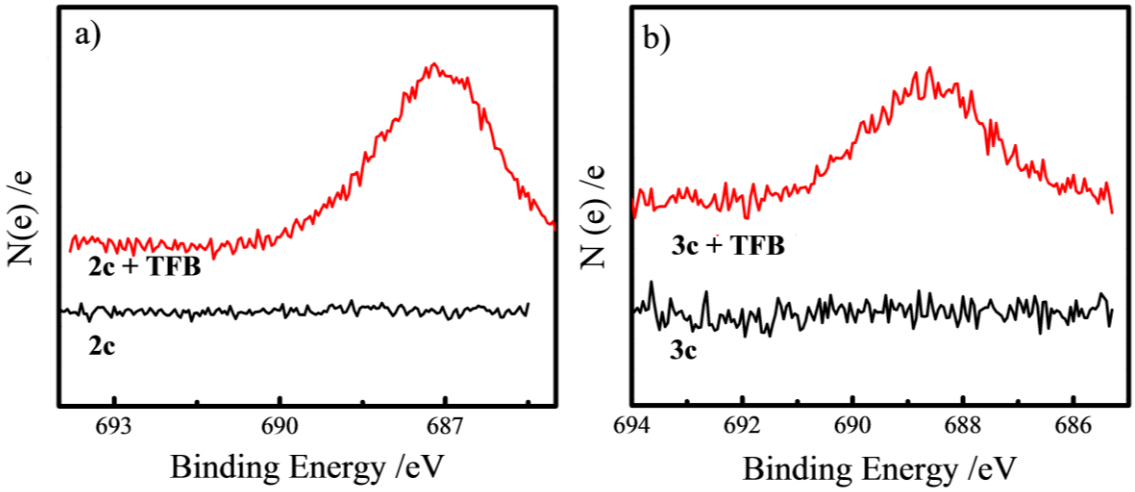

Figure 4.10 High resolution F 1s XP spectra after etherification reaction of TFB with (a) ***2c*** and (b) ***3c***.

than type ***1*** surfaces (Table 4.4) but still demonstrated reasonable levels of passivation on the order of 10^2 cm s^{-1}.Over 4 days, the surface recombination velocities fluctuated with time and increased slightly for type ***2*** surfaces. Type ***2a*** surfaces exhibited *S* values measurably larger than for type ***2*** but these values *decreased* over the course of 4 days. In comparison, the methylation 'back-fill' step yielded noticeably lower *S* values for types ***2b*** and ***2c*** surfaces relative to types ***2*** and ***2a*** surfaces. Type ***2b*** surfaces (i.e. functionalized with 3,4-(methylenedioxy)phenyl and methyl groups) showed a general trend of slightly increasing surface recombination velocities over time. Conversely, type ***2c*** surfaces (i.e. functionalized with 3,4-benzenediol and methyl groups) like type ***2a*** surfaces showed *S* values that slightly *decreased* over time.

4.3.3 Passivated Surfaces Featuring Chemisorbed Phenylamine

Type ***3*** surfaces were prepared after reaction with 4-[bis(trimethylsilyl)amino]phenyl magnesium bromide. As-prepared **3** surfaces showed a detectable but low N 1s signal intensity. A peak at 925 cm^{-1} was observed in the IR spectrum which agreed with the Si-N stretch in trimethylsilyl groups (Figure 4.11).[55,56] Deprotection of the surface groups by reaction with acid (i.e. H- replaced the trimethylsilyl groups) resulted in type ***3a*** surfaces. These surfaces did not initially possess substantial oxide (Figure 4.12a) and the N 1s signal in the XP spectrum became more pronounced (Figure 4.12b). The integrated intensity of this signal corresponded to a fractional coverage of 0.49 phenylamine groups per atop Si atom. Further, the wettability towards water increased, with a change in the water contact angle from 70 ± 6° to 57 ± 4° (Table 4.3). In addition, a peak at 3330 cm^{-1} consistent with NH_2 symmetric stretches was now evident in the IR spectra (Figure 4.12c). After aging in ambient conditions for 48 h, types ***3*** and ***3a*** surfaces had oxide layer thicknesses of 0.21 and 0.033 nm, respectively. Type ***3a*** surfaces were selectively reactive towards 4-(trifluoromethyl)benzyl bromide, yielding a surface coverage of 0.22 grafted groups per atop Si atom (Figure 4.12d), indicating not all underlying phenylamine groups were alkylated. Reaction of ***3*** with CH_3MgCl prior to deprotection of the phenylamine groups yielded type ***3b*** surfaces. After deprotection to give type ***3c*** surfaces, the integrated intensity in the N 1s spectra corresponded to a fractional coverage of phenylamine groups of 0.5 per atop Si atom, similar to type ***3a*** surfaces. Type ***3c*** surfaces were similarly reactive towards alkylation via reaction

with 4-(trifluoromethyl)benzyl bromide (Figure 4.10b), yielding a surface coverage of 0.18 grafted groups per atop Si atom.

Type ***3*** surfaces exhibited an initial surface recombination velocity (100 ± 40 cm s^{-1}), which steadily increased over time. The deprotection step that converted type ***3*** to type ***3a*** surfaces increased the measured value of *S* even though the measured oxide content had not substantially increased (*vide supra*). In addition, these surfaces deteriorated significantly over 4 days, yielding the largest value of *S* among all the surface types that were analyzed (345 ± 100 cm s^{-1}). Unexpectedly, type ***3b*** surfaces (i.e. functionalized with [bis(trimethylsilyl)amino]phenyl and methyl groups) did not possess lower *S* values as compared to type ***3*** surfaces either initially and after 4 days in air (Table 4.3). Steric blocking by the bis(trimethylsilyl)amino]phenyl groups may have prevented sufficient access to populate unreacted sites with -CH_3 groups. Still, type ***3***c surfaces (i.e. functionalized with phenylamine and methyl groups) demonstrated more stable and lower values of *S* relative to type ***3a*** surfaces, implying a sufficient amount of -CH_3 groups to render some improved passivating effect.

4.4 DICUSSION

The presented data cumulatively show three separate surface types that achieve some level of chemical stability, possess proton donating/accepting character, and have low defect density. Here we discuss their respective virtues, the observed correlations between surface stability and electronic passivation, and the prospects for employing such surface chemistry to interfaces beyond Si. Lewis and co-workers previously showed allyl-terminated Si(111) prepared by a Grignard reaction possesses surface recombination velocities ranging from 50 to 90 cm s^{-1},[49,51] in line with what was observed here. They later proved that mixed monolayers with allyl-groups demonstrate *S* values as small as 30 cm s^{-1} if 10% of the surface is decorated with allyl groups and the remaining 90% is covered by CH_3- groups.[51] A more recent advancement by this same group was the oxidation of the fraction of allyl groups to primary aldehydes, resulting in a low defect surface amenable for ALD coating.[52] However, the wetting properties were not detailed. The type ***1a*** surfaces reported here are designed to achieve a similar goal but are simpler to prepare (i.e. fewer reaction steps) and have a defined hydrophilicity. However, the initial surface recombination velocity is decidedly be tolerable depending on the specific application. For reference, the initial *S* value for type ***1a*** surfaces is

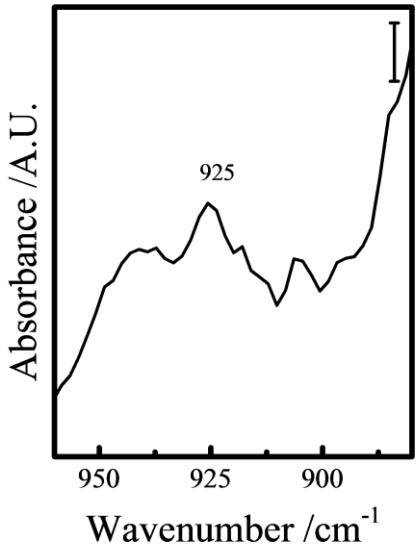

Figure 4.11 GATR-FTIR of surface ***3***. Scale bar is 1 x 10^{-4} A.U.

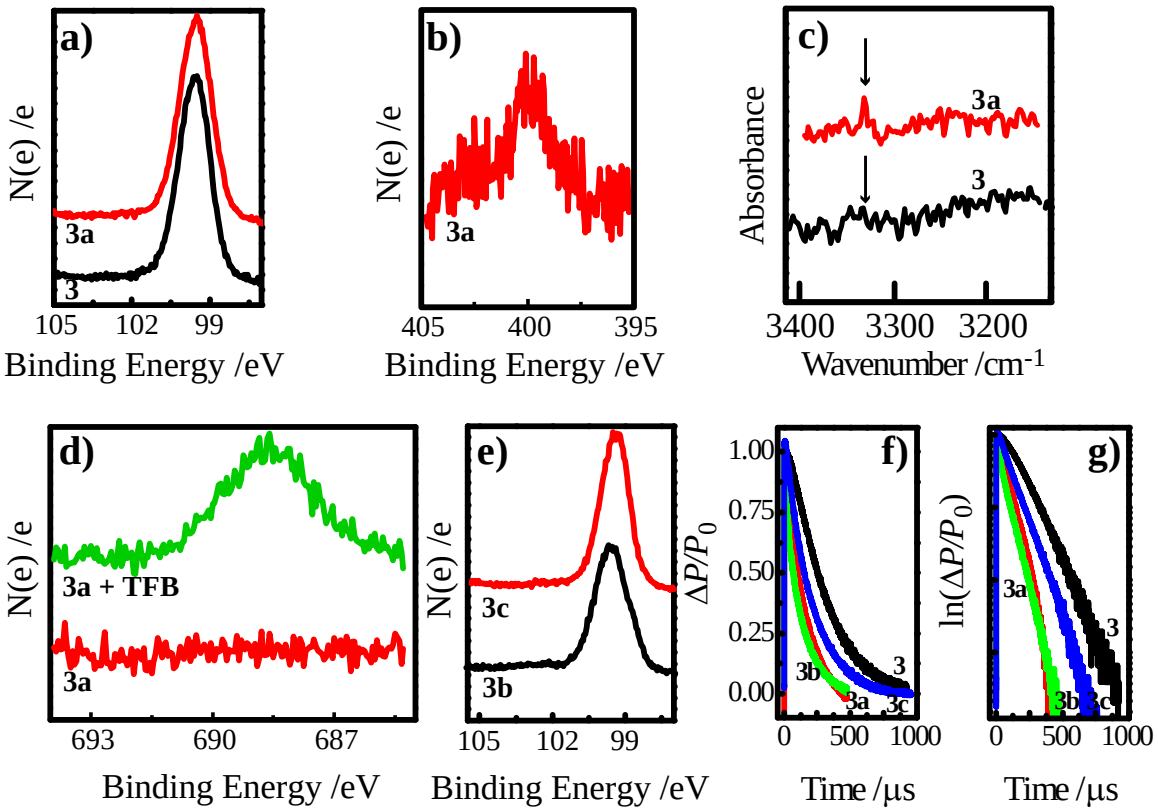

Figure 4.12 (*a*) Comparison of Si 2p XP spectra for freshly prepared type ***3*** and ***3a*** surfaces. (*b*) High resolution N1s XP spectrum of a freshly prepared type ***3a*** surface. (*c*) Comparison of infrared spectra for freshly prepared type ***3*** and ***3a*** surfaces. (*d*) Comparison of F 1s XP spectra before and after reaction of a type ***3a*** surface with 4-(trifluoromethyl)benzyl bromide. (*e*) Comparison of Si 2p XP spectra for freshly prepared type ***3b*** and ***3c*** surfaces. All spectra offset vertically for clarity. Representative microwave photoconductivity transients presented as (*f*) normalized and (*g*) natural log signal vs time.

still reasonably good compared to the native oxide higher for these type ***1a*** surfaces, which may or may not of Si and is in fact on par with unannealed thermal oxides.[57] For further comparison, a recent report demonstrating Si(111) surfaces terminated with 4-trifluoromethylsulfonylbenzene exhibited surface recombination velocities of 1372 ± 30 cm s^{-1}.[58] Still, if a lower initial surface recombination velocity is necessary, surface types ***2a***, ***2c***, ***3a***, and ***3c*** are all viable options. Again, surface types ***2a*** and ***3a*** retain the practical advantage of a minimal number of preparative steps. Further, type ***2a*** surfaces exhibit the greatest wettability towards water in comparison to surface ***3a***, a feature which may aid in coatings cast from aqueous solutions. In comparison to alkyl-terminated Si surfaces rendered hydrophilic by oxidation with oxygen-containing plasmas,[59,60] the wet chemical approach shown here is both controllable and more amenable to 'short' surface layers suited for heterogeneous charge transfer.

The surface stability and surface recombination velocities of some of the surfaces studied here tracked with time in unexpected ways. Surfaces that did not intentionally have any proton donating/accepting character (i.e. type ***1***, ***2, 2b, 3,*** and ***3b***) all exhibited surface recombination velocities that either remained statistically unchanged or slightly increased over time. This observation itself is unsurprising given these surfaces are not indefinitely stable against oxidation and the act of oxidation should introduce strained bonding that act as electronic traps. However, the majority of surfaces that did have explicit proton donating/accepting character (i.e. type ***1a***, ***2a,*** and ***2c***) had surface recombination velocities that *decreased* over time even though the underlying surface oxide layer *increased*. That is, even though these surfaces were somewhat susceptible to oxidation of the underlying substrate, the resultant oxide growth did not add significant numbers of new electrical traps. Surface type ***1a*** is a noteworthy example, as the surface oxide that grew after 24 h (0.55 nm) in air was greater than the thickness of a complete oxide monolayer on Si(111) (0.4 nm),[61] yet the measured surface recombination velocity was actually lower than the initial value. Although the present dataset does not provide any direct microscopic insight on the cause of this observation, we comment on two possibilities. First, the presence of the grafted surface groups imparted some directing effect on the growth of any new oxide. Similar arguments have been made previously for modified surfaces whose surface recombination velocities decrease over time[62,63] and there is no data to conclusively rule out this scenario. Still, since the physicochemical nature of the modifying groups in these three sets of surfaces differ

significantly, an equivalent 'oxide templating' effect seems unlikely. Second, the acid/base functionality of the modified surfaces influences/introduces charge within the growing oxide. Such oxides could artificially lower the observable surface recombination velocity through charge screening.[9] A hallmark of such an effect is a strong dependence of the surface recombination velocity with illumination intensity.[9] The accessible illumination intensities were limited by the linearity of the microwave reflection method only at low charge carrier concentrations.[64] Nevertheless, we did not observe any significant dependence of the measured lifetimes with changes in laser intensity, arguing against this possibility. Hence, additional studies are necessary to explain this curious phenomenon.

The wet chemical strategies applied here are not limited to just Si interfaces. The approaches demonstrated in this work to convert the grafted moieties into alcohols and amines should generally apply to these same groups when bonded to other semiconductors. We have shown previously that III-V semiconductor surfaces (e.g. GaAs(111)A, GaP(111)A, GaN(0001))[65-67] are reactive towards Grignard reagents and therefore these interface could be initially functionalized in a similar manner as explored here. Since the intrinsic instability of the native surfaces of these III-V semiconductors substantially complicates coating these semiconductors with either solid dielectrics[68,69] or molecular films,[70] such wet chemical methods should prove useful. Work in our group to attain similar levels of control over wetting, stability, and interfacial defect densities on III-V semiconductor surfaces is ongoing.

4.5 SUMMARY

Three separate wet chemical reaction sequences were performed on Si(111) to achieve hydrophilic, chemically stable, and electronically passivated surfaces. These general features were attained although an unexpected improvement in the apparent surface recombination velocities was observed for many of the surfaces with acid/base character. These modified Si surfaces should be amenable for contacting methods such as ALD or spin-casting of solutions of oxo-clusters. With regards to ALD, these interfaces ought to provide a high number of nucleating sites during the initial deposition cycles, potentially leading to more uniform films. In the context of solution-cast oxides, the low level of initial defects and good chemical stability should improve the quality of the resultant junction. Separate studies are needed to rigorously test these hypotheses. This study adds three sets of Si surfaces to the

number of interfaces that are quantitatively categorized in terms of their stability, wettability, and electrical quality. This work thus defines protocols and benchmarks so as to evaluate these surfaces in heterojunctions as well as to apply to other semiconductor interfaces.

4.6 REFERENCES

(1) Ilic, S.; Brown, E. S.; Xie, Y.; Maldonado, S.; Glusac, K. D. Sensitization of p-GaP with Monocationic Dyes: The Effect of Dye Excited-State Lifetime on Hole Injection Efficiencies. *The Journal of Physical Chemistry C* **2016**, *120*, 3145-3155.

(2) Leskela, M.; Ritala, M. Atomic Layer Deposition (ALD): From Precursors to Thin Film Structures. *Thin Solid Films* **2002**, *409*, 138-146.

(3) Kim, H. J.; Kearney, K. L.; Le, L. H.; Pekarek, R. T.; Roses, M. J. Platinum-Enhanced Electron Transfer and Surface Passivation through Ultrathin Film Aluminum Oxide (Al2O3) on Si(111)-CH3 Photoelectrodes. *ACS Appl. Mater. Interfaces* **2015**, *7*, 8572-8584.

(4) Oleksak, R. P.; Ruther, R. E.; Luo, F.; Fairley, K. C.; Decker, S. R.; Stickle, W. F.; Johnson, D. W.; Garfunkel, E. L.; Herman, G. S.; Keszler, D. A. Chemical and Structural Investigation of High-Resolution Patterning with HafSOx. *ACS Appl. Mater. Interfaces* **2014**, *6*, 2917-2921.

(5) Wager, J. F.; Yeh, B.; Hoffman, R. L.; Keszler, D. A. An Amorphous Oxide Semiconductor Thin-Film Transistor Route to Oxide Electronics. *Current Opinion in Solid State & Materials Science* **2014**, *18*, 53-61.

(6) Masteika, V.; Kowal, J.; Braithwaite, N. S. J.; Rogers, T. A Review of Hydrophilic Silicon Wafer Bonding. *ECS J. Solid State Sci. Technol.* **2014**, *3*, Q42-Q54.

(7) Royea, W. J.; Juang, A.; Lewis, N. S. Preparation of Air-Stable, Low Recombination Velocity Si(111) Surfaces through Alkyl Termination. *Appl. Phys. Lett.* **2000**, *77*, 1988-1990.

(8) Eades, W. D.; Swanson, R. M. Calculation of Surface Generation and Recombination Velocities at the Si/SiO2 Interface. *J. Appl. Phys.* **1985**, *58*, 4267-4276.

(9) Yablonovitch, E.; Allara, D. L.; Chang, C. C.; Gmitter, T.; Bright, T. B. Unusually Low Surface-Recombination Velocity on Silicon and Germanium Surfaces *Phys. Rev. Lett.* **1986**, *57*, 249-252.

(10) Titova, L. V.; Hoang, T. B.; Jackson, H. E.; Smith, L. M.; Yarrison-Rice, J. M.; Kim, Y.; Joyce, H. J.; Tan, H. H.; Jagadish, C. Temperature Dependence of Photoluminescence from Single Core-Shell GaAs-AlGaAs Nanowires. *Appl. Phys. Lett.* **2006**, *89*.

(11) George, S. M. Atomic Layer Deposition: An Overview. *Chem. Rev.* **2010**, *110*, 111-131.

(12) Khaselev, O.; Turner, J. A. Electrochemical Stability of p-GaInP2 in Aqueous Electrolytes Toward Photoelectrochemical Water Splitting. *J. Electrochem. Soc.* **1998**, *145*, 3335-3339.

(13) Gerischer, H. Electrolytic Decomposition and Photo-decomposition of Compound Semiconductors in Contact with Electrolytes *J. Vac. Sci. Technol.* **1978**, *15*, 1422-1428.

(14) Price, M. J.; Maldonado, S. Macroporous n-GaP in Nonaqueous Regenerative Photoelectrochemical Cells. *J. Phys. Chem. C* **2009**, *113*, 11988-11994.

(15) Mukherjee, J.; Erickson, B.; Maldonado, S. Physicochemical and Electrochemical Properties of Etched GaP(111)A and GaP(111)B Surfaces. *J. Electrochem. Soc.* **2010**, *157*, H487-H495.
(16) Gershenzon, M.; Mikulyak, R. M. Radiative Pair Recombination and Surface Recombination in GaP Photoluminescence. *Appl. Phys. Lett.* **1966**, *8*, 245-247.
(17) Stringfellow, G. B. Effect of Surface Treatment on Surface Recombination Velocity and Diode Leakage in GaP. *J. Vac. Sci. Technol.* **1976**, *13*, 908-913.
(18) Bansal, A.; Lewis, N. S. Electrochemical Properties of (111)-Oriented n-Si Surfaces Derivatized with Covalently-Attached Alkyl Chains. *J. Phys. Chem. B* **1998**, *102*, 1067-1070.
(19) Bocarsly, A. B.; Walton, E. G.; Bradley, M. G.; Wrighton, M. S. 2-Electron Oxidations at Illuminated n-Type Semiconducting Silicon Electrodes-Use of Chemically Derivatized Photoelectrodes. *J. Electroanal. Chem.* **1979**, *100*, 283-306.
(20) Bocarsly, A. B.; Walton, E. G.; Wrighton, M. S. Use of Chemically Derivatized n-Type Silicon Photoelectrodes in Aqueous Media-Photo-oxidation of Iodide, Hexacyanoiron(II), and Hexaammineruthenium(II) at Ferrocene-Derivatized Photoandoes. *J. Am. Chem. Soc.* **1980**, *102*, 3390-3398.
(21) Bansal, A.; Li, X. L.; Lauermann, I.; Lewis, N. S.; Yi, S. I.; Weinberg, W. H. Alkylation of Si Surfaces Using a Two-Step Halogenation Grignard Route. *J. Am. Chem. Soc.* **1996**, *118*, 7225-7226.
(22) Bansal, A.; Lewis, N. S. Stabilization of Si Photoanodes in Aqueous Electrolytes Through Surface Alkylation. *J. Phys. Chem. B* **1998**, *102*, 4058-4060.
(23) Aberle, A. G. Surface Passivation of Crystalline Silicon Solar Cells: A Review. *Prog. Photovoltaics* **2000**, *8*, 473-487.
(24) Buriak, J. M. Organometallic Chemistry on Silicon and Germanium Surfaces. *Chem. Rev.* **2002**, *102*, 1271-1308.
(25) Waltenburg, H. N.; Yates, J. T. Surface Chemistry of Silicon *Chem. Rev.* **1995**, *95*, 1589-1673.
(26) Filler, M. A.; Bent, S. F. The Surface as Molecular Reagent: Organic Chemistry at the Semiconductor Interface. *Prog. Surf. Sci.* **2003**, *73*, 1-56.
(27) Cicero, R. L.; Linford, M. R.; Chidsey, C. E. D. Photoreactivity of Unsaturated Compounds with Hydrogen-Terminated Silicon(111). *Langmuir* **2000**, *16*, 5688-5695.
(28) Sun, Q. Y.; de Smet, L.; van Lagen, B.; Giesbers, M.; Thune, P. C.; van Engelenburg, J.; de Wolf, F. A.; Zuilhof, H.; Sudholter, E. J. R. Covalently Attached Monolayers on Crystalline Hydrogen-Terminated Silicon: Extremely Mild Attachment by Visible Light. *J. Am. Chem. Soc.* **2005**, *127*, 2514-2523.
(29) Linford, M. R.; Fenter, P.; Eisenberger, P. M.; Chidsey, C. E. D. Alkyl Monolayers on Silicon Prepared from 1-Alkenes and Hydrogen-Terminated Silicon *J. Am. Chem. Soc.* **1995**, *117*, 3145-3155.
(30) Wasserman, S. R.; Tao, Y. T.; Whitesides, G. M. Structure and Reactivity of Alkylsiloxane Monolayers Formed by Reaction of Alkyltrichlorosilanes on Silicon Substrates. *Langmuir* **1989**, *5*, 1074-1087.

(31) Toledano, T.; Biller, A.; Bendikov, T.; Cohen, H.; Vilan, A.; Cahen, D. Controlling Space Charge of Oxide-Free Si by in Situ Modification of Dipolar Alkyl Monolayers. *J. Phys. Chem. C* **2012**, *116*, 11434-11443.
(32) Chhabra, B.; Bowden, S.; Opila, R. L.; Honsberg, C. B. High Effective Minority Carrier Lifetime on Silicon Substrates using Quinhydrone-Methanol Passivation. *Appl. Phys. Lett.* **2010**, *96*.
(33) Takato, H.; Sakata, I.; Shimokawa, R. Quinhydrone/Methanol Treatment for the Measurement of Carrier Lifetime in Silicon Substrates. *Jpn. J. Appl. Phys. 2* **2002**, *41*, L870-L872.
(34) Takato, H.; Sakata, I.; Shimokawa, R. Surface Passivation Effect of Silicon Substrates due to Quinhydrone/Ethanol Treatment. *Jpn. J. Appl. Phys. 2* **2001**, *40*, L1003-L1004.
(35) Bansal, A.; Li, X. L.; Yi, S. I.; Weinberg, W. H.; Lewis, N. S. Spectroscopic Studies of the Modification of Crystalline Si(111) Surfaces with Covalently-Attached Alkyl Chains using a Chlorination/Alkylation Method. *J. Phys. Chem. B* **2001**, *105*, 10266-10277.
(36) Leblanc, Y.; Fitzsimmons, B. J.; Adams, J.; Perez, F.; Rokach, J. The Total Synthesis of 12-HETE and 12,20-diHETE. *J. Org. Chem.* **1986**, *51*, 789-793.
(37) Barr, T. L.; Seal, S. Nature of the Use of Adventitious Carbon as a Binding-Energy Standard. *J. Vac. Sci. Technol., A* **1995**, *13*, 1239-1246.
(38) *Practical Surface Analysis*; Briggs, D.; Seah, M. P., Eds.; John Wiley & Sons: Chichester, 1983.
(39) Asami, K.; Hashimoto, K.; Shimodaira, S. XPS Determination of Compositions of Alloy Surfaces and Surface Oxides on Mechanically Polished Iron-Chromium Alloys. *Corros. Sci.* **1977**, *17*, 713-723.
(40) Laibinis, P. E.; Bain, C. D.; Whitesides, G. M. Attenuation of Photoelectrons in Monolayers of Normal-Alkanethiols Adsorbed on Copper, Silver, and Gold. *J. Phys. Chem.* **1991**, *95*, 7017-7021.
(41) Pies, W., Weiss, A. *Crystal Structure Data of Inorganic Compounds*; Springer-Verlag: Berlin, 1979.
(42) Wagner, C. D.; Davis, L. E.; Zeller, M. V.; Taylor, J. A.; Raymond, R. H.; Gale, L. H. Empirical Atomic Sensitivity Factors for Quantitative Analysis by Electron Spectroscopy for Chemical Analysis. *Surf. Interface Anal.* **1981**, *3*, 211-225.
(43) Sturzenegger, M.; Prokopuk, N.; Kenyon, C. N.; Royea, W. J.; Lewis, N. S. Reactions of Etched, Single Crystal (111)B-Oriented InP to Produce Functionalized Surfaces with Low Electrical Defect Densities. *J. Phys. Chem. B* **1999**, *103*, 10838-10849.
(44) Allen, F. H.; Kennard, O.; Watson, D. G.; Brammer, L.; Orpen, A. G.; Taylor, R. Tables of Bond Lengths Determined by X-ray and Neutron-Diffraction. 1. Bond Lengths in Organic Compounds. *Journal of the Chemical Society-Perkin Transactions 2* **1987**, S1-S19.
(45) Clough, A. J.; Yoo, J. W.; Mecklenburg, M. H.; Marinescu, S. C. Two-Dimensional Metal-Organic Surfaces for Efficient Hydrogen Evolution from Water. *J. Am. Chem. Soc.* **2015**, *137*, 118-121.

(46) Eady, S. C.; Peczonczyk, S. L.; Maldonado, S.; Lehnert, N. Facile Heterogenization of a Cobalt Catalyst via Graphene Adsorption: Robust and Versatile Dihydrogen Production Systems. *Chem. Commun.* **2014**, *50*, 8065-8068.
(47) Horanyi, T. S.; Pavelka, T.; Tutto, P. In-Situ Bulk Lifetime Measurement on Silicon with a Chemically Passivated Surface. *Appl. Surf. Sci.* **1993**, *63*, 306-311.
(48) Rosling, M.; Bleichner, H.; Jonsson, P.; Nordlander, E. The Ambipolar Diffusion-Coefficient in Silicon--Dependence on Excess-Carrier Concentration and Temperature. *J. Appl. Phys.* **1994**, *76*, 2855-2859.
(49) Plass, K. E.; Liu, X. L.; Brunschwig, B. S.; Lewis, N. S. Passivation and Secondary Functionalization of Allyl-Terminated Si(111) Surfaces. *Chem. Mat.* **2008**, *20*, 2228-2233.
(50) Zhong, Y. L.; Bernasek, S. L. Direct Photochemical Functionalization of Si(111) with Undecenol. *Langmuir* **2011**, *27*, 1796-1802.
(51) O'Leary, L. E.; Johansson, E.; Brunschwig, B. S.; Lewis, N. S. Synthesis and Characterization of Mixed Methyl/Allyl Monolayers on Si(111). *J. Phys. Chem. B* **2010**, *114*, 14298-14302.
(52) O'Leary, L. E.; Strandwitz, N. C.; Roske, C. W.; Pyo, S.; Brunschwig, B. S.; Lewis, N. S. Use of Mixed CH3-/HC(O)CH2CH2-Si(111) Functionality to Control Interfacial Chemical and Electronic Properties During the Atomic-Layer Deposition of Ultrathin Oxides on Si(111). *J. Phys. Chem. Lett.* **2015**, *6*, 722-726.
(53) Lattimer, J. R. C.; Brunschwig, B. S.; Lewis, N. S.; Gray, H. B. Redox Properties of Mixed Methyl/Vinylferrocenyl Monolayers on Si(111) Surfaces. *J. Phys. Chem. C* **2013**, *117*, 27012-27022.
(54) Li, F.; Basile, V. M.; Pekarek, R. T.; Rose, M. J. Steric Spacing of Molecular Linkers on Passivated Si(111) Photoelectrodes. *ACS Appl. Mater. Interfaces* **2014**, *6*, 20557-20568.
(55) Smith, A. L. Infrared Spectra--Structure Correlations for Organosilicon Compounds. *Spectrochim. Acta* **1960**, *16*, 87-105.
(56) Badawi, H. M.; Forner, W.; Ali, S. A. A Comparative Study of the Infrared and Raman Spectra of Aniline and o-, m-, p-Phenylenediamine Isomers. *Spectrochim. Acta, Part A* **2013**, *112*, 388-396.
(57) Opsal, J.; Taylor, M. W.; Smith, W. L.; Rosencwaig, A. Temporal Behavior of Modulated Optical Reflectance in Silicon. *J. Appl. Phys.* **1987**, *61*, 240-248.
(58) Seo, J.; Kim, H. J.; Pekarek, R. T.; Rose, M. J. Hybrid Organic/Inorganic Band-Edge Modulation of p-Si(111) Photoelectrodes: Effects of R, Metal Oxide, and Pt on H-2 Generation. *J. Am. Chem. Soc.* **2015**, *137*, 3173-3176.
(59) Rosso, M.; Giesbers, M.; Schroen, K.; Zuilhof, H. Controlled Oxidation, Biofunctionalization, and Patterning of Alkyl Monolayers on Silicon and Silicon Nitride Surfaces using Plasma Treatment. *Langmuir* **2010**, *26*, 866-872.
(60) Aureau, D.; Morscheidt, W.; Etcheberry, A.; Vigneron, J.; Ozanam, F.; Allongue, P.; Chazalvielt, J. N. Controlled Oxidation of Alkyl Monolayers Grafted onto Flat Si(111) in an Oxygen Plasma of Low Power Density. *J. Phys. Chem. C* **2009**, *113*, 14418-14428.
(61) Kobayashi, Y.; Sugii, K. Thermal Decomposition of Very Thin Oxide Layers on Si(111). *J. Vac. Sci. Technol., A* **1992**, *10*, 2308-2313.

(62) Webb, L. J.; Lewis, N. S. Comparison of the Electrical Properties and Chemical Stability of Crystalline Silicon(111) Surfaces Alkylated using Grignard Reagents or Olefins with Lewis Acid Catalysts. *J. Phys. Chem. B* **2003**, *107*, 5404-5412.
(63) Nemanick, E. J.; Hurley, P. T.; Brunschwig, B. S.; Lewis, N. S. Chemical and Electrical Passivation of Silicon (111) Surfaces through Functionalization with Sterically Hindered Alkyl Groups. *J. Phys. Chem. B* **2006**, *110*, 14800-14808.
(64) Kunst, M.; Beck, G. The Study of Charge Carrier Kinetics in Semiconductors by Microwave Conductivity Measurements. *J. Appl. Phys.* **1986**, *60*, 3558-3566.
(65) Mukherjee, J.; Peczonczyk, S.; Maldonado, S. Wet Chemical Functionalization of III-V Semiconductor Surfaces: Alkylation of Gallium Phosphide Using a Grignard Reaction Sequence. *Langmuir* **2010**, *26*, 10890-10896.
(66) Peczonczyk, S. L.; Mukherjee, J.; Carim, A. I.; Maldonado, S. Wet Chemical Functionalization of III-V Semiconductor Surfaces: Alkylation of Gallium Arsenide and Gallium Nitride by a Grignard Reaction Sequence. *Langmuir* **2012**, *28*, 4672-4682.
(67) Peczonczyk, S. L.; Brown, E. S.; Maldonado, S. Secondary Functionalization of Allyl-Terminated GaP(111)A Surfaces via Heck Cross-Coupling Metathesis, Hydrosilylation, and Electrophilic Addition of Bromine. *Langmuir* **2014**, *30*, 156-164.
(68) Granados-Alpizar, B.; Muscat, A. J. Surface Reactions of TiCl4 and Al(CH3)(3) on GaAs(100) During the First Half-Cycle of Atomic Layer Deposition. *Surf. Sci.* **2011**, *605*, 1243-1248.
(69) Delabie, A.; Brunco, D. P.; Conard, T.; Favia, P.; Bender, H.; Franquet, A.; Sioncke, S.; Vandervorst, W.; Van Elshocht, S.; Heyns, M.; Meuris, M.; Kim, E.; McIntyre, P. C.; Saraswat, K. C.; LeBeau, J. M.; Cagnon, J.; Stemmer, S.; Tsai, W. Atomic Layer Deposition of Hafnium Oxide on Ge and GaAs Substrates: Precursors and Surface Preparation. *J. Electrochem. Soc.* **2008**, *155*, H937-H944.
(70) Chitambar, M.; Wang, Z. J.; Liu, Y. M.; Rockett, A.; Maldonado, S. Dye-Sensitized Photocathodes: Efficient Light-Stimulated Hole Injection into p-GaP Under Depletion Conditions. *J. Am. Chem. Soc.* **2012**, *134*, 10670-10681.

APPENDIX A

Functionalization of As-Prepared Gallium Phosphide Nanowires

A1. INTRODUCTION

Gallium phosphide (GaP) is a known material for photocathodes in solar energy conversion systems. Due to its indirect band gap, photon absorption is inefficient in thin planar films. However, thick films increase the probability of charge recombination in the bulk, lowering conversion efficiencies. One way to mitigate this effect is to utilize nanostructured GaP with high aspect ratios. These structures have been achieved through anodic etching,[1] vapor-liquid-solid growth (VLS),[2] or solution-liquid-solid growth.[3]

Another challenge is the inherent instability of GaP surfaces toward chemical attack in air. Oxidation of the surface creates surface traps which facilitate recombination at the interface. Several wet chemical techniques have been employed on crystalline GaP surfaces.[3-7] Macroporous GaP has been coated with PEDOT:PSS polymer in order to affect a solid state device and was shown to have good performance in air.[8] However, no wet chemical strategies have been employed on nanostructured GaP. With the increased surface area of these high aspect ratio nanostructures, wet chemical passivation strategies are crucial for extending the performance of these devices in photoelectrochemical systems.

By scanning electron microscopy, there are some visible regions of the nanowires that have <111> crystal planes exposed. However, these surfaces are not exclusively present. Therefore, we assume that the nanowires have mixed composition of surface atoms (gallium and phosphorus present and exact bonding orbital(s) available were unknown).

In this appendix, preliminary results of two chemical strategies are discussed. Nanowires (NW) prepared through published protocols were used (GaP on Si substrate).[2] NW were treated with Williamson ether type reactions with benzyl bromides or through

chlorination/Grignard reaction sequences that were previously developed for planar GaP(111) surfaces (Figure A.1). Williamson ether type reaction can likely react with both Ga-OH and P-OH surface species while chlorination/Grignard reaction sequence targets atop Ga atoms. Lastly, towards dye-sensitized photocathode systems, modified Coomassie Blue dye was attached to the NW.

A.2 EXPERIMENTAL

A.2.1 Materials

Gallium phosphide NW samples were prepared as previously published. Reagents were identical to those previously listed in Chapters 2 and 3 and published works.[6,9] N-chlorosuccinimide (Sigma-Aldrich, 98%) was dried under vacuum >3 h and brought into nitrogen atmosphere glovebox.

NW samples are fragile and care was taken not to scratch the surface with the Teflon tweezers during handling, as this destroys the NW structures touched. GaP NW were reacted by two general strategies shown in Figure A.1.

A.2.2 X-ray Photoelectron Spectroscopy

All X-ray photoelectron (XP) spectra were collected with a PHI 5400 analyzer using an Al Kα (1486.6 eV) source without a monochromator. Spectra were collected without charge neutralization at a base pressure of < 2.5×10^{-9} Torr. A 6 mA current emission and a 12 kV anode high tension were used. Survey scans were recorded between 0 and 1350 eV at pass energy of 117.40 eV. High resolution spectra were collected at a pass energy of 23.5 eV. The binding energies of all spectra were corrected using the expected binding energy for adventitious carbon (284.6 eV).[29,30]

A.2.3 Static Sessile Drop Contact Angle Measurements

The contact angles formed between a droplet of distilled water (2.2 μL) and a GaP interface were recorded with a CAM 100 optical contact angle meter (KSV instrument, Helsinki, Finland) and analyzed using the KSV software analysis package. It should be noted that due to inherently non-uniform surface and inconsistent NW packing on the substrate, measured contact angle values should be treated with caution and require extensive repetition before publication. Over six samples of etched NW samples, the average was 39.5 ± 18°, a very large standard deviation. Error was mitigated in this

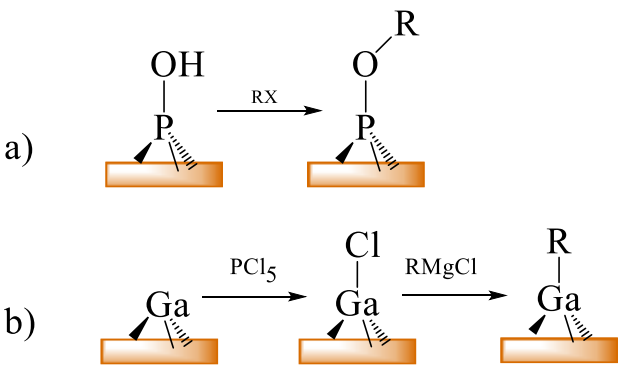

Figure A.1 Schemes determined for a) phosphorus atop atoms of planar GaP(111)B and b) gallium atop atoms of planar GaP(111)A.

preliminary study by comparing each reacted sample to the etched contact angle of the same substrate.

A.3. RESULTS

A.3.1. Williamson Ether Type Reaction

After etching NW samples carefully for 30 seconds in concentrated H_2SO_4(aq), NW were reacted with 4-(trifluoromethyl)benzyl bromide (TFB) in acetonitrile with potassium bis(trimethyl)silylamide promoter at 60°C for 1 h. Figure A.2 shows high resolution F 1s XP spectra for etched NW samples (contact angle ~ 10°) and after treatment with TFB (contact angle ~80°). Figure A.2b shows small peaks in the C 1s spectrum which correlate to C-F bonding.

A.3.2 Chlorination

While Chlorination/Grignard reaction sequences are only likely viable for atop Ga atoms, the stability of these surfaces is as yet unparalleled, resisting oxidation on the order of several months in ambient conditions.[5]

Previous preliminary studies by S.L. Peczoncyzk (unpublished) on GaP NW have shown instability towards the standard chlorination step of crystalline GaP, where crystalline GaP was reacted with PCl_5 in chlorobenzene with benzoyl peroxide initiator at 90°C for 50 min. The bright yellow color (indicative of GaP NW) was nearly completely removed from Si substrates under these conditions. Similar results were achieved used 6 M HCl. Lower concentrations and times of exposure to acidic solutions resulted in low signals of Cl 2p in XP spectra.

N-chlorosuccinimide (NCS) was used as the chlorinating agent in dimethylformamide for short times under room temperature in the glovebox. Scanning electron micrographs in Figure A.3 show NW structure after 15 min and 30 min treatment with NCS. The NW structure seems to have degraded into less straight, more globule looking structures. The quantity also appeared diminished visibly by a more dull yellow color and by the resolution of the SEM. High resolution Cl 2p and Au 4f XP spectra are shown in Figure A.4. Cl 2p signal intensity is higher for 30 min chlorination. Au 4f signal, arising from the catalyst for NW growth, appeared to be larger on 30 min chlorination samples, which was consistent with the removal of GaP material through

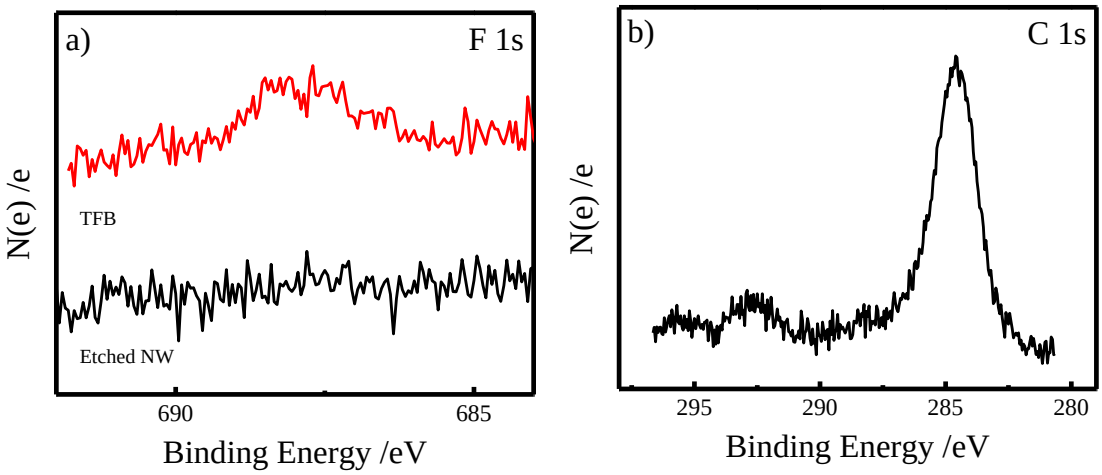

Figure A.2 High resolution XP spectra of a) F 1s region of GaP NW after etching (bottom) and after reaction with TFB. Spectra offset for clarity. XP spectra of b) C 1s region of GaP NW after reaction with TFB.

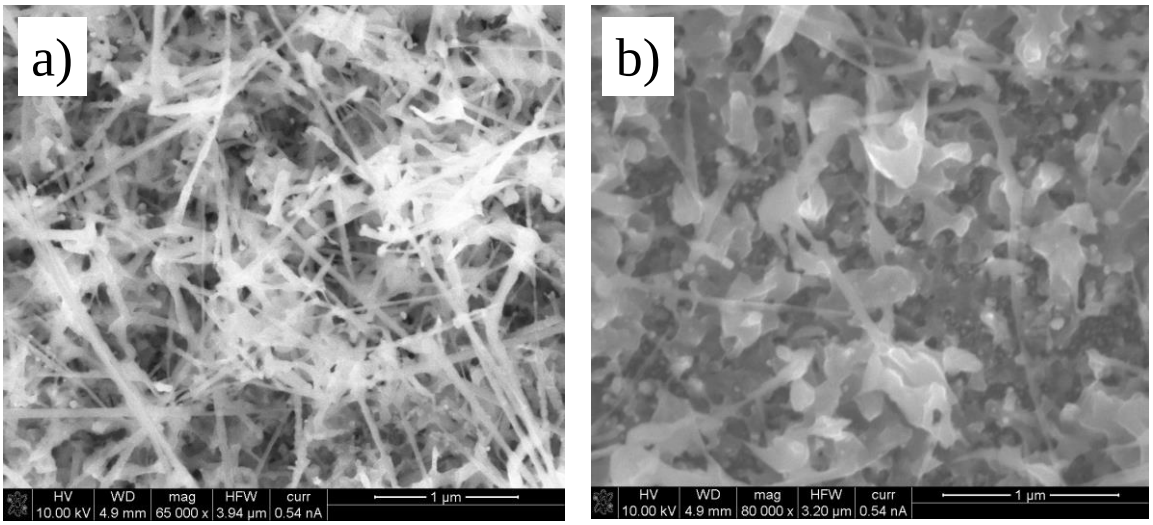

Figure A.3 SEM of GaP NW after a) 15 min and b) 30 min in NCS solution. Micrographs courtesy of Dr. W.Wen.

etching. NCS reaction times of 45 min and 1 h completely removed the yellow mat of wires from the substrate, so no further data was acquired from those samples. Chlorinated GaP NW samples were then reacted with CH_3MgCl overnight. Samples did not undergo any visible changes. Cl 2p XP signal decreased on the 15 min chlorinated sample, likely indicating a conversion of nearly all chlorinated surface atoms to organic $–CH_3$ groups. The Cl 2p of 30 min chlorination samples decreased slightly, but was still significantly large. No C-Ga shoulder was observed in any of the C 1s XP spectra, as observed previously at 282 eV.[5]

Grignard reactions were also performed with longer chain alkyl groups, $C_nH_{2n+1}MgCl$ where n = 2, 4, 8, 14, 18. Contact angle values are shown in Table A.1. Some samples were wetted, where the droplet of water dispersed in between the NW, mostly for n = 1, 2, and 4. For n = 8, 14, and 18, sometimes the droplet would wick completely off the sample due to extremely hydrophobic surfaces.

A.3.3 Dye Attachment

Through the same reaction scheme employed previously,[6] modified Coomassie Blue was attached to GaP NW through Williamson ether type linkages after 55°C for 1 h in methanol. XP spectra shown in Figure A.5 displayed low PO_x, and significant N 1s, S 2p, and Cl 2p signatures consistent with chemisorbed dye. However, the substrate did not undergo any visible color change.

A.3.4 Oxidation in Water

Treated NW samples were subjected to oxygenated water for several hours to investigate stability against chemical attack. Over 12 h, F 1s signal in XP spectra shown in Figure A.6 decreased significantly. Aged contact angles were also affected. While contact angle of etched NW samples increased to 20°, aged TFB-NW decreased to about 70°.

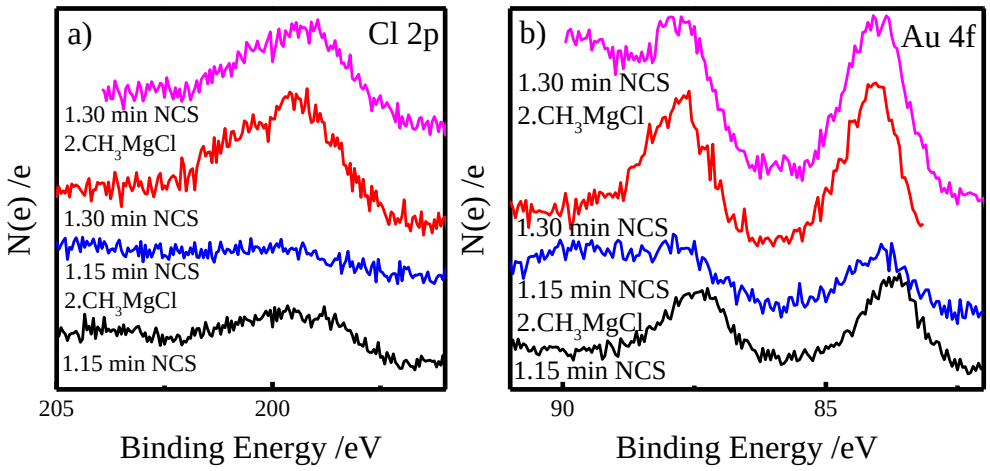

Figure A.4 High resolution XP a) Cl 2p and b) Au 4f spectra of samples after chlorination with NCS for 15 min (black) or 30 min (red) and after reaction with CH_3MgCl (blue and pink, respectively). Spectra are offset for clarity.

Table A.1 Contact Angle Values for Modified NW Samples.

$C_nH_{2n+1}MgCl$ where n =	Contact Angle Avg /°	No. of samples
1	24 ± 11	2
2	17	1
4	22 ± 11	2
8	153 ± 4	3
14	142 ± 4	4
18	155 ± 13	5

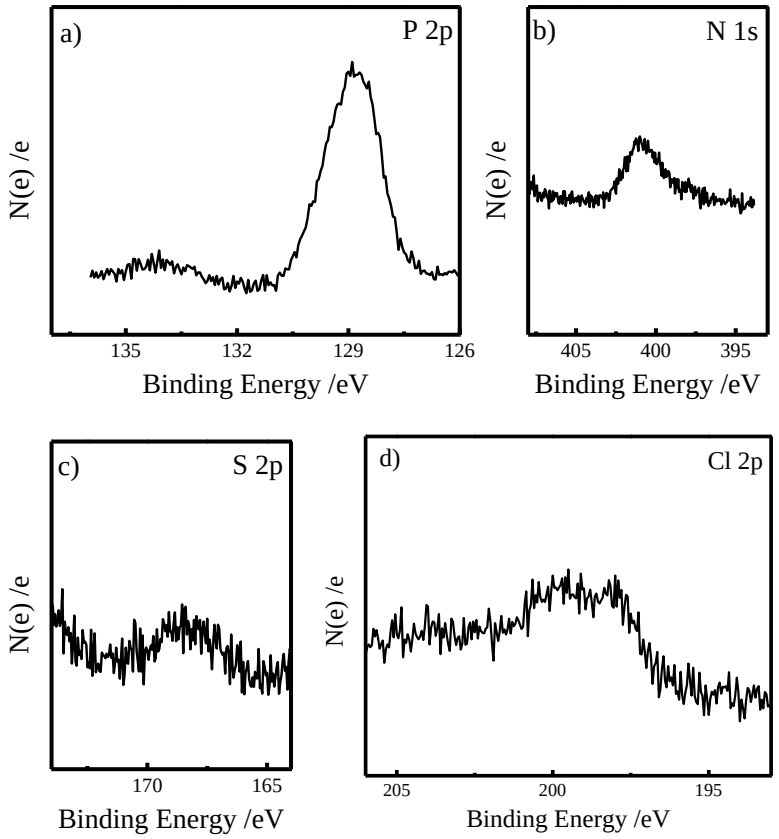

Figure A.5 High resolution XP a) P 2p, b) N 1s, c) S 2p, and d) Cl 2p spectra for GaP NW reacted with modified Coomassie Blue dye.

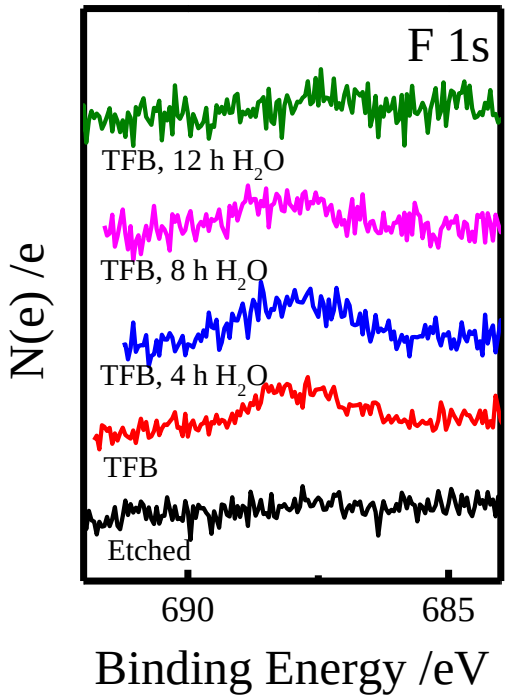

Figure A.6 High resolution F 1s XP spectra of modified GaP NW. Increased signal at 688 eV was observed from etched NW (black) to spectra taken immediately after reaction with TFB (red). Peak signal changes after aging reacted NW samples in water for 4 h (blue), 8 h (pink), and 12 h (green). Spectra are normalized and offset for clarity.

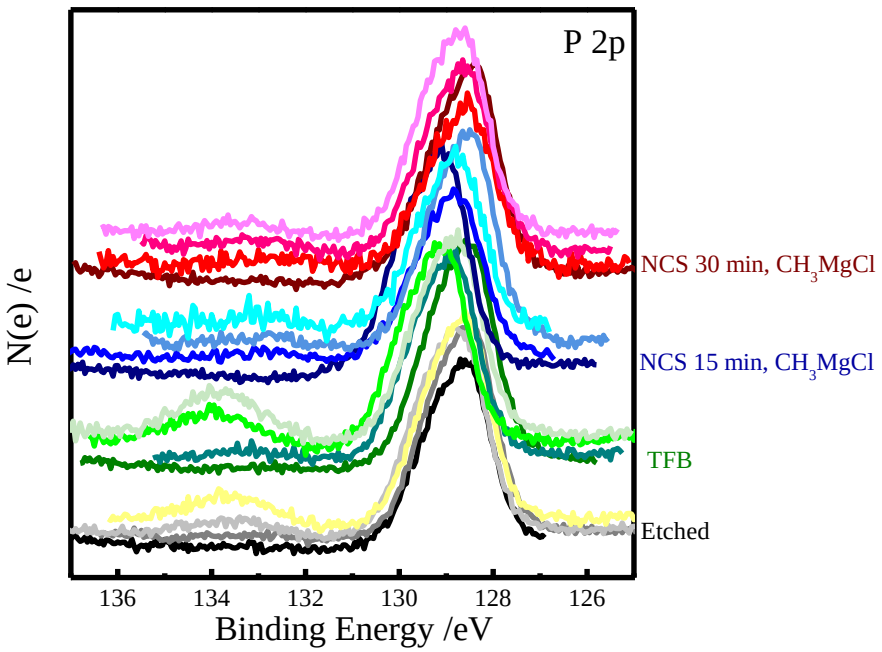

Figure A.7 High resolution XP P 2p spectra for modified GaP NW immediately after reaction (bottom traces) and after several hours oxidation in water (4 h, 8 h, 12 h). Each spectra is offset a small amount for clarity. Each modified surface is grouped together, where etched is black, TFB-reacted is green, NCS (15 min) and CH_3MgCl is blue, and NCS (30 min) and CH_3MgCl is red.

In Figure A.7, the P 2p XP spectra are shown over oxidation in water for 0 h, 4 h, 8 h, and 12 h of etched GaP NW, TFB functionalized NW, and 15 min and 30 min chlorinated samples subsequently reacted with CH_3MgCl. PO_x at 133 eV exhibited the extent of oxidation of these surfaces. TFB reacted samples resulted the highest oxidation while etched surfaces resulted in nearly as high oxidation levels. Samples chlorinated for 15 min and reacted with CH_3MgCl affected surfaces most resistant towards oxidation. There was no change in contact angle of aged chlorinated/Grignard reacted samples (~16°).

A.4 DISCUSSION

More uniform NW samples would be required to calculate the surface coverage of these molecules and oxide thickness.

Based upon the contact angle data after reaction with alkyl Grignard reagents of varying chain length, the average inter-wire distance was approximated as being between smaller than the length of C_8H_{17}- but larger than C_4H_9- molecules. Our working hypothesis was that the longer chains completely cover the surface of the NW structures so as to affect a very hydrophobic surface, but do not completely cover all available surface area.

Due to the high loading expected for NW substrates, no color change could indicate improper coverage of the wires deep in between the interlocking wires. This is not unexpected for closely packed wires, as the average distance between wires is smaller than the diameter of the Coomassie Blue dye molecule.

Grignard chemistry seemed to be the most promising way of reducing surface states and chemical attack and oxidation over time. Dye sensitization and functionalization with long alkyl chains will be feasible with NW of defined spacing, perhaps utilizing patterning techniques previously developed. [10,11]

Additional advances are required before photoelectrochemical measurements of photocathode GaP NW systems can be acquired. Possible areas for modification of GaP NW grown through VLS are changes in the seed catalyst (Au), alternative strategies for Au removal, and secondary annealing after atomic layer deposition of zinc oxide to drive dopant into the NW structure.

A.5. REFERENCES

(1) Price, M. J.; Maldonado, S. Macroporous n-GaP in Nonaqueous Regenerative Photoelectrochemical Cells. *J. Phys. Chem. C* **2009**, *113*, 11988-11994.

(2) Wen, W.; Carim, A. I.; Collins, S. M.; Price, M. J.; Peczonczyk, S. L.; Maldonado, S. Structural and Photoelectrochemical Properties of GaP Nanowires Annealed in NH3. *J. Phys. Chem. C* **2011**, *115*, 22652-22661.

(3) Flores-Perez, R.; Zernlyanov, D. Y.; Ivanisevic, A. Quantitative Evaluation of Covalently Bound Molecules on GaP (100) Surfaces. *J. Phys. Chem. C* **2008**, *112*, 2147-2155.

(4) Richards, D.; Zemlyanov, D.; Ivanisevic, A. Assessment of the Passivation Capabilities of Two Different Covalent Chemical Modifications on GaP(100). *Langmuir* **2010**, *26*, 8141-8146.

(5) Mukherjee, J.; Peczonczyk, S.; Maldonado, S. Wet Chemical Functionalization of III-V Semiconductor Surfaces: Alkylation of Gallium Phosphide Using a Grignard Reaction Sequence. *Langmuir* **2010**, *26*, 10890-10896.

(6) Brown, E. S.; Peczonczyk, S. L.; Maldonado, S. Wet Chemical Functionalization of GaP(111)B through a Williamson Ether-Type Reaction. *J. Phys. Chem. C* **2015**, *119*, 1338-1345.

(7) Peczonczyk, S. L.; Brown, E. S.; Maldonado, S. Secondary Functionalization of Allyl-Terminated GaP(111)A Surfaces via Heck Cross-Coupling Metathesis, Hydrosilylation, and Electrophilic Addition of Bromine. *Langmuir* **2014**, *30*, 156-164.

(8) Wang, Z.; Brown, E. S.; Maldonado, S. Hybrid solar cells constructed of macroporous n-type GaP coated with PEDOT:PSS. *Chinese Chemical Letters* **2015**, *26*, 469-473.

(9) Brown, E. S.; Peczonczyk, S. L.; Wang, Z. J.; Maldonado, S. Photoelectrochemical Properties of CH3-Terminated p-Type GaP(111)A. *J. Phys. Chem. C* **2014**, *118*, 11593-11600.

APPENDIX B

Dye Sensitization With A New Set of Triarylmethane Dyes after Surface Modification of GaP(111)A

B.1. INTRODUCTION

The potential for GaP photocathodes in dye-sensitized photoelectrochemical systems has been previously recognized and physisoprtion with commercially available dyes has been recorded.[1-3] Previously reported dyes all contain several characteristics, such as absorption >540 nm and highest occupied molecular orbital levels of >0.9 V vs. Ag/AgCl to align with the valence band of GaP (0.85 V vs Ag/AgCl).[1,2] However, more recent reports observed a shift in valence band potential to lower energies (0.6 V vs Ag/AgCl).[4] Here, several commercially available dyes were tested with absorptions >540 nm and HOMO levels between 0.85 V and 0.65 V vs Ag/AgCl. The band energetics are displayed pictorially in Figure B.1. Specifically, pinacyanol chloride, Stains All, and Coomassie Blue were tested, which exhibit HOMO levels of 0.695, 0.7, and 0.75 V vs Ag/AgCl, respectively.[5]

B.2 EXPERIMENTAL

B.2.1 Materials

Chemicals and used as received. Indocyanine green, ethyl violet, pinacyanol chloride, Stains All, Coomassie Blue G, were purchased from Sigma Aldrich. Potassium chloride was purchased from Mallinckrodt. All chemicals were used as received. Other chemicals used were previously described.[4]

Water with a resistivity of > 18.2MΩ cm^{-1} (Barnsted Nanopure system) was used throughout. P-type GaP(111)A was purchased and prepared equivalent to published procedures.[4]

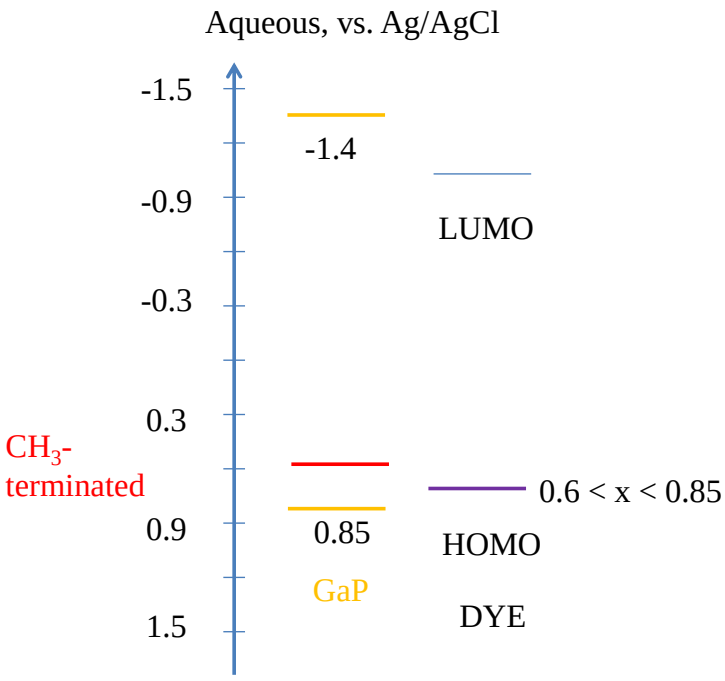

Figure B.1 Band diagram for GaP etched (orange), after modification with PCl_5 and subsequently CH_3MgCl (red), and the HOMO and LUMO levels for the hole-injecting dye.

B.2.2 Photoelectrode Preparation

Ohmic contact to the backside of GaP wafers (0.5 cm^2) was prepared by etching with concentrated H_2SO_4 (aq), rinsing with distilled H_2O, soldering a thin, even film of In:Zn onto the surface, and annealing for 10 minutes at 400°C in forming gas. Electrodes were prepared by using silver print (GC Electronics) to attach the GaP section to a copper wire coil threaded through a glass tube and sealed with inert epoxy (Hysol C). Exposed epoxy was wrapped in Teflon tape to prevent absorption of reactants or solvent. Electrodes were degreased, etched, and reacted as mentioned previously. Photoelectrochemical measurements were acquired in an airtight glass cell with an optically flat bottom. A Pt counter electrode and Ag/AgCl reference electrodes were used. For all photoelectrochemical measurements, the distance between the optical window and the GaP photoelectrode face was ~1 mm. An aqueous solution of potassium chloride (1 M) was used as the background electrolyte, with 10 micromolar dye concentration added when noted.

B.2.3 Photoelectrochemical Measurements

All measurements were performed at room temperature (23±3°C). All photoelectrochemical measurements were performed in a three-electrode cell under potentiostatic control (Princeton Applied Research 267A) and with stirring. The net photocurrent collected per incident light intensity is reported here as an external quantum yield on a scale from 0 to 1. Wavelength-dependent external quantum yield measurements were taken with a setup described previously.[3] Illumination intensities ranged from ~0.1 to 1.0 mW cm^{-2}.

B.3. RESULTS

Figure B.2 shows external quantum yield past the band gap of GaP due to sensitization from physisorbed pinacyanol chloride, Stains All, and Coomassie Blue dyes, respectively.

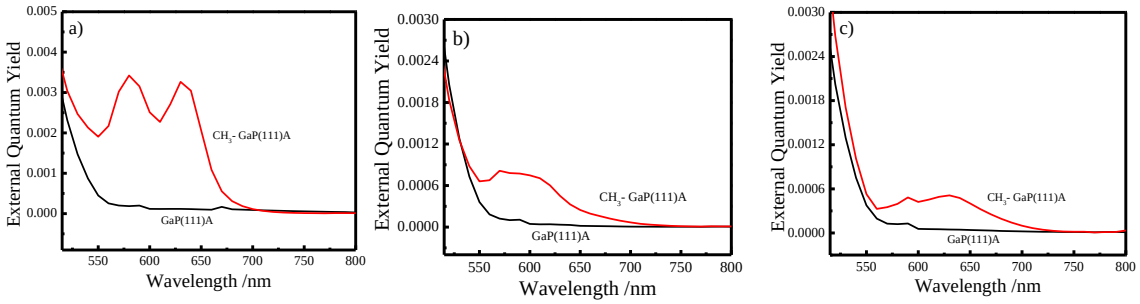

Figure B.2 External quantum yield measured in the sub-band gap region of GaP (>550 nm) for 10 μM a) pinacyanol chloride, b) Stains All, or c) Coomassie Blue in 1 M KCl electrolyte. Etched GaP(111)A responses are shown in black and CH_3-terminated GaP(111)A responses are shown in red.

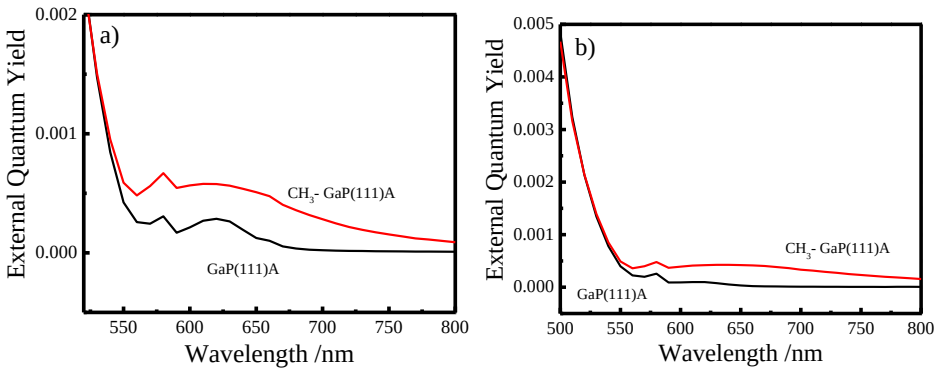

Figure B.3 External quantum yield measured in the sub-band gap region of GaP (>550 nm) for 10 μM a) ethyl violet and b) indocyanine green in 1 M KCl electrolyte. Etched GaP(111)A responses are shown in black and CH_3-terminated GaP(111)A responses are shown in red.

Figure B.3 shows EQY response of positive control ethyl violet and negative control indocyanine green which have HOMO levels of 1.15 V and 0.45 V vs Ag/AgCl, respectively.

B.4 DISCUSSION

These plots show proof of concept that the covalent attachment of organic groups (in this case, $-CH_3$) does impact the valence band potential as measured by impedance[4] and that now a new class of target molecules can be accessed such as dyes, catalysts, sensors, etc.

B.5. REFERENCES

(1) Chitambar, M.; Wang, Z. J.; Liu, Y. M.; Rockett, A.; Maldonado, S. Dye-Sensitized Photocathodes: Efficient Light-Stimulated Hole Injection into p-GaP Under Depletion Conditions. *J. Am. Chem. Soc.* **2012**, *134*, 10670-10681.

(2) Choi, D.; Rowley, J. G.; Parkinson, B. A. Dye Sensitization of n and p Type Gallium Phosphide Photoelectrodes. *J. Electrochem. Soc.* **2012**, *159*, H846-H852.

(3) Memming, R.; Tributsch, H. Electrochemical Investigations on Spectral Sensitization of Gallium Phosphide Electrodes. *J. Phys. Chem.* **1971**, *75*, 562-570.

(4) Brown, E. S.; Peczonczyk, S. L.; Wang, Z. J.; Maldonado, S. Photoelectrochemical Properties of CH3-Terminated p-Type GaP(111)A. *J. Phys. Chem. C* **2014**, *118*, 11593-11600.

(5) Parkinson, B. A. Dye Sensitization of van der Waals Surfaces of SnS2 Photoanodes. *Langmuir* **1988**, *4*, 967-976.

APPENDIX C

Fluorination of Si(111) through Covalent Attachment of $-CF_3$ Groups

C.1. INTRODUCTION

Surface chemistry on Si(111) has been widely studied. Popular methods result in Si-C bond formation, which was noted to be very stable against oxidation and chemical attack.[1-4] Herein, alternative routes were attempted. In particular, a CF_3-terminated Si(111) surface was endeavored. The highly electron-withdrawing $-CF_3$ group would likely impart large shifts on the electronic band structure of Si(111)[5] and affect a very hydrophobic surface.[6] In addition, by endeavoring to use a new reaction method, more insight could be shed into the mechanisms of reactions at the surface.

Homogeneous reactions of silyl chlorides were adapted for Cl-terminated Si(111). First, an exchange reaction with trifluorotmethyltrimethysilyl ($TMSCF_3$) was attempted. Next, reactions with trifluorophenyl sulfides ($PhSCF_3$) and sulfoxides ($PhSO_2CF_3$) were tried. Last, a copper reagent was used to facilitate fluorination of Si(111).

C.2. EXPERIMENTAL

C.2.1 Materials and Chemicals

All chemicals were freeze-pump-thawed for three cycles or placed under vacuum for several hours and subsequently brought into the glovebox. All chemicals were purchased from Sigma Aldrich unless otherwise noted. Trifluoromethyltrimethylsilyl, phenyl trifluoromethylsulfone (Carbosynth), 4-(trifluoromethyl)phenyl sulfoxide, benzoyl peroxide (≥ 97%, Fluka), phosphorus (V) chloride (95%), magnesium powder (99.5%), mercury (II) chloride, potassium butoxide, 1,10-phenanthroline, copper (I) chloride. Methanol (anhydrous, 99.8%), acetone (HPLC-grade, Fisher), tetrahydrofuran (anhydrous, ≥ 99.9%), dimethylformamide (anhydrous, 99%), 40% ammonium fluoride

(Transene Electronic Chemicals, semiconductor grade) were used as purchased. Water with a resistivity of >18 MΩ cm (Barnsted Nanopure system) was used throughout. For surface characterization studies, one-side polished, n-type Si (111) wafers doped with As were purchased from Wafer Works Corp. and had thickness of 525 ± 15 μm. For SRV measurements, float-zone (FZ), intrinsically-doped Si(111) (El-Cat) wafers with a resistivity equal to 16500 ± 3500 Ω·cm, a thickness of 460 ± 15 μm, and both sides polished were used.

C.2.2 Sample Preparation

Samples were diced into 0.5 cm by 0.5 cm squares for surface characterization and into 1 cm by 1.5 cm rectangles for SRV measurements. Si(111) samples were etched prior to use in 40% NH_4F solution for 5 minutes while continuously purging with nitrogen gas, rinsed with water, and dried in a stream of nitrogen gas. Immediately after etching, wafers were transferred to a nitrogen-purged glove box. Freshly etched wafers were chlorinated at 90°C for 50 minutes using a saturated solution of phosphorous (V) pentachloride in chlorobenzene, to which a few grains of benzoyl peroxide were added.[7] Following the chlorination step, samples were washed with THF, dried in the glovebox, and transferred to reaction vessels to which fluorinating reagents were added either in the glovebox ($TMSCF_3$ or $TMSCF_3$ with CuCl, 1,10-phenathroline, potassium butoxide) or in a Schlenk flask in a freezer ($PhSCF_3$, $PhSO_2CF_3$).

C.2.3 X-ray Photoelectron Spectroscopy

Elemental composition of functionalized Si(111) surfaces was collected using a PHI 5400 analyzer equipped with Al K α(1486.6 eV) source, without a monochromator. Acquisition took place at a pressure of < $2.5x10^{-9}$ torr, without the need for charge neutralization due to the natural conductivity of the samples. A 6 mA current emission and a 12 kV anode high tension were used. For each sample survey scans were recorded between 0 and 1350 eV at pass energy of 117.40 eV. While high resolution spectra were collected at pass energy of 23.5 eV. All binding energies were referenced to the expected binding energy for adventitious carbon (284.6 eV).[8] Spectrum analysis was performed with CASA XPS 2.3.13 software. Further characterization of the surfaces were performed by calculating oxide thickness using a simplified substrate/overlayer model[9] and calculating fractional monolayer coverage of the surface using three-layer model.[10]

C.2.4 Static Sessile Drop Contact Angle Measurements

Surface wettability was determined by recording the contact angles of water droplets formed on functionalized surfaces. CAM 100 optical contact angle meter (KSV instrument, Helsinki, Finland) and KSV software analysis package were utilized during data collection and analysis.

C.2.5 Surface Recombination Velocity Measurement

A custom-built microwave photoconductivity system[10,11] was used to measure the minority carrier lifetime in Si wafer sections after various surface treatments. Float-grown Si with low resistivity (R > 13000 ohm cm) and a thickness of 0.046 cm was used exclusively for these measurements. A Continuum Minilite Nd:YAG laser operating at λ = 1064 nm was used to produce excitation pulses with a full-width at half-maximum of < 10 ns. Photoexcitation was performed on the sample side opposite of where microwave radiation was incident. The microwave source was a HP 8350B Sweep Oscillator with a 83570A module operating at a frequency of 18.670 GHz and a nominal output power of 3.16 mW. The reflected signal was measured with an Advanced Control Devices diode (ACSP2644NZ, rise time < 1 ns) connected to a Tektronix TDS 1002B digital oscilloscope. The transient responses were normalized by the reflected signal at t = 0 and plotted as '$\Delta P/P_0$'. The apparent photoconductivity lifetime, τ, was then determined from plots of $\Delta P/P_0$ vs t through a fit with a single exponential function. The explicit relation between τ and the surface recombination velocity, S, is given: [12]

$$\frac{1}{\tau} = \frac{1}{\tau_b} + \left(\frac{2S\pi^2 D}{W\pi^2 D + 2SW^2} \right)$$

Equation C.1 Relation between lifetime and surface state recombination velocity.

where τ_b is the bulk lifetime of the Si wafer section, D is the ambipolar diffusion constant in crystalline Si (10 cm^2 s^{-1} at T = 300 K)[13], and W is the wafer thickness. Figure C.1 defines several important bounds. The shortest time constant (= $W^2\pi^{-2}D^{-1}$) occurs when S is infinitely large. For the materials used here, the shortest measurable value of τ is 2 x 10^{-5} s. The largest possible value of τ occurs when S = 0 cm s^{-1} and corresponds exactly to τ_b. According to the manufacturer, τ_b > 2 x 10^{-3} s for the wafers used here. All values of τ measured between these

two bounds thus report on *S*. Since $\pi^2 D >> 2SW$ for $S < 10^3$ cm s^{-1} for all measured samples, the following approximation was used to estimate *S*.

$$\frac{1}{\tau} = \frac{1}{\tau_b} + \frac{2S}{W}$$

Equation C.2 Approximation for surface state recombination velocity.

C.3. RESULTS

C.3.1 Exchange reaction with $TMSCF_3$

After chlorination reaction, Si(111) samples were reacted through a variety of conditions with $TMSCF_3$ in the glovebox at room temperature, utilizing different solvents and reaction times. The reaction conditions and corresponding contact angle data is shown in Table C.1.

Representative high resolution XP spectra of Si 2p (99.5 eV) and SiO_x (~102 eV) is shown in Figure C.1 for entries 5, 7, and 6 from Table C.1. Though these samples exhibit high contact angle, which could be indicative of a surface covered by several F-containing groups, the XP spectra showed little F 1s signal and very high SiO_x signals. These oxide signals indicated that the self-exchange was not dominating the reactivity of these surfaces under these conditions.

C.3.2 Radical reaction of •CF3

After chlorination reaction, Si(111) samples were reacted with $PhSCF_3$ or $PhSO_2CF_3$ with Mg^0 in DMF following reaction parameters identified by Prakash, et al.[14] Figure C.2 displays the Si 2p XP spectra for two conditions of the reaction with $PhSCF_3$. Though F 1s present in significant qualities, SiO_x was present even when reaction temperature reduced to 0°C. This oxide would likely be detrimental to device performance, as oxides can form surface states if they are non-uniform. As temperature of reactions with $PhSO_2CF_3$ was decreased, SiO_x signal decreased and F 1s signal increased (Figure C.3). Contact angle values are shown in Table C.2. Contact angles are not dramatically hydrophobic, even when significant amounts of F 1s are observed. Due

Table C.1 Contact Angle Values for $TMSCF_3$ Reactions.

Entry	Reagent	Conditions	N	Contact Angle /°
1	THF only	1 h	2	98.5
2	DMF only	1 h	2	93.0
3	$TMSCF_3$, neat	1 h, set 1	5	56.8 ± 2
4	$TMSCF_3$, neat	3 h, set 1	3	73.3 ± 5
5	$TMSCF_3$, neat	1 h, set 2	11	102.5 ± 6
6	$TMSCF_3$, neat	3 h, set 2	4	103 ± 2
7	$TMSCF_3$, neat	1 h, set 2, 5 min methanol sonication	2	100
8	$TMSCF_3$, THF	1 h	4	105 ± 1
9	$TMSCF_3$, DMF	1 h	3	104 ± 2

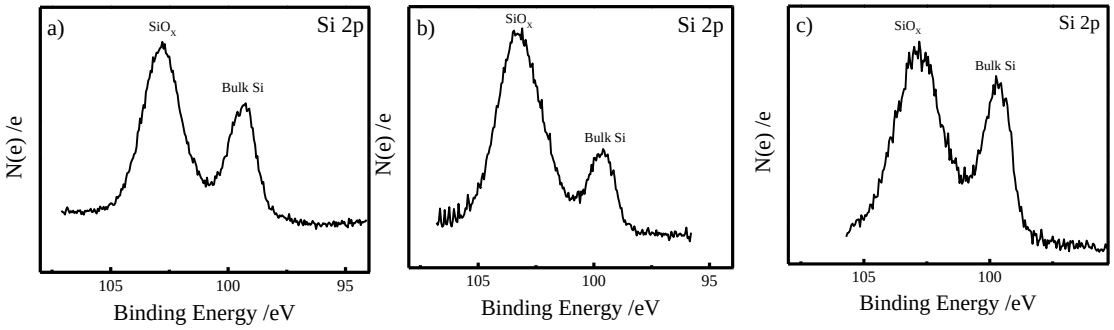

Figure C.1 High resolution Si 2p XP spectra for Si(111) reacted with PCl_5 and then a) $TMSCF_3$ for 1 h, b) $TMSCF_3$ for 1 h followed by sonication in methanol, and c) $TMSCF_3$ for 3 h.

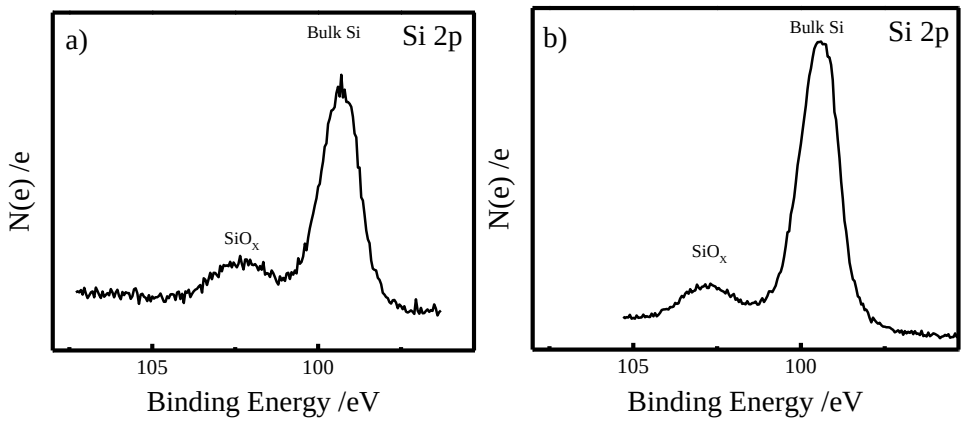

Figure C.2 High resolution Si 2p XP spectra for Si(111) reacted with PCl_5 and then with Mg^0 and a) $PhSCF_3$ for 4 h and b) $PhSCF_3$ for 24 h at 0^0C, followed by sonication in methanol.

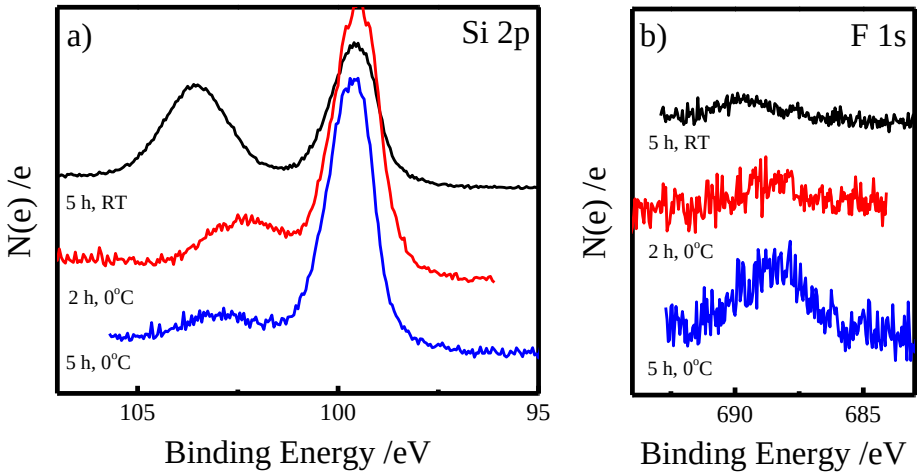

Figure C.3 High resolution a) Si 2p and b) F 1s XP spectra for Si(111) reacted with PCl_5 and subsequently with $PhSO_2CF_3$ and Mg^0 for 5 h at room temperature (black), for 2 h at 0°C (red), and for 5 h at 0°C (blue). Spectra are offset for clarity.

Table C.2 Contact Angle Values for $PhSCF_3$ and $PhSO_2CF_3$.

Entry	Reagent	Conditions	N	Contact Angle /°
1	Cl-Si(111)		3	50 ± 8
2	$PhSCF_3$	4 h	2	43.5
3	$PhSCF_3$	24 h	2	44
4	$PhSCF_3$	1 h, 0°C	3	56 ± 1
5	$PhSO_2CF_3$	5 h	4	46.7 ± 1
6	$PhSO_2CF_3$	2 h, 0°C	3	69.7 ± 9
7	$PhSO_2CF_3$	5 h, 0°C	2	35.5
8	$PhSO_2CF_3$	2 h, -30°C	3	67.6 ± 1
9	$PhSO_2CF_3$	24 h, -30°C	3	63.6 ± 3

to lowest oxide levels, ideal reaction temperature was chosen to be -30°C and used here on out.

Additional reaction considerations showed even more reduced amounts of SiO_x. In particular, the order that reagents were added together impacted surface reactions. When Cl-Si(111) wafers were added last to the reaction mixtures and at cold temperatures (<0°C), SiO_x was negligible (Figure C.4). Mixing of reagents prior to wafer addition also impacted results. When reagents were mixed together and then added to the Si wafer, two different F 1s peaks were often observed at 688 eV and 686 eV (Figure C.5, blue traces). These peaks correspond to different oxidation states of F 1s, often cited as F-C bonding (covalent) and fluoride (ionic), respectively. In contrast, when the reagents are injected to a flask containing the wafer simultaneously, only one F 1s peak appears at 688 eV, though the total intensity of the signal is lower (Figure C.5, green traces).

As shown in Figure C.6, the high resolution F 1s and Cl 2p spectra are shown for various reaction times at -30°C. Under these conditions, the smallest amount of F 1s and largest amount of Cl 2p were observed for reaction of Cl-Si(111) with $PhSCF_3$ for 24 h, indicative of very little conversion of Si-Cl bonds to Si-CF_3. For $PhSO_2CF_3$, Cl 2p decreases with reaction time, possibly indicating the reaction going towards higher completion. However, the F 1s signal shifts from covalent, F-C oxidation state at 689 eV to ionic type F at 686 eV. Only slight decreases in contact were observed as reaction time increased. No peaks indicative of $–CF_3$ were observed by grazing-angle attenuated total reflectance infrared spectroscopy.

Additives were employed to probe alternative methods of bonding.[15,16] Over all reaction conditions tested, no F 1s spectrum showed only a single peak corresponding to covalent F at 688 eV. Representative spectra of reactions with $HgCl_2$ and potassium butoxide are shown in Figure C.7.

C.3.3 Metal-Ligand Assisted Fluorination with 1,10-phenathroline and CuCl

Reaction conditions were adapted from copper-assisted reaction identified by Morimoto, et al.[17] CuCl (0.1g), potassium butoxide (0.03g), and 1,10-phenathroline (0.2g) were mixed in DMF for 30 min at room temperature. $TMSCF_3$(0.2 mL) was slowly added and mixed for about an hour. Finally, Cl-Si(111) wafers were added to the

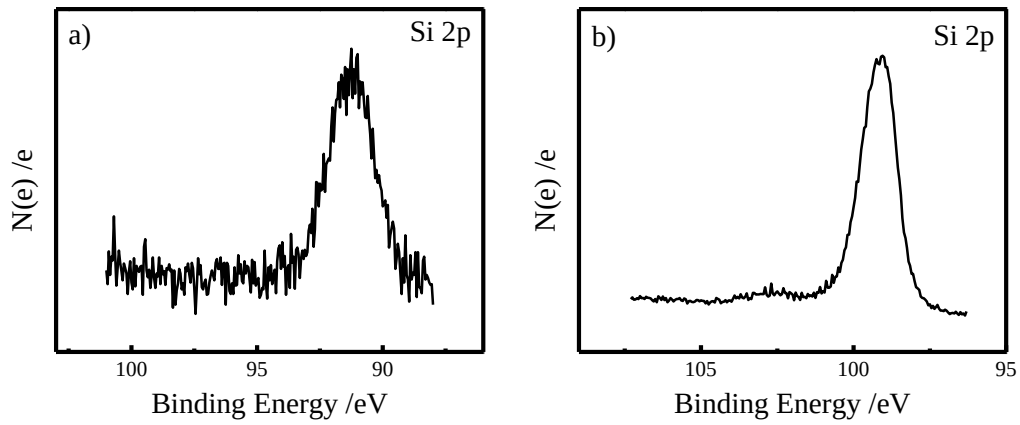

Figure C.4 High resolution Si 2p XP spectra for Si(111) reacted with PCl_5 and then with $PhSO_2CF_3$ and Mg^0 a) for 2 h at 0°C and b) for 2 h at -30°C. Procedure for these reactions required the reagents to be mixed prior to adding to the Cl-Si(111).

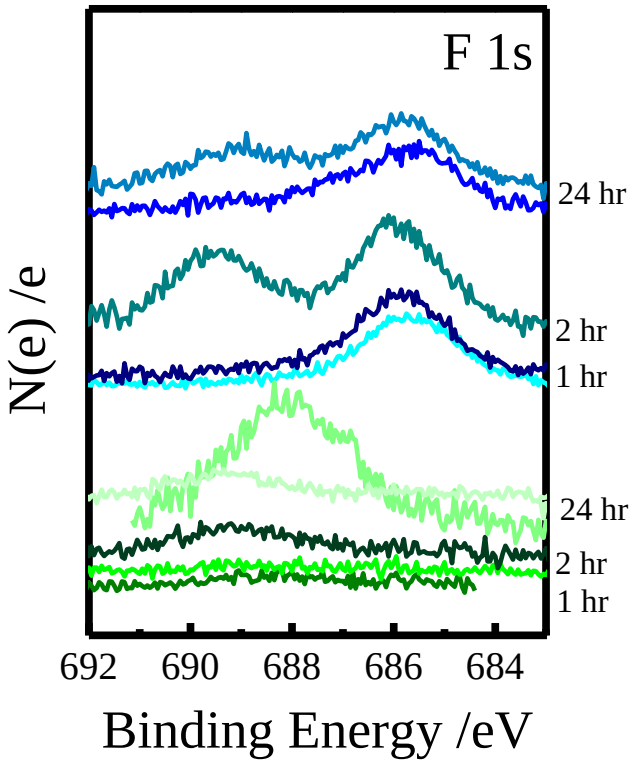

Figure C.5 High resolution XP spectra of Cl-Si(111) after reaction with $PhSO_2CF_3$ and Mg^0 in DMF at -30°C for different reaction times. Blue traces indicate reactions where all reagents are mixed together before adding Si substrate while green traces indicate reactions where all reagents were injected simultaneously into a vessel containing the Si substrate.

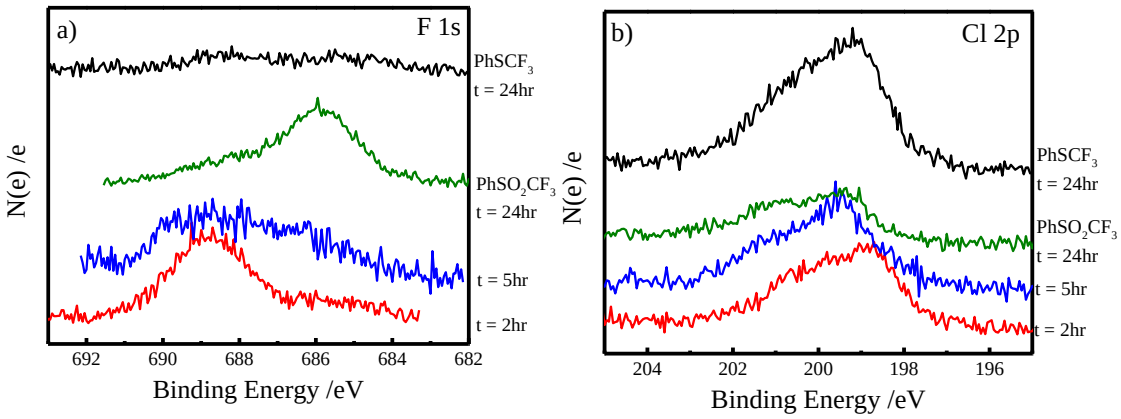

Figure C.6 High resolution a) F 1s and b) Cl 2p XP spectra for Cl-Si(111) reacted at -30°C with Mg^0 and $PhSCF_3$ for 24 h (green) or $PhSO_2CF_3$ for 2 h (red), 5 h (blue), or 24 h (green).

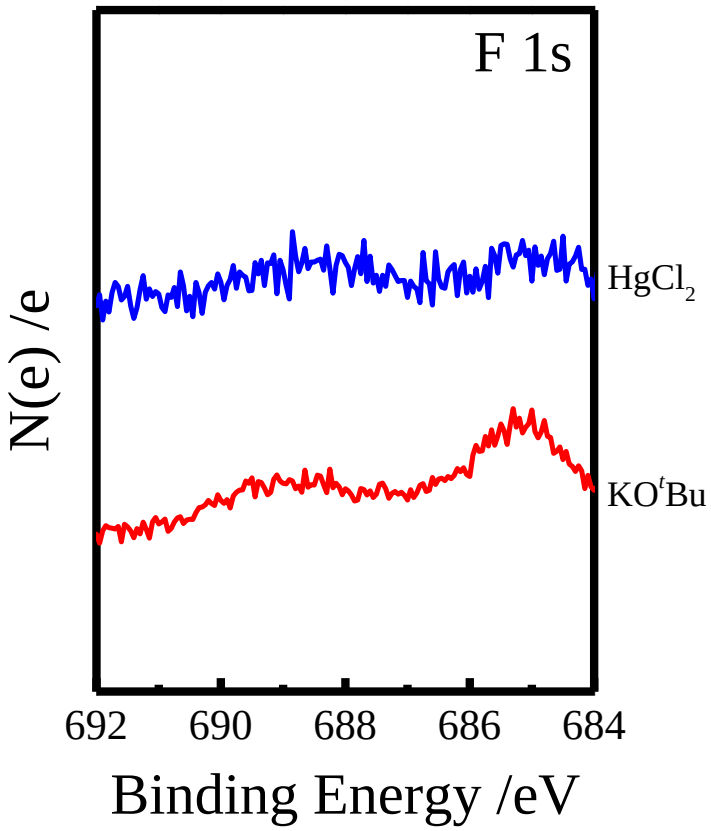

Figure C.7 Representative high resolution F 1s XP spectra for Cl-Si(111) reacted at -30°C with Mg^0 and $PhSO_2CF_3$ for 2 h in the presence of $HgCl_2$ (blue) or potassium butoxide (red) additives.

mixture and were reacted for 12 to24 h at 55°C. Reactions initially were performed in an evacuated and purged Schlenk flask but were moved into the glovebox to help with consistency. Samples were rinsed and sonicated in acetone before characterization. Contact angle was 112 ± 10° with N = 10.

Several reaction conditions were characterized in Figure C.8. For reactions containing only $TMSCF_3$ or standard conditions without CuCl, oxide was observed with ionic F signal around 686 eV. Non-chlorinated Si surfaces reacted through standard conditions showed high oxide and high ionic F signal. Temperature impacted oxide content and type of F signal. Samples reacted at 25°C showed some oxide and ionic F signal, 50°C showed some oxide and more covalent F at 687.5 eV, 55°C showed high oxide and high covalent F signal at 688 eV, and 90°C showed exclusively SiO_x and medium covalent F signal. The spectra shown in Figure C.8 were chosen due to no Cu 2p contamination. There was some sample variance within each set of conditions. The reaction mixture tends to form sludge at the bottom of the reaction vessel and sometimes a plaque would form on the wafer which was not removable by sonication in a number of solvents. This plaque was not identified, though it contained low Cu 2p and high SiO_x, as shown in Figure C.9 where it is compared to a clean area of the same sample wafer.

Stability was tested by aging samples in ambient conditions. As shown in Figure C.10, SiO_x increased and F 1s signal decreased over 1 day in ambient. Average monolayer coverage was calculated to be 0.67 for pristine samples, 0.62 after aging in ambient conditions for 1 day, and 0.59 after aging in ambient for 6 days.

C.3.4 Preliminary Assessment of Surface States after Surface Modification

Float zone Si(111) was modified as listed in Table C.3 and charge carrier lifetimes were measured using a microwave conductivity set up. Surface recombination velocity values were roughly 50 times higher than ideally passivated CH_3-Si(111) surfaces.

C.4. DISCUSSION

C.4.1 Exchange reaction with $TMSCF_3$

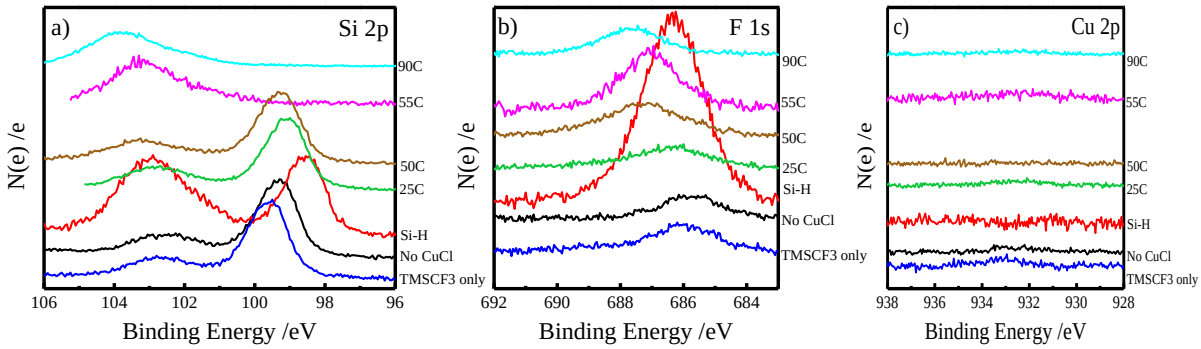

Figure C.8 High resolution a) Si 2p, b) F 1s, and c) Cu 2p XP spectra of several reaction conditions of Cl-Si(111) reacted with $TMSCF_3$ with CuCl, 1,10-phenathroline, and potassium butoxide in DMF.

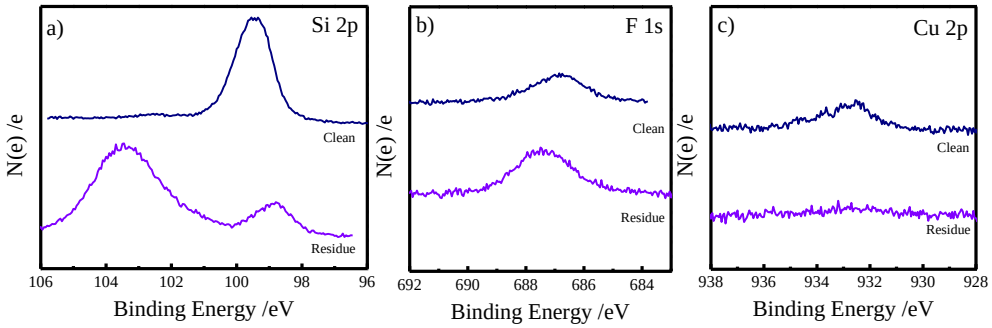

Figure C.9 High resolution a) Si 2p, b) F 1s, and c) Cu 2p XP spectra of two sections of the same wafer after reaction of Cl-Si(111) with $TMSCF_3$ with CuCl, 1,10-phenathroline, and potassium butoxide in DMF at 55°C for 18 h. One section, termed 'clean', looked optically shiny after rinsing while another section contained a plaque that was not removable by sonication in different solvents, termed 'residue.

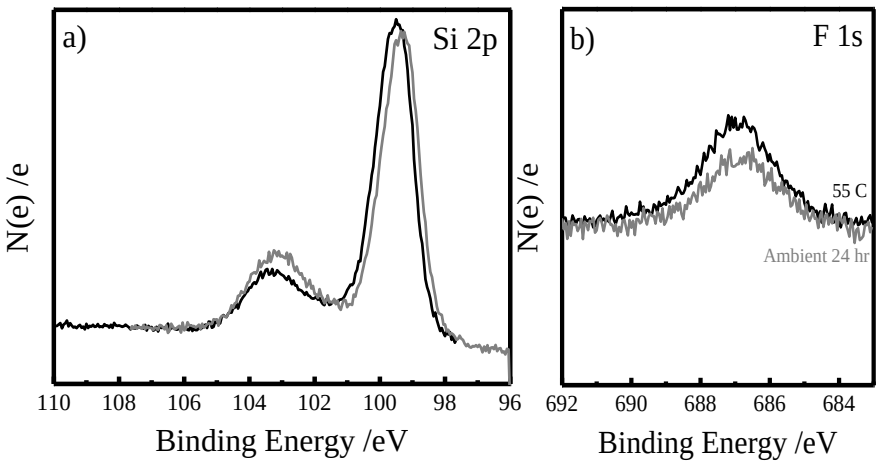

Figure C.10 High resolution a) Si 2p and b) F 1s XP spectra for Cl-Si(111) with $TMSCF_3$ with CuCl, 1,10-phenathroline, and potassium butoxide in DMF at 55°C for 18 h (black) and after 1 day in ambient conditions (gray).

Table C.3 Lifetime and Surface Recombination Velocity of Modified Si(111).

Sample	Lifetime /μs^{-1}	Surface Recombination Velocity /cm s^{-1}
CH_3-Si(111)	638	37
Cl-Si(111)+PhSO2CF_3, -30°C, 24 h	6.15	2460
Cl-Si(111)+TMSCF_3, CuCl, phen, 55°C	9.20	1630

Self-exchange reactions are likely kinetically slow, especially when steric limitations are imposed for surface reactions. The mechanism of oxide growth during these reactions is unknown, especially as these reactions took place in air-free environments such as the glovebox or purged Schlenk flasks.

C.4.2 Radical reaction of •CF_3

When reagents are added together before they come in contact with Si-Cl, some radical could be forming and doing a side reaction before they come in contact with Si-Cl. When reagents are added to the Si-Cl simultaneously but separately, a majority of radical that is formed could react directly with Si-Cl before participating in side reactions. Side reactions could include CF_3 radicals annihilated to C_2F_6 or CF_3 radicals could abstract H to CF_3H.[18]

C.4.3 Metal-Ligand Assisted Fluorination with 1,10-phenathroline and CuCl

Catalyst-assisted reaction at the surface could be promising. Limitations or potential areas for improvement could be in controlling reaction temperature and eliminating 'sludge' from the reaction conditions.

C.4.4 Surface state measurement of Attempted CF_3-Si(111)

Surface recombination velocities, and proportionally, surface state densities, are much higher for our attempted CF_3-Si(111) surfaces than chlorination/Grignard reacted CH_3-Si(111) surfaces, which are known to have full monolayers. Chemical strategies for $–CF_3$ passivation need more development because likely too much oxide was introduced using the methods described here. The introduction of these oxides and likely low monolayer coverage of $–CF_3$ groups make these reactions unaccommodating towards highly efficient interfaces for electronic devices.

C.5. CONCLUSIONS AND FUTURE OUTLOOK

No electronically passivating and highly hydrophobic monolayers of $–CF_3$ were yet achieved using several different reaction strategies. Alternative methods of $–CF_3$ reaction could be probed, looking at anionic or cationic $–CF_3$ reactions, delving into the mechanism of different reactions, or even halogenating the Si(111) surface with a better leaving group, e.g., bromination of H-Si(111) with N-bromosuccinimide.

C.6. REFERENCES

(1) Bansal, A.; Li, X. L.; Lauermann, I.; Lewis, N. S.; Yi, S. I.; Weinberg, W. H. Alkylation of Si Surfaces Using a Two-Step Halogenation Grignard Route. *J. Am. Chem. Soc.* **1996**, *118*, 7225-7226.

(2) Bansal, A.; Lewis, N. S. Stabilization of Si Photoanodes in Aqueous Electrolytes Through Surface Alkylation. *J. Phys. Chem. B* **1998**, *102*, 4058-4060.

(3) Selzer, Y.; Salomon, A.; Cahen, D. The importance of chemical bonding to the contact for tunneling through alkyl chains. *J. Phys. Chem. B* **2002**, *106*, 10432-10439.

(4) Cohen, R.; Zenou, N.; Cahen, D.; Yitzchaik, S. Molecular electronic tuning of Si surfaces. *Chem. Phys. Lett.* **1997**, *279*, 270-274.

(5) Bruening, M.; Moons, E.; Yaronmarcovich, D.; Cahen, D.; Libman, J.; Shanzer, A. Polar ligand adsorption controls semiconductor surface-potentials. *J. Am. Chem. Soc.* **1994**, *116*, 2972-2977.

(6) Wei, W.; Huang, X. B.; Zhao, X. L.; Zhang, P.; Tang, X. Z. A Rapid and Efficient Strategy for Preparation of Super-Hydrophobic Surface with Cross-Linked Cyclotriphosphazene/6F-bisphenol A Copolymer Microspheres. *Chem. Commun.* **2010**, *46*, 487-489.

(7) Bansal, A.; Li, X. L.; Yi, S. I.; Weinberg, W. H.; Lewis, N. S. Spectroscopic Studies of the Modification of Crystalline Si(111) Surfaces with Covalently-Attached Alkyl Chains using a Chlorination/Alkylation Method. *J. Phys. Chem. B* **2001**, *105*, 10266-10277.

(8) Barr, T. L.; Seal, S. Nature of the Use of Adventitious Carbon as a Binding-Energy Standard. *J. Vac. Sci. Technol., A* **1995**, *13*, 1239-1246.

(9) *Practical Surface Analysis*; Briggs, D.; Seah, M. P., Eds.; John Wiley & Sons: Chichester, 1983.

(10) Asami, K.; Hashimoto, K.; Shimodaira, S. XPS Determination of Compositions of Alloy Surfaces and Surface Oxides on Mechanically Polished Iron-Chromium Alloys. *Corros. Sci.* **1977**, *17*, 713-723.

(11) Eady, S. C.; Peczonczyk, S. L.; Maldonado, S.; Lehnert, N. Facile Heterogenization of a Cobalt Catalyst via Graphene Adsorption: Robust and Versatile Dihydrogen Production Systems. *Chem. Commun.* **2014**, *50*, 8065-8068.

(12) Horanyi, T. S.; Pavelka, T.; Tutto, P. In-Situ Bulk Lifetime Measurement on Silicon with a Chemically Passivated Surface. *Appl. Surf. Sci.* **1993**, *63*, 306-311.

(13) Rosling, M.; Bleichner, H.; Jonsson, P.; Nordlander, E. The Ambipolar Diffusion-Coefficient in Silicon--Dependence on Excess-Carrier Concentration and Temperature. *J. Appl. Phys.* **1994**, *76*, 2855-2859.

(14) Prakash, G. K. S.; Hu, J. B.; Olah, G. A. Preparation of tri- and difluoromethylsilanes via an unusual magnesium metal-mediated reductive tri- and difluoromethylation of chlorosilanes using tri- and difluoromethyl sulfides, sulfoxides, and sulfones. *J. Org. Chem.* **2003**, *68*, 4457-4463.

(15) Prakash, G. K. S.; Wang, F.; Zhang, Z.; Haiges, R.; Rahm, M.; Christe, K. O.; Mathew, T.; Olah, G. A. Long-Lived Trifluoromethanide Anion: A Key

Intermediate in Nucleophilic Trifluoromethylations. *Angewandte Chemie-International Edition* **2014**, *53*, 11575-11578.

(16) Zhao, Y.; Zhu, J.; Ni, C.; Hu, J. Magnesium Metal-Mediated Reductive Trifluoromethylation of Aldehydes with Phenyl Trifluoromethyl Sulfone. *Synthesis* **2010**, 1899-1904.

(17) Morimoto, H.; Tsubogo, T.; Litvinas, N. D.; Hartwig, J. F. A Broadly Applicable Copper Reagent for Trifluoromethylations and Perfluoroalkylations of Aryl Iodides and Bromides. *Angewandte Chemie-International Edition* **2011**, *50*, 3793-3798.

(18) Majer, J. R.; Naman, S. A. M.; Robb, J. C. Hydrogen Abstraction from Aromatic Aldehydes by Trifluoromethyl Radicals. *Transactions of the Faraday Society* **1969**, *65*, 3295-&.